Synthesis, spectroscopic and nonlinear optical properties of metal-free and nickel β substituted binuclear phthalocyanines

A thesis submitted in fulfilment of the requirement for the degree of

MASTER OF SCIENCE

AT

RHODES UNIVERSITY

By

KAPAMBWE PETER KABWE

January 2016

DEDICATION

TO MY LATE FATHER

ABRAHAM KABWE

AND

THE ENTIRE KABWE'S FAMILY

ACKNOWLEDGEMENT

I would like to acknowledge the efforts and support from all the people who contributed to the completion of this research project.

In particular, I give my heartfelt appreciations to my supervisor Dr Samson Khene for his guidance, encouragements, criticism and the confidence he built in me. He played a major role from the start up to the end of the research project, thank you so much. May GOD guide you as you continue with this wonderful career.

I would like also to appreciate and thank my friends, Grace Ngubeni, Daniel Mwanza, Marcel and Zainab Makinde for the support they gave me during my research. My special thanks go to my entire family for their love, care and encouragements; they gave me whilst doing my research. I am deeply grateful to you all. May the Almighty God prolong your lives.

Lastly, I would like to extend my sincere gratitude to the HEART PROJECT of Copperbelt University (Zambia) in partnership with VU University Amsterdam, (Netherlands) for financial assistance.

ABSTRACT

In this project, nickel and metal-free 4β-(4-*tert*-butylphenoxy) phthalocyanine, biphenyl bridged binuclear 4-*tert*-butylphenoxy phthalocyanine and naphthalene bridged binuclear 4-*tert*-butylphenoxy phthalocyanine have been synthesised. The Z-scan technique has been employed to comparatively study their second order nonlinear optical (NLO) properties. This work, shows that the presence of H-aggregation in binuclear Pcs of metal-free and nickel 4β-(4-*tert*-butylphenoxy) phthalocyanines do not have an effect on the magnitude of second order nonlinear absorption coefficient (β) as compared to monomeric Pcs.

Density functional (DFT) calculations of dipolar/octupolar contributions were performed, in order to explain experimentally determined β values. Spectroscopic and photophysical properties of the synthesised compounds have been determined using a range of different spectroscopic techniques, including magnetic circular dichroism (MCD), time correlated single photon counting spectroscopy (TCSPC), UV-visible absorption spectroscopy, mass spectroscopy and IR Spectroscopy.

TABLE OF CONTENT

LIST OF ABBREVIATIONS

Abs	Absorption
Bi-Pcs	Binuclear phthalocyanines
DBU	Diazabicxylo-undec- 7- ene
DCM	Dichloromethane
DFT	Density functional theory
DMF	Dimethylformamide
DMSO	Dimethylsulfoxide
DR	Depolarization ratio
Em	Emission
Exc	Excitation
HCl	Hydrochloric acid
HOMO	Highest occupied molecular orbital
HRS	Hyper-Rayleigh Scattering
IR	Infrared
Lcp	Left circular polarized
LUMO	Lowest unoccupied molecular orbital
MDC	Magnetic circular dichroism
mJ	millijoules
mmol	millimolar
MOs	Molecular orbitals
mpa.s	millipascal second
MPcs	Metalated phthalocyanines
NLO	Nonlinear optical

Nm	Nanometers
NMR	Nuclear magnetic resonance
Ns	Nanoseconds
Pcs	Phthalocyanines
PDT	Photodynamic therapy
Ppm	parts per million
Rcp	Right circular polarized
RSA	Reserve saturable absorption
RT	Room temperature
TCSP	Time correlated single photon counting
TD-DFT	Time dependant density functional theory
THF	Tetrahydrofuran
UV-Vis	Ultraviolet visible

LIST OF SYMBOLS

β	Nonlinear absorption coefficient
ε	Extinction coefficient
G	Giga
h	Planck's constant
H_Z	Hertz
J	Joules
κ	Boltzmann constant
K	Kelvin
L	Sample length
Le_{ff}	Effective propagation length in the material
m	Meters
N	Number of active species per unit volume
ρ	Nonlinear anisotropy parameter
ρ_0	peak power of the pulses
T	Temperature
τ	Fluorescence lifetime
$q_0 (z_s)$	Parameter characterizing the strength of the nonlinearity
Vm	Molecular volume
W	Watts
Wo	Beam width of the sample
W (Zs)	Beam width of the sample
Zo	Location of the beam focus
Z_R	Rayleigh length

Φ	Anisotropy rotational correlation time
$\Phi_{J=1}$	Dipolar contribution
$\Phi_{J=3}$	Octupolar contribution
λ	Wavelength
μ	Micro
η	Viscosity
π (π*)	Pi bonding (anti pi bonding)
ΔE	Change in energy

LIST OF FIGURES

LIST OF SCHEMES

LIST OF TABLES

CHAPTER ONE: INTRODUCTION

1. Introduction

1.1 Phthalocyanines

Phthalocyanines (Pcs) are synthetic compounds that are made up of four isoindole units joined together by aza nitrogen atoms, with an 18 π-electron system within the macrocycles [1], **Figure 1.1**. Pcs are interesting compounds due to their physical and chemical properties such as, conductivity, thermal and chemical stability towards environmental influences. Pcs are well known by their blue or green colours which are used as pigments in printing inks, paints and plastics [1, 2, 3]. These interesting compounds have a variety of technological applications such as photodynamic therapy (PDT) [4], gas and chemical sensors [5], catalysis [6], photovoltaic cells [7], semi-conductors devices [8] and nonlinear optics [9]. Pcs can be modified by coordination with different metals and substitution of peripheral or non-peripheral positions with different substituents. These modifications on Pcs can increase their specificity in various applications. Peripheral or non-peripheral positions are generally referred to as **β** and **α** position respectively (**Figure 1.1**).

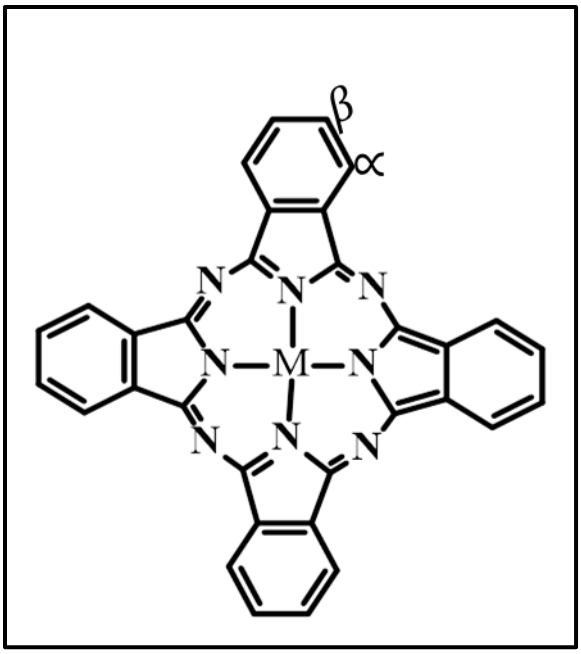

Figure 1.1: General structure of phthalocyanine (Pc), (metalated form MPc and metal-free form H2Pc)

1.2 Electronic Absorption Spectra of Phthalocyanines

Pcs spectra generally shows two major absorption bands referred to as Q and B band (Soret band), **Figure 1.2**. The strong colours of Pcs arise from the Q band which is a strong band in the far red of the visible spectrum around **660** and **720** nm. The most energetic set of transitions referred to as B bands (soret) are less intense and lie to the blue of the electromagnetic spectrum between **320-400** nm. These intense absorption bands are due to transitions from bonding to anti-bonding orbitals, $\pi \rightarrow \pi^*$ transitions.

In phthalocyanines, the highest occupied molecular orbital (HOMO) is labelled a_{1u} (π) and the next low lying orbital is labelled a_{2u} (π). The lowest unoccupied molecular orbital (LUMO) is doubly degenerate and labelled e_g (π^*) and the one after it is labelled b_{1u} (π^*) [10].

The π-π* transition involve a_{1u} to e_g transition results in the intense Q-band and the less intense B band is due to the second π-π* transitions which involves a_{2u} and/ or b_{2u} to e_g transitions. The electronic energy level diagram summarising the energy level labelling is shown in **Figure 1.3.**

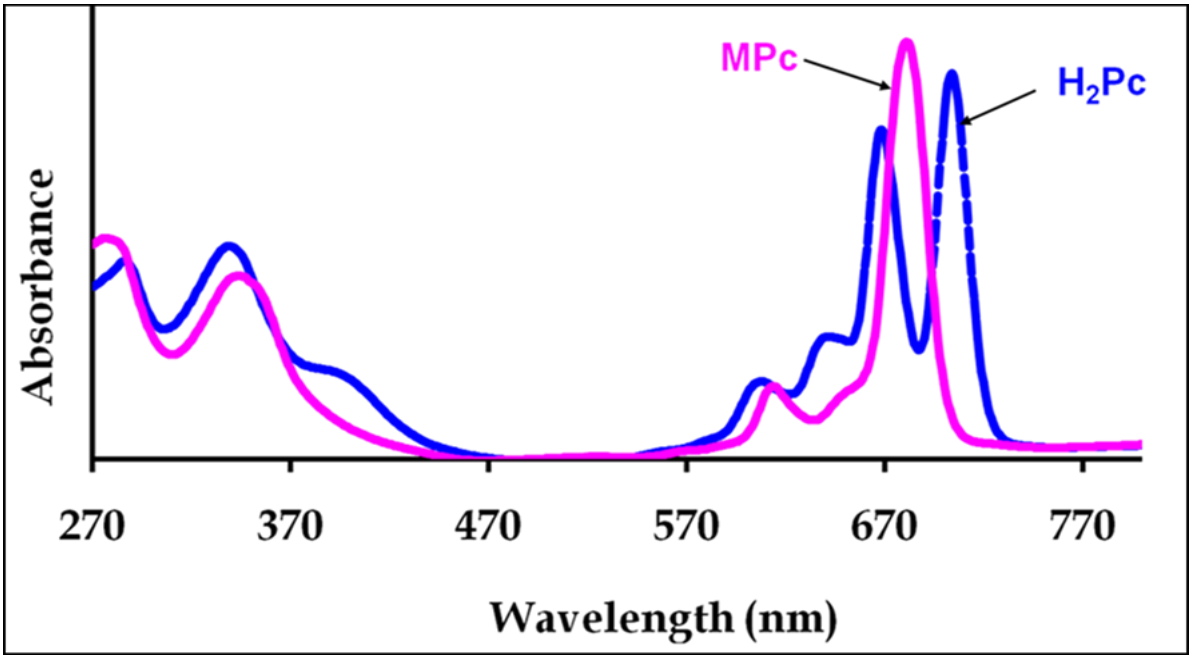

Figure 1.2 UV/Vis spectra of Metalated (MPc) and metal-free (H_2Pc) phthalocyanine in Chloroform [11]

Metal-free Pcs have lower D_{2h} molecular symmetry, while metalated Pcs have higher D_{4h} molecular symmetry. Due to the lower molecular symmetry of metal-free Pcs, the e_g energy levels are not degenerate; hence they have a split Q band, **Figure 1.2.** Metalated Pc Q band is not split due a higher molecular symmetry which causes the e_g energy level to be degenerate, (as shown in **Figure 1.2).** Aggregation which is enhanced by van der Waals attractive forces between the rings of larger planar molecules also lowers the molecular symmetry of Pcs and results in the broadening and splitting of the Q band. Aggregated Pc couples between rings of

two or more π-system which leads to the blue or red shifting of the Q band. Aggregation lowers solubility, prevents photo chemistry and makes purification difficult [12].

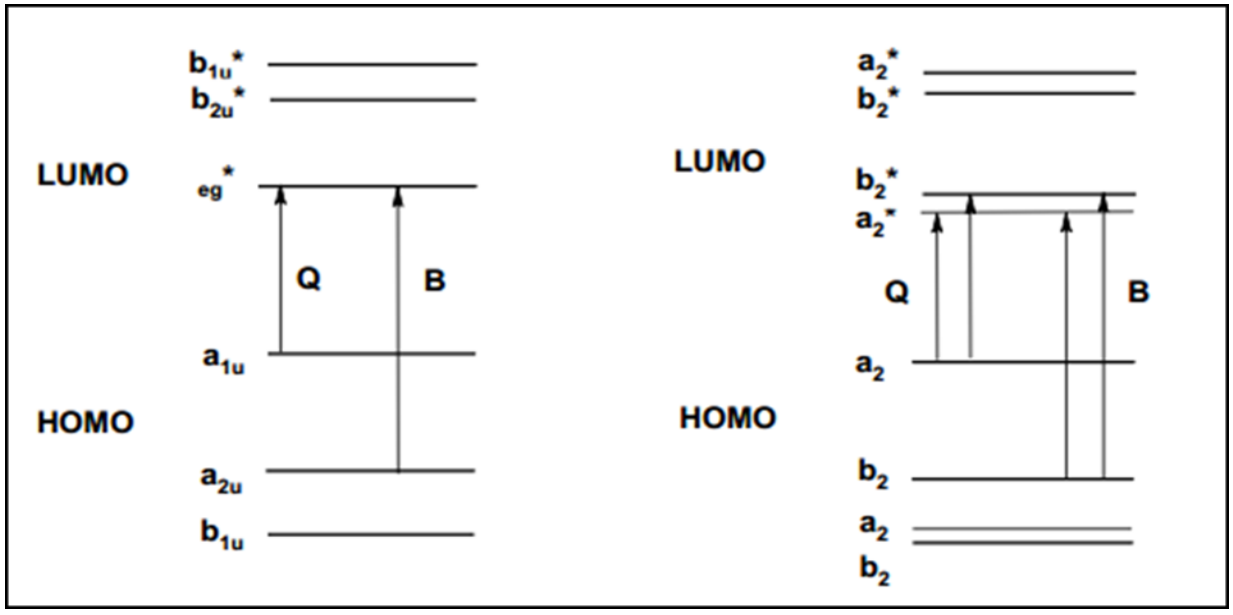

Figure 1.3 Electronic energy levels for Metalated Pc (left) and Metal-free Pc (right) [11]

The Q-band wavelength changes when oxidation potential of the central metal ion changes. The wavelength shift of the Q-band is also observed in the presence of coordinating solvents or when coordinating ligands are added [13]. When electron-donating group is introduced at the α position of the Pc, the Q band shifts to the longer wavelength, while at the β position, the Q band shifts to the shorter wavelength [14]. For electron-withdrawing groups, the effect is completely opposite with regards to α and β positions. Introducing the electron-withdrawing group at the α position shifts the Q band to the short wavelength while at the β position, the Q band shifts to the longer wavelength [14].

1.3 General synthesis of phthalocyanines

Synthesis of Pcs can be done using different methods. The nature of the precursors and availability of the substituents as the study materials determine the method of making these Pcs [15]. The most common synthetic method used involves the heating of substituted phthalonitriles derivatives as the starting materials in the presence of other reagents such as 1,8-diazabicylo-[5,4,0]-undec-7-ene (DBU) or lithium (used as catalysts), solvent (e.g. pentanol, octanol) and metal salt in the case of metalated Pcs [15], **Scheme 1.1.**

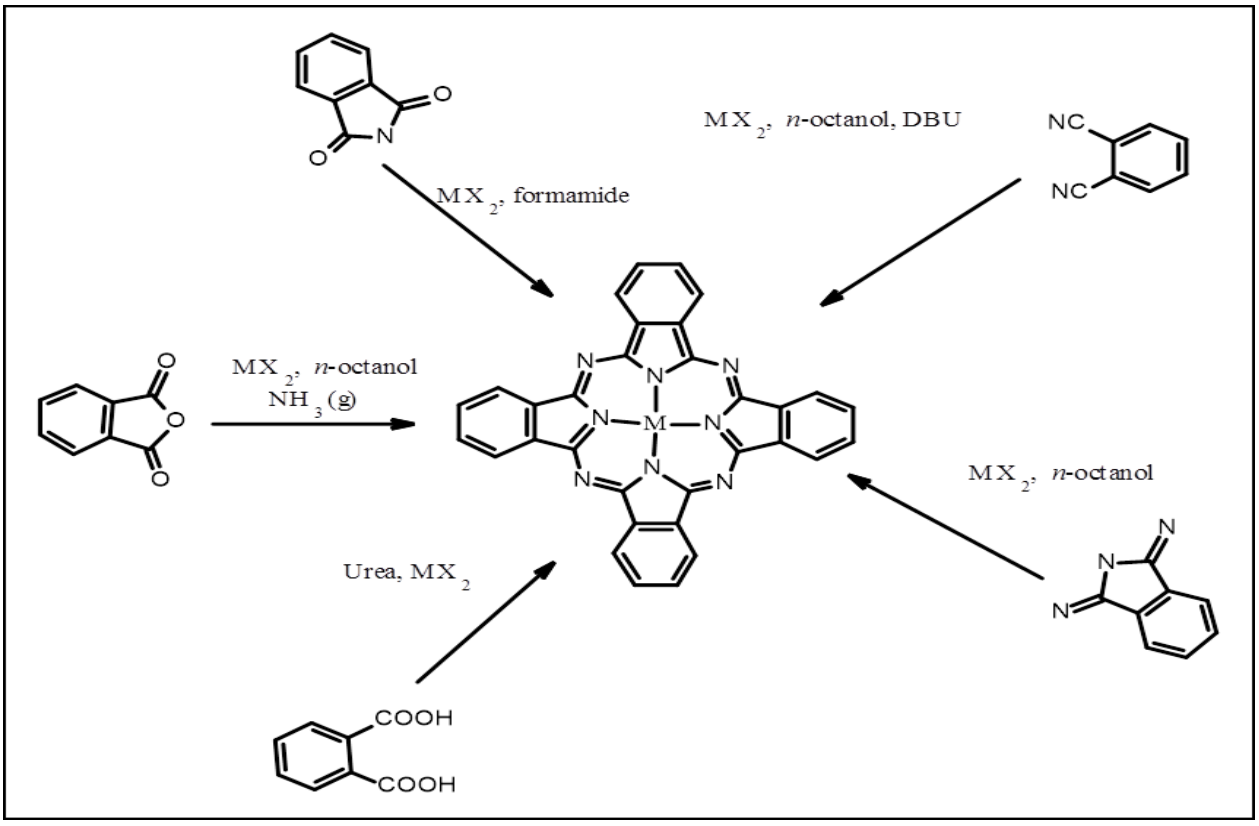

Scheme 1.1: General synthesis of phthalocyanines, MX_2=Metal salt [16].

1.3.1 Synthesis of peripheral tetra substituted phthalocyanines.

Phthalocyanine's solubility in some organic solvents can be improved by the addition of substituents at the β or α position of macrocycles. Substituents improve Pc dissolution due to the increase in distance between the stacked molecules [17]. In this work, β tetra substituted Pc is studied. Synthetic route for peripheral tetra substituted phthalocyanine is shown below in (**Scheme 1.2**) involving the nucleophilic substitution reaction of 4-nitrophthalonitrile (**1**) and an alcohol in the presence of K_2CO_3 as a base and dry polar aprotic solvent to produce the 4-alkoxyphthalonitrile (**2**) [18]. **Scheme 1.2** also shows the synthesis of β tetra substituted Pc using microwave method. Microwave method involves heating of phthalic anhydride with urea in the presence of a catalyst mainly ammonium molybdate or aluminium oxide. These substances are mixed together and irradiate in a domestic microwave oven for less than 5 minutes. This method is fast and cheap however purification takes time [19].

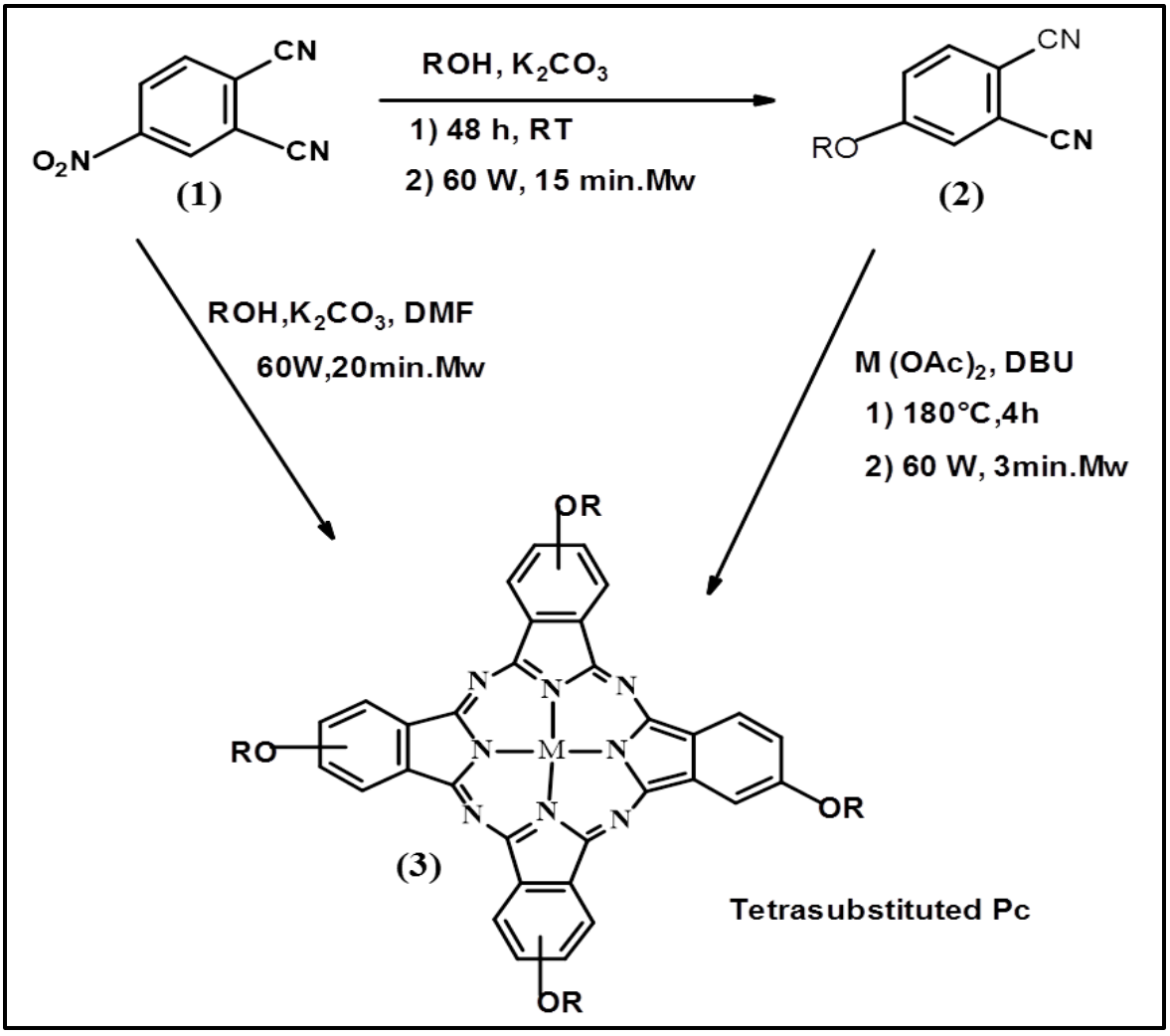

Scheme 1.2: Synthesis of peripheral tetra substituted phthalocyanine, OR=any functional group [18].

1.4 Second order nonlinear optical activity (NLO)

Studies on organic second-order nonlinear optical (NLO) materials have been conducted in the recent past. NLO materials have gained promising applications in practical areas such as optical sensors, laser frequency conversion devices, optical information storage and higher speed electro-optic switching [20-24]. Second-order optical nonlinearity in many organic compounds

arises from highly polarizable π-conjugated system capped with groups of different electron affinities. Traditional inorganic materials have been studied for their NLO properties in the past. It has been reported in literature [25], that these inorganic materials have some disadvantages such as difficulty of substitution, low response coefficient and delayed response. However, these drawbacks have been overcome by using organic dipolar molecules such as phthalocyanines.

1.4.1 Second-Order nonlinear optical activity in phthalocyanines

Phthalocyanines are applied as potential nonlinear optical materials based on two-photon absorption (2PA) and the nonlinear reverse saturable absorption (RSA) mechanism [26].Two photon absorption is a process in which an atom absorbs two-photons at the same time. In this process, an electron from a lower energy level (ground state) is promoted to a higher energy level referred to as the excited state. The sum of the two photon energies is equal to the total energy of the transition [27]. RSA mechanism is observed when nonlinear excited state absorption is larger than the ground state absorption. RSA mechanism depends on the 2PA mechanism. **Figure 1.4** shows how RSA is rationnalised. It is understood that Pc molecule lie within the vibration manifold of one of the five electronic states. The ground state, $\mathbf{S_0}$, one of the two excited singlet states, $\mathbf{S_1}$or $\mathbf{S_2}$ and one of the two excited triplet states $\mathbf{T_1}$ or $\mathbf{T_2}$. The absorption cross section for the transition $\mathbf{S_0 \rightarrow S_1}$, $\mathbf{S_1 \rightarrow S_2}$ and $\mathbf{T_1 \rightarrow T_2}$ are denoted as $\boldsymbol{\sigma_G}$, $\boldsymbol{\sigma_S}$ and $\boldsymbol{\sigma_T}$ respectively. The excited state cross sections ($\boldsymbol{\sigma_S}$, $\boldsymbol{\sigma_T}$) are larger than the ground state cross section ($\boldsymbol{\sigma_G}$) for RSA mechanism. The decays $\mathbf{S_1 \rightarrow S_0}$, $\mathbf{S_1 \rightarrow T_1}$ and $\mathbf{T_1 \rightarrow S_0}$ have rate constant $\mathbf{k_{SG}}$, $\mathbf{k_{ISC}}$ and $\mathbf{k_{TG}}$ respectively [27].

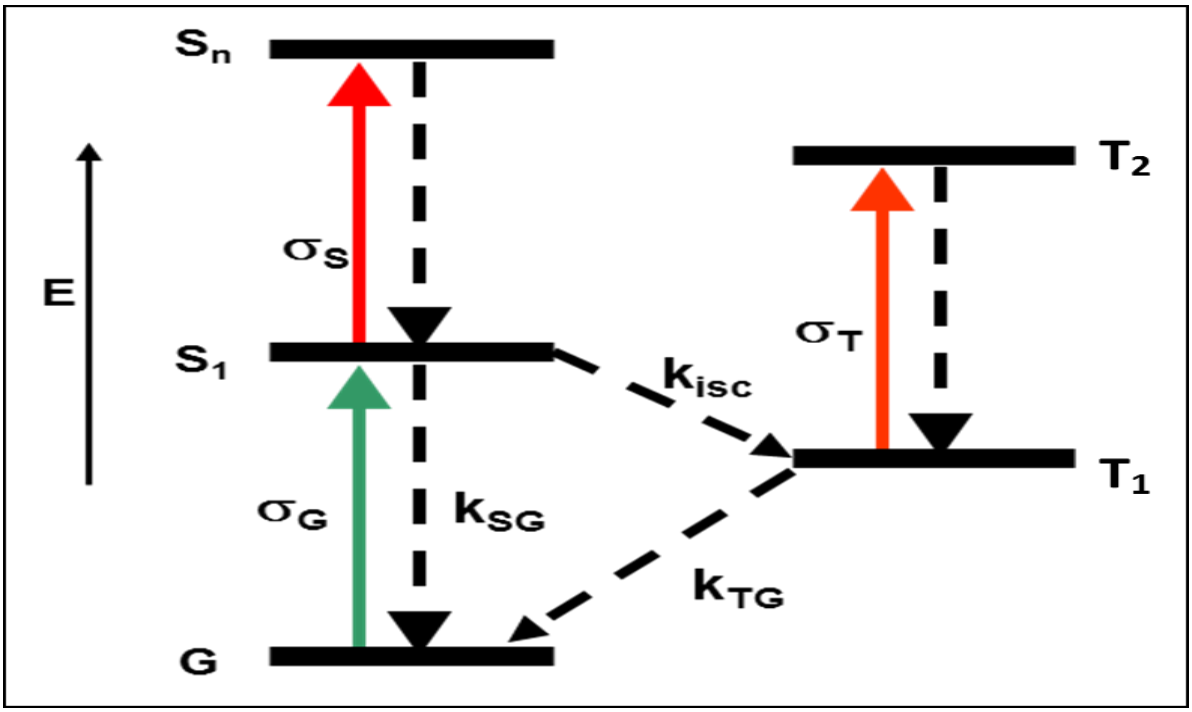

Figure 1.4: Five energy level diagram [27].

Pcs have a network of conjugated 18 π-electrons, which enables them to have high polarizability and fast charge redistribution when they interact with rapidly varying intense electromagnetic fields of laser radiation [28]. Pcs also take up high position as NLO materials due to their high excellent chemical and thermal stability and can easily be prepared [28]. In addition, Pcs have high threshold for damage [30]. Pcs are very good candidate for NLO optics, because they show high second- order nonlinear absorption coefficient (β) over a broad spectra bandwidth, which appears within a nanoseconds response time. Nonlinear absorption coefficient is the nonlinear optical property of the material that changes in the presence of high intensity light [29]. **Table 1.1** gives the summary of some known Pcs and their β values that have been reported in literature for the last 10 years. The β value is obtained by a nonlinear fit of q_0 (z_s), a parameter that

describes the strength of the nonlinearity. Literature reports that the higher the β value, the better the nonlinear optical material [29]. β values can be determined using different methods such as; electric field induced second-harmonic generation (EFISHG) measurements, hyper-Rayleigh light scattering (HRS) measurements and Z-scan measurents. It is reported in literature that analysis of results obtained from these different measurements show consistent results, although results may not be exactly the same [31].

Table 1.1: Summary of some selected known Pcs with their second order β values for the last 10 years.

Compound (Pc)	**β value (x10 $^{-10}$ m/W)**	**Reference**
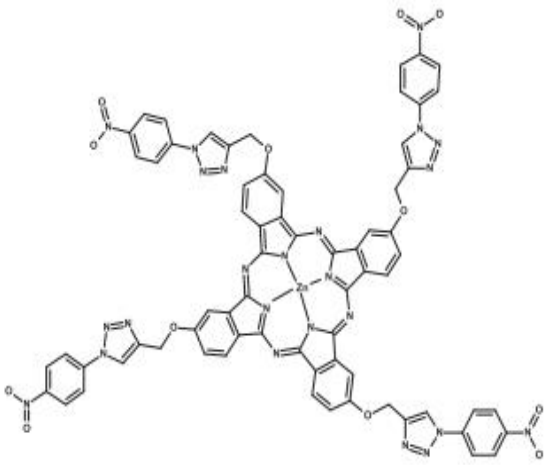	**0.15** Z-scan measurements in DMSO	**[32]**

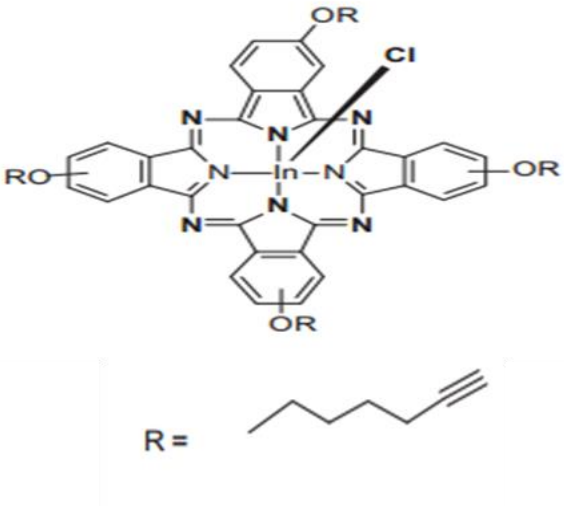	**0.43** Z-scan measurements in DMSO	**[33]**
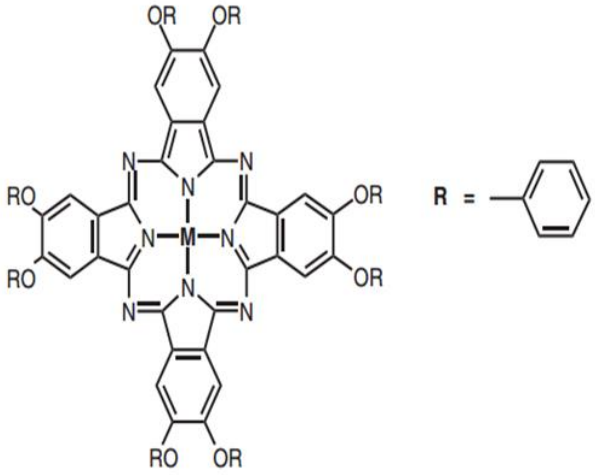	**0.36** Z-scan measurements in DMSO	**[34]**
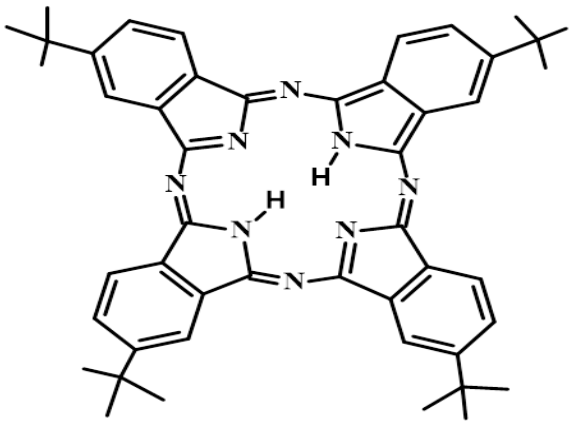	**0.15** Z-scan measurements in Chloroform	**[35]**

2,3,9,10,16,17,23,24-octakis-(heptyloxy) phthalocyanine	**6.00** Z-scan measurements in DMSO	**[36]**
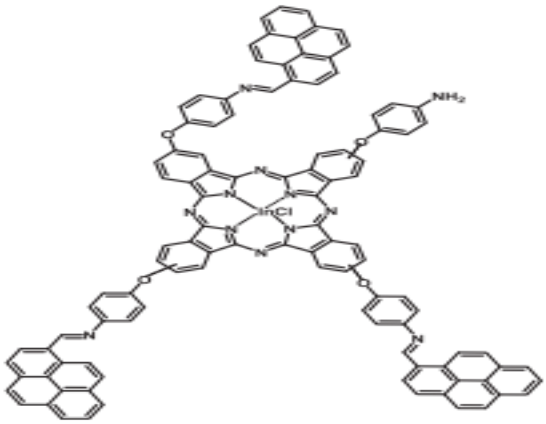	**5.38** Z-scan measurements in DMSO	**[37]**
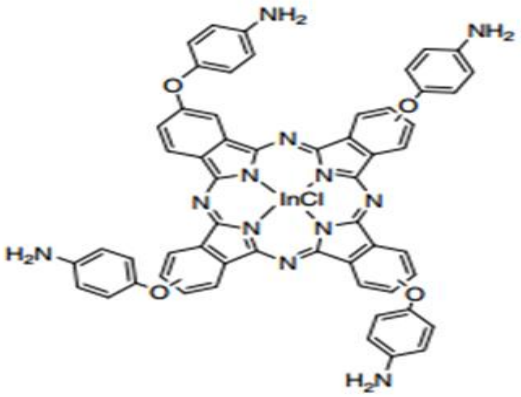	**0.22** Z-scan measurements in DMSO	**[38]**

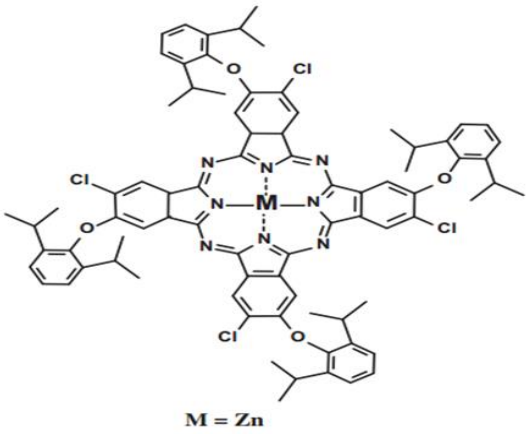	**0.29** Z-scan measurements in Toluene	**[39]**
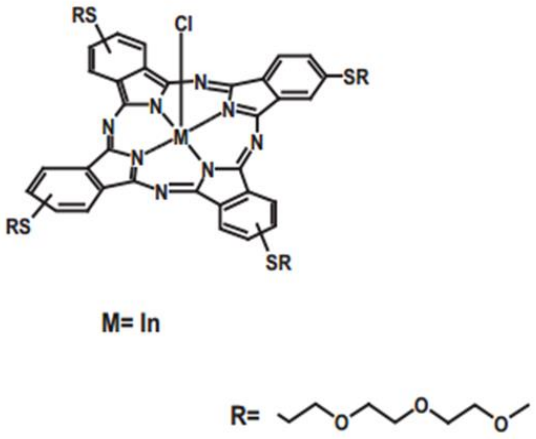	**0.39** Z-scan measurements in Chlororm	**[40]**
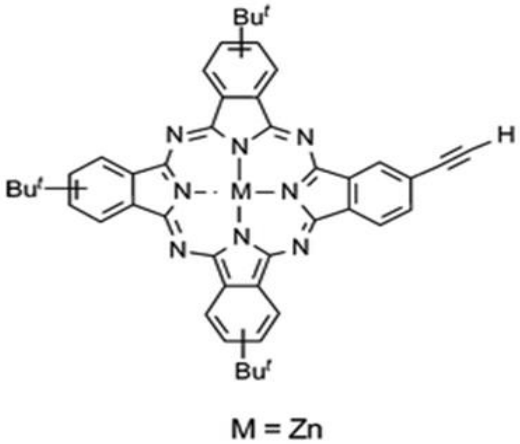	**3.50** Z-scan measurements in Toluene	**[41]**

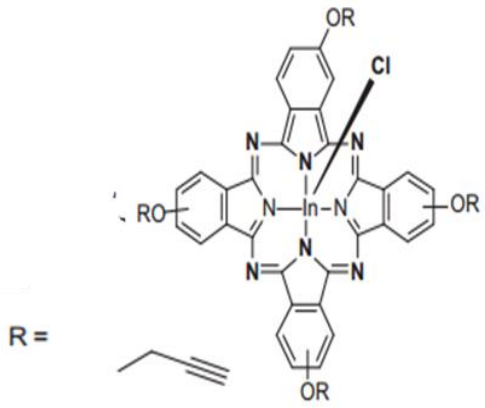	**0.44** Z-scan measurements in DMSO	**[33]**
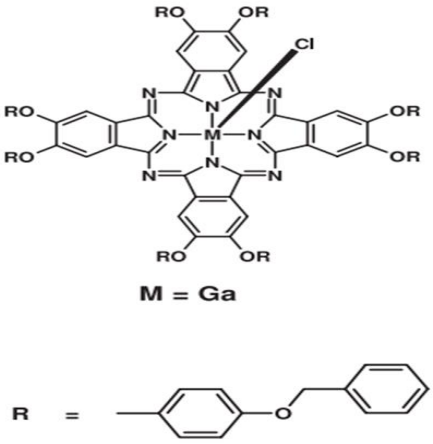	**0.16** Z-scan measurements in Chlororm	**[42]**

Although Pcs have been studied extensively and used as NLO materials due to high second order nonlinear absorption coefficient (β), they possess some barriers that prevent further improvement of nonlinear optical activities, such as aggregation. Aggregation reduces active absorbing excited state and lifetime of the Pcs based material causing a drastic decay in their optical properties such as reduction in second order nonlinear absorption coefficient [12, 39, 40]. There are two types of aggregation, namely; H and J aggregations. With respect to Q band, H aggregation is blue shifted and J aggregation is red shifted [43]. Density functional theory (DFT) calculations

also show that phthalocyanines being dipolar molecules due the presence of dipole moments tend to arrange in antiparallel ways that enables the formation of crystalline larger materials (aggregates), which contributes to the reduction of second order nonlinear activity [44].

Some second order nonlinear optical applications require materials that display high transparency in the red region of their UV-Vis spectra, which cannot be achieved by phthalocyanines due their extended conjugated π-electron system [45].Increased conjugation length causes a loss in optical transparency [46], which reduces the second order β value. Despite phthalocyanines having these barriers, there are various ways that can be done to further improve their NLO activities.

Some of the ways include, firstly, changing the central metal in the cavity of the phthalocyanines ring. Literature reports that Pcs containing heavy metals such as Indium [47] promotes intersystem crossing which results in improved NLO behaviour that is different from a metal-free Pc. In this work, nickel is used. Nickel is used as a central metal because it has good chelating and stability properties and possesses enhanced NLO properties. [48].

Secondly, alteration of peripheral, non-peripheral or axial substituents in Pcs can also modify the molecular structural arrangement and enhance the solubility of Pcs, which has an effect on improving the NLO activity [49, 50]. It is reported that phthalocyanines with substituents at the peripheral positions, provide better NLO activity compared to non-peripheral substitution [51]. Hence, this work looks at peripheral substituted Pcs and introduction of binuclear phthalocyanines (Bi-Pcs) as potential molecules to overcome some the challenges faced by monomeric Pcs.

1.5 Binuclear phthalocyanines

Binuclear phthalocyanines have two phthalocyanines units connecting one another via covalent bonding, **Figure 1.5**. Bi-Pcs are formed by fusing two chromophores directly or linking through different types of conjugated or non-conjugated bridges. These binuclear complexes can exist in various conformations depending upon the nature of the bridging unit, such as co-facial, planar and clamshell [52]. Bi-Pcs that are covalently linked with highly conjugated species have received attention in the recent past [53, 54]. The presence of highly conjugated species enables Bi-Pcs to have a lot of applications, hence the attention.

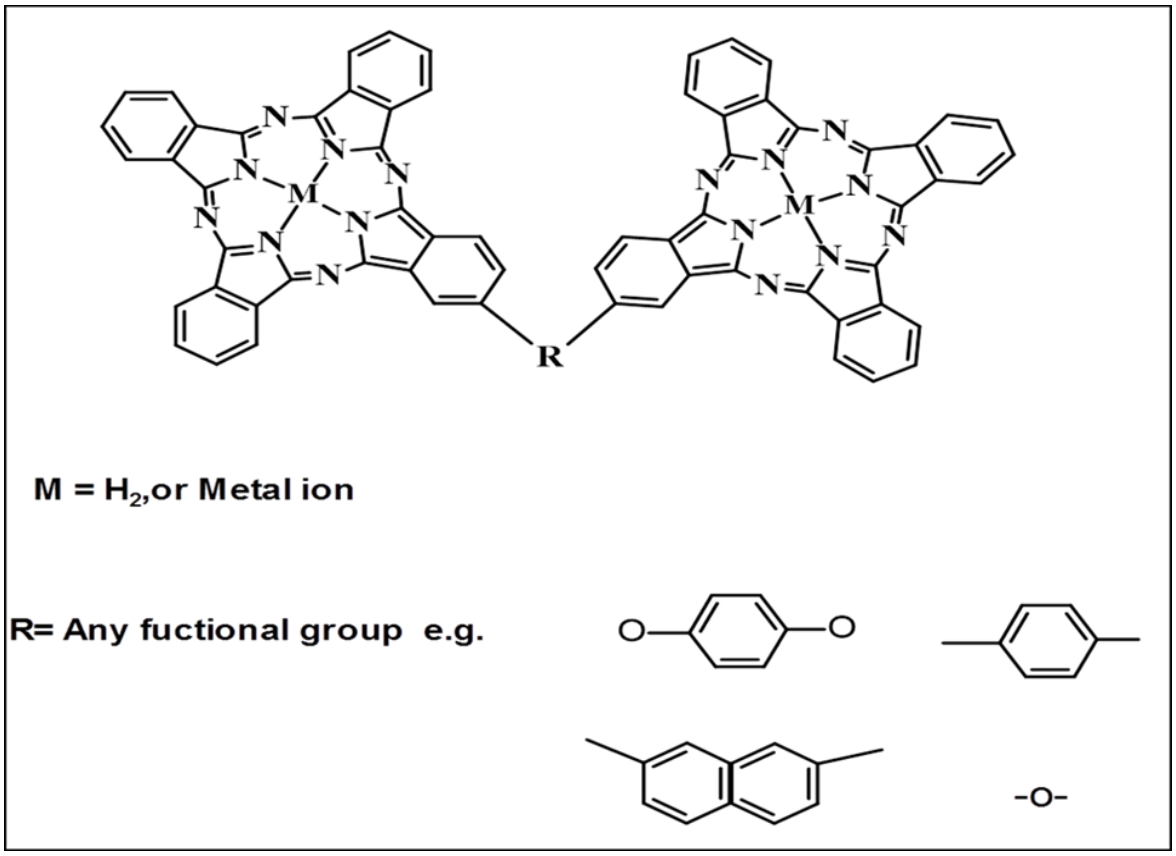

Figure 1.5: General structure of binuclear phthalocyanine

The two linked Bi-Pcs nuclei couple between electronic states, which lead to important variation in the absorption spectra of the molecules. These make Bi-Pcs play significant roles as serious building blocks with high excitonic properties for the construction of multicomponent photo which brings about electron transfer supramolecular systems [53]. Excellent chemical, thermal stability, bright colour and conductivity have made Bi-Pcs very desirable for many applications, such as in electrochemical sensor, single molecular magnets, organic light-emitting diode [52]. Spectroscopic properties of Bi-Pcs are similar to that of monomeric Pcs because the Pc units are covalently linked through a bridge

1.5.1 Binuclear phthalocyanine synthesis

Bi-Pcs have been synthesised in order to look for excitonic or electronic interactions within the rings of the molecules so as to change the electrical and optical behaviour of the binuclear systems more than mononuclear parent compounds. **Table 1.2,** gives some examples Bi-Pcs and their second order β values that have been reported in literature for the last fifteen years

The synthesis of Bi-Pc is usually carried out by statistical condensation reaction. In this reaction, dicyano substituted intermediate reacts with a large excess selected phthalonitrile. Unfortunately, this reaction produces more monomeric phthalocyanines than binuclear phthalocyanine. **Scheme 1.3,** shows an example of a typical statistical condensation reaction. In statistical condensation reaction, two different phthalonitriles or diiminoisoindolines are used as starting materials for the synthesis of Bi-Pcs and other condensation products [55]. The use of diiminoisoindoline is the preferred method when the reactivity of the phthalonitrile is very low, because diiminoisoindoline is more reactivity than phthalonitrile. Phthalonitrile is a precursor for diiminoisoindoline. Diiminoisoindoline is prepared by refluxing phthalonitrile in methanol in the presence of ammonia gas and sodium metal as a catalyst [56].

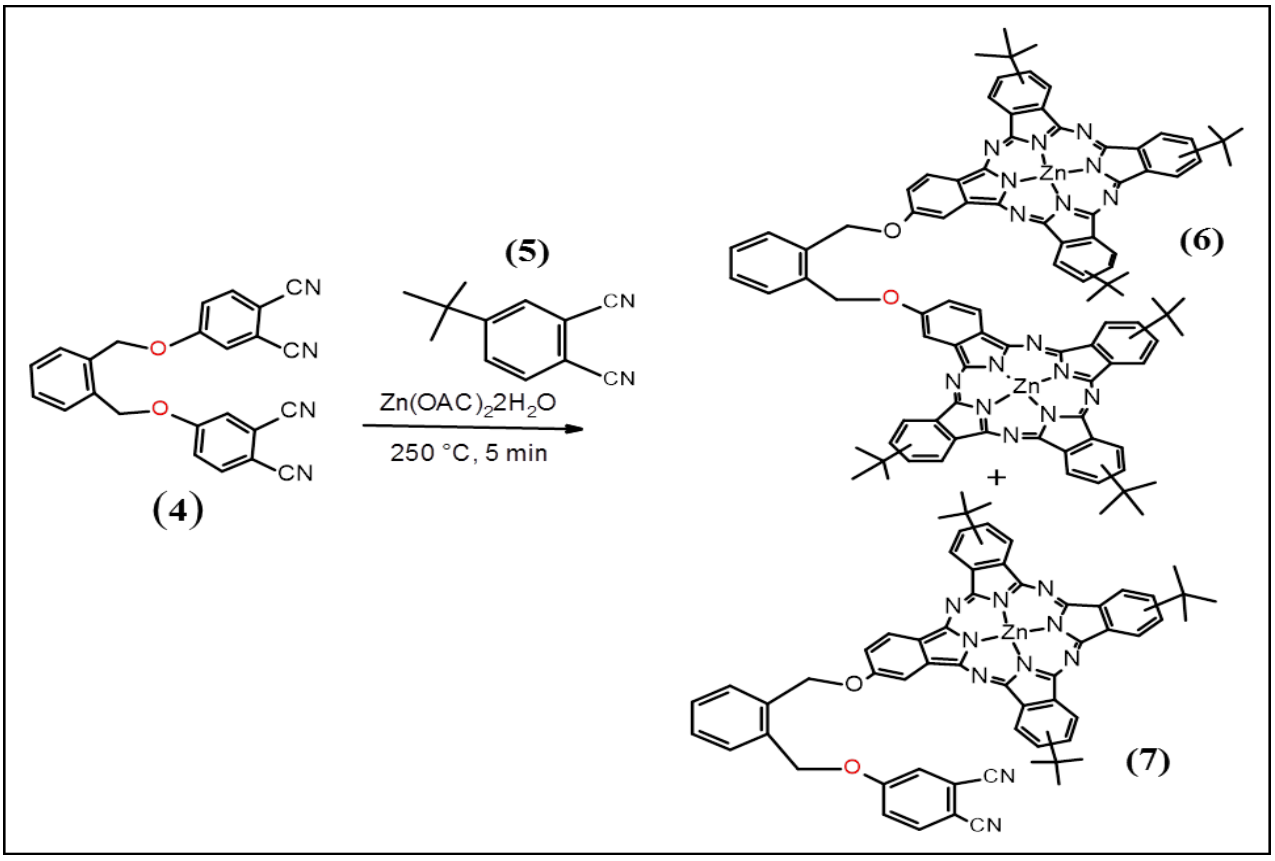

Scheme 1.3: Example of a condensation reaction used to synthesise binuclear phthalocyanine [55].

1.5.2 Second-order NLO Activity in Binuclear Pthalocyaniness

Second-order nonlinear optical properties have been mainly studied on monomeric Pcs, and few studies have been conducted on Bi-Pcs. Hence, this work focuses on the second order hyperpolarizability (β) of Bi-Pcs, in order to further contribute to the study of the material with NLO properties. Bi-Pcs are non-centrosymmetric and therefore expected to show an enhanced second β term, which in turn has a direct impact on the macroscopic second order NLO response. Bi-Pcs have the potential to transform D_{2h} symmetry Pc unit to a D_2 or D_{2d} symmetry. This can be achieved by changing the angles corresponding to the torsional relationship between the Pc

unit and the linker least square plane [57], **Figure 1.6**. Almost all known NLO octupolars have either a D_{3h} or T_d symmetry. The D_2 and D_{2d} symmetry could be exploited in the design of octupolar compounds. Timothy et al has shown that a strongly coupled D_2 symmetry oscillator can provide an important design for NLO chromospheres with enhanced NLO properties [57]. **Figure 1.6** shows that torsional angle of $\theta = -\phi < 45^{\circ}$ correspond to D_2 symmetry with Hyper-Rayleigh Scattering (HRS) active, $\theta = -\phi = 45^{\circ}$ correspond to D_{2d} symmetry, with maximum HRS active and $\theta = -\phi = 0^{\circ}$ correspond to D_{2h} symmetry with HRS silent. In general, Multinuclear Pcs have shown potential of improving β values [58-62].

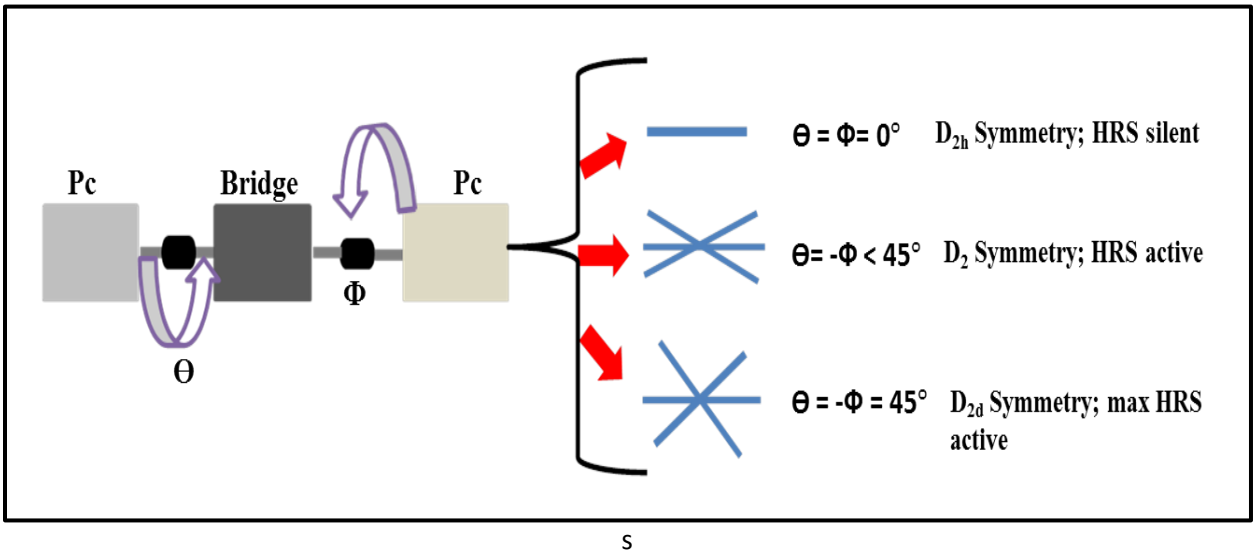

s

Figure 1.6: Formation of D_{2h}, D_2 and D_{2d} symmetry [57]

Low symmetry Pcs are known to possess variable degrees of dipolarity and octupolarity ratio [63], which contribute to the measured second order β values.

Molecules which are more octupolar are known to show great potential as novel second-order NLO material, due to their diverse and complex charge distribution [63, 64]. Compared to their dipolar counterparts, octupolar molecules possess favourable characteristics such as insensitivity

to polarization, increased transparency and absence of dipole moment. However, Bi-Pcs are known to form strong H-aggregation in solution [65, 66], which in turn could contribute to the reduction of β values [67].

Although, synthesis of Bi-Pcs has been reported, less work has been done on the application of Bi-Pcs as second order nonlinear optical material, through the determination of second order nonlinear absorption coefficient (β) as indicated in the **Table 1.2.**Therefor, much work needs to be done in this area.

Table 1.2: Selected reported Bi-Pcs and their second order β values for the last fifteen years

Binuclear Pc	**β value (x10^{-10} m/W)**	**References**
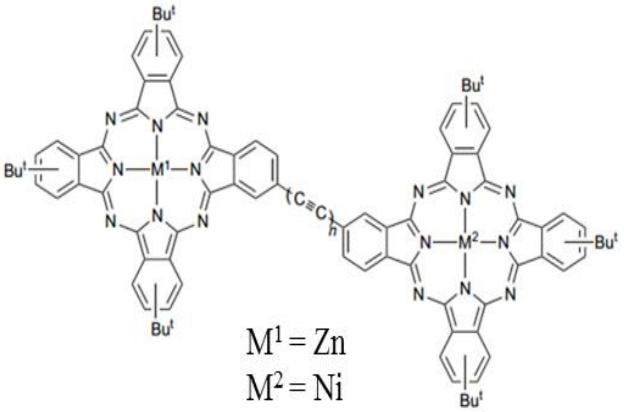	**3.50** Z-scan measurements in Toluene	[40]

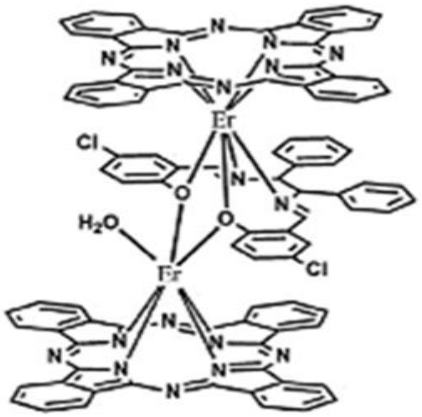	**2.50** Z-scan measurements in DC	[68]

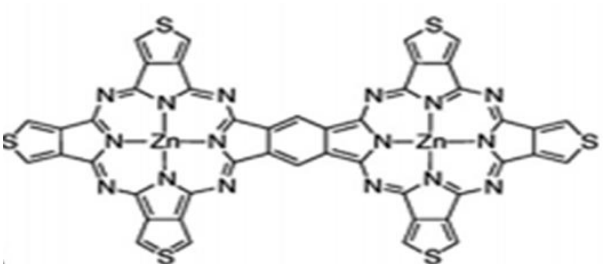	-	**[69]**
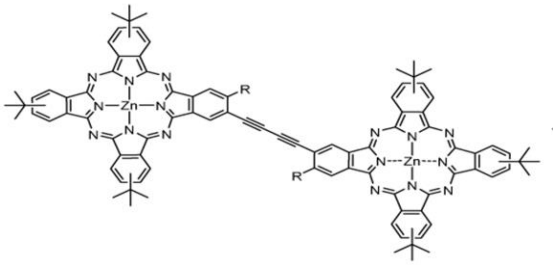	-	**[70]**
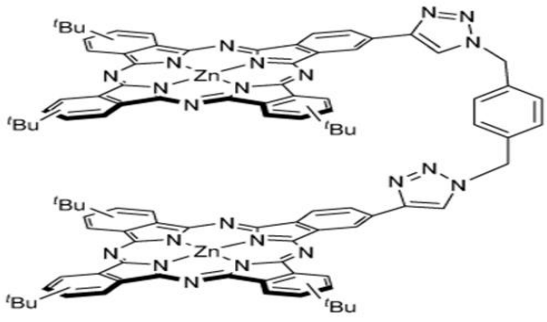	-	**[71]**

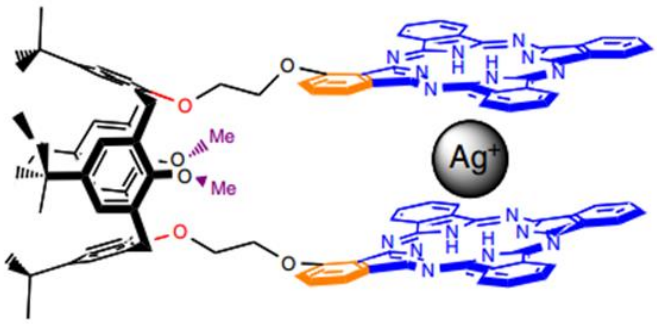	-	[72]
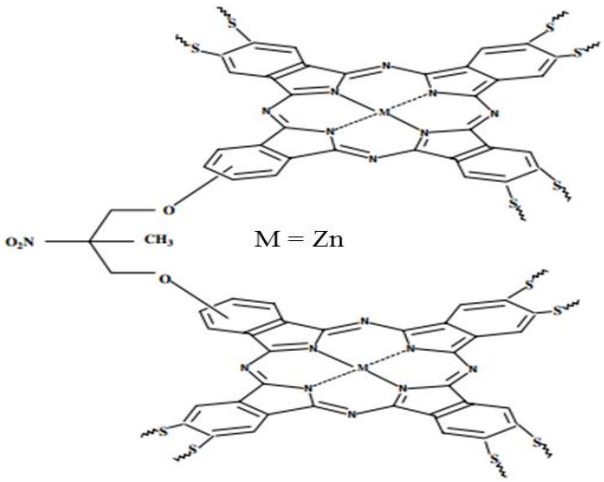	-	[73]
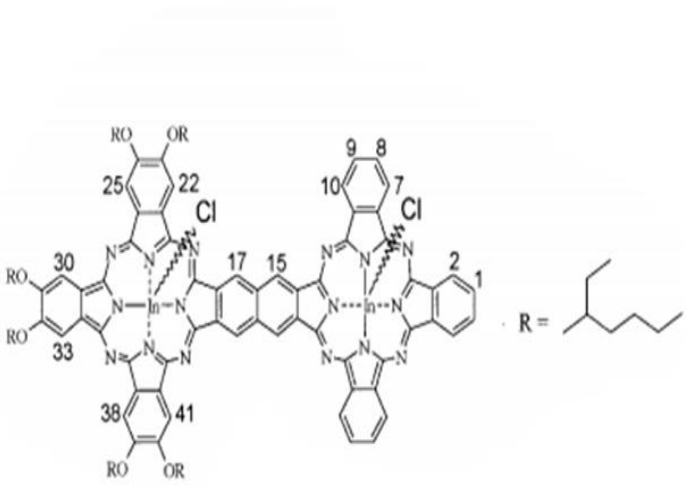	-	[74]

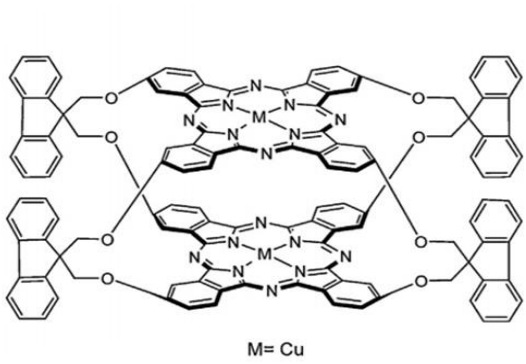	-	**[75]**
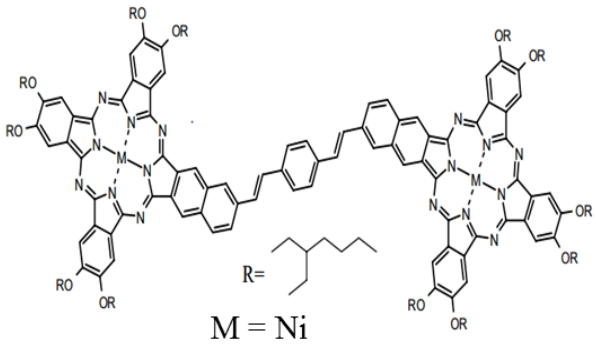	-	**[76]**

1.6 Spectroscopic characterization

This section discusses briefly some of the spectroscopic techniques used in this thesis.

1.6.1 Magnetic Circular Dichroism (MCD)

Magnetic Circular Dichroism spectroscopy is an extremely powerful technique used to investigate the electronic structures and spectra of paramagnetic transition metal complexes. This technique has clear advantage compared to UV-Vis absorption spectroscopy because of better

resolution of electronic transitions. The polarizations of the electronic transitions are accessible by MCD in samples of randomly oriented molecules [**77**]. MCD spectroscopy provides the ground and excited state degeneracy information required to fully understand the electronic structure of the high symmetry complexes of heteroaromatic π-systems such phthalocyanines on the basis of the orbital angular momentum properties of the frontier π-molecular orbitals (MOs). The additional information provided by the MCD technique is derived from the three highly characteristic spectra features, the Faraday $\boldsymbol{A_1}$, $\boldsymbol{B_0}$ and $\boldsymbol{C_0}$ terms based, on the Zeeman splitting of the absorption bands for left circular polarized (lcp) and right circular polarized (rcp) light, the field induced mixing of the zero-field states and the Zeeman splitting based ground state population adjustment [**78**]. The A_1term, **Figure 1.7:** arises from the Zeeman splitting of an orbitally degenerate excited state. There is a highly distinctive first derivative band shape due to the separation of the band centres for the absorption of lcp and rcp light. [79].

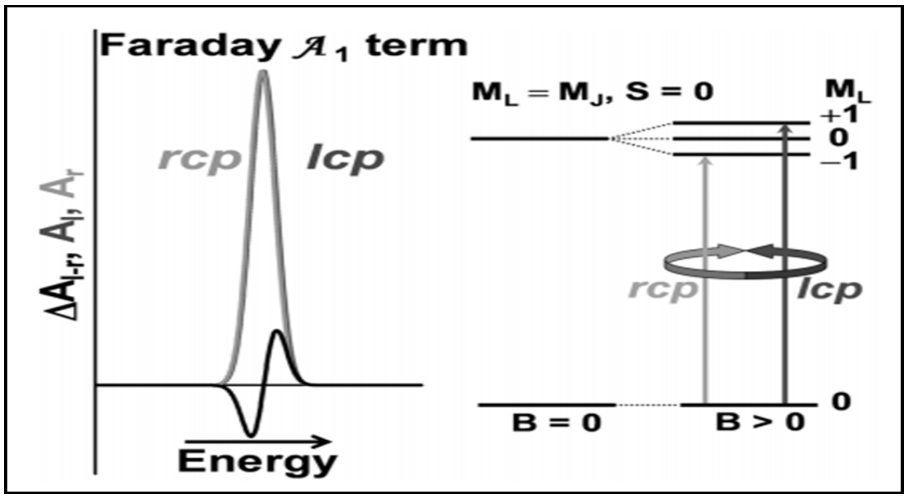

Figure 1.7: Faraday A_1 terms [79].

The $\boldsymbol{B_0}$ term arises from second order effects based on the field induced mixing of the zero field states. $\boldsymbol{B_0}$ terms completely dominate the MDC spectrum when there is no three-fold or higher

rotation axis, since there are no orbitally degenerate states that can be split due to the Zeeman effect [78, 79].

When a structural modification results in a small zero–field splitting, relative to the spectral band width of what would otherwise be an orbitally degenerate π-π* excited state, the resulting derivative-shaped signal is often referred to as a pseudo-$\boldsymbol{A_1}$ term**, Figure 1.8, [79],** since there is a dependence on the energy separation of states J and K (ΔE_{KJ}) mixed by the field.

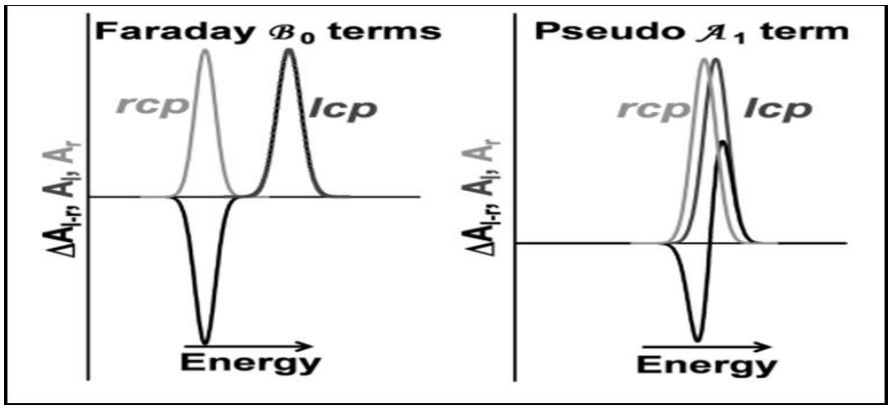

Figure 1.8: Faraday B_0 terms [79].

The $\boldsymbol{B_0}$ terms can be readily distinguished from $\boldsymbol{C_0}$ terms by measuring spectra at both room and cryogenic temperatures since they lack 1/kT temperature dependence, [78, 79].

An MCD band shape which peaks nearly at the absorption maximum and whose magnitude is temperature-dependent is generally called a faraday $\boldsymbol{C_0}$ term, and its sign and magnitude are related to the sign and magnitude of splitting of the ground state, **Figure 1.9**, [78].

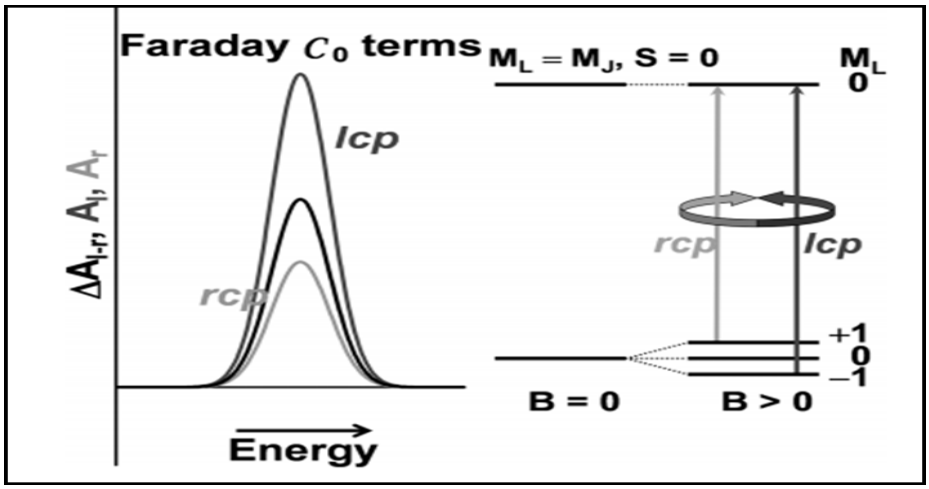

Figure 1.9: Faraday C_0 terms [79**].**

Thus a non-zero C_0 term requires the presence of a degenerate ground state and a non-zero A_1 term requires either a degenerate ground state or excited state. Mathematical expressions for the Faraday A_1, B_0 and C_0 terms are reported in literature [78-80] and not repeated here.

As mentioned before, the spectra of phthalocyanines consist generally of two regions. The one in the **600-750** nm region is the called the Q band and the other in the **300-450** nm is called the **B** band (soret).In case of metalated phthalocyanines (MPcs) with D_{4h} symmetry, the intense **Q** band is related to a single transition from the non-degenerate ground state to a doubly degenerate excited state, while the B band contains a set of transitions of less intensity. The **B** band of the MPcs includes at least one transition from the non-degenerate ground state to a doubly – degenerate excited state. Thus, MPcs show Faraday A_1 terms at both the **B** and **Q** bands. In contrast, metal-free Pcs exhibit only Faraday B_0 terms through all regions since there is no degeneracy at either ground or excited states. MDC curves can have both plus and minus signs, [79, 80], **Figure 1.10.**

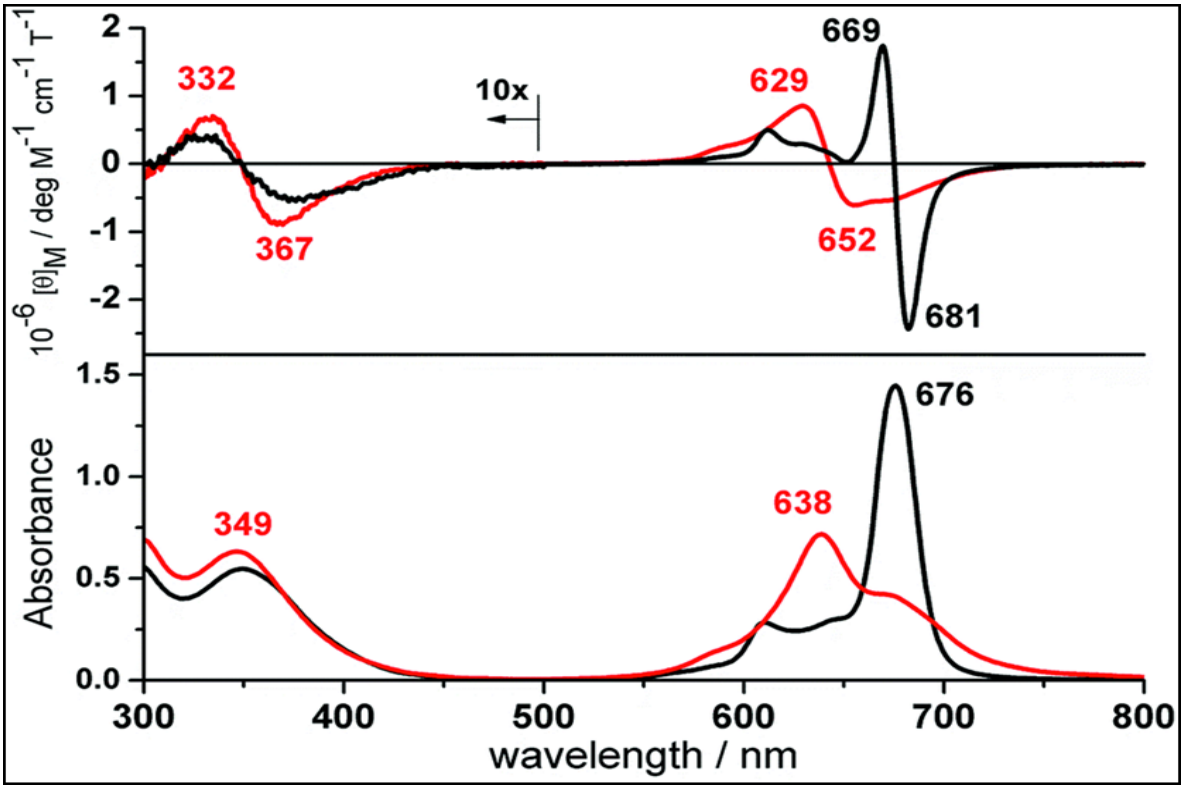

Figure 1.10: Absorption (bottom) and MCD (top) of MPc (black) and MBi-Pc (red) in Toluene [81].

1.7 Time-correlated single photon counting (TCSPC) technique

Time-Correlated Single Photon Counting (TCSPC) is based on the detection of single photons of a periodical light signal, the measurement of the detection times of the individual photons within the signal period, and the reconstruction of the waveform from the individual time measurements. The TCSPC technique makes use of the fact that for low level, high repetition rate signals the light intensity is usually so low that the probability to detect one photon in one signal period is much less than one. Therefore, the detection of several photons per signal period can be neglected [82].The TCSPC measurements relies on the concept that the probability distribution for emission of a single photon after an excitation yields the actual intensity against

time distribution of all the photons emitted as a result of the excitation[82]. TCSPC measures fluorescence emission, excitation, lifetimes and rotational correlation time (anisotropy).

The time it takes for any molecule to rotate one radian is referred to as rotational correlation time [82,83]. Rotational correlations time depends on the particle size of the molecule and the viscosity of solvent. Less work in literature has been reported on determining the rotational correlation time of Pcs. Therefore, in this work, rotational correlation time of β tetra substituted Pcs and Bi-Pcs are measured.

1.8 Z-scan technique

Figure 1.11, depicts the schematic of the experiment set up for the Z-scan measurements. The Z-scan works on the principle of moving the sample under investigation through the focus of a tightly focussed Gaussian laser beam. The interaction of the medium with the laser light changes as the sample is moved. This is because the sample experiences different intensities, dependent on the sample position (Z) relative to the focus [82].

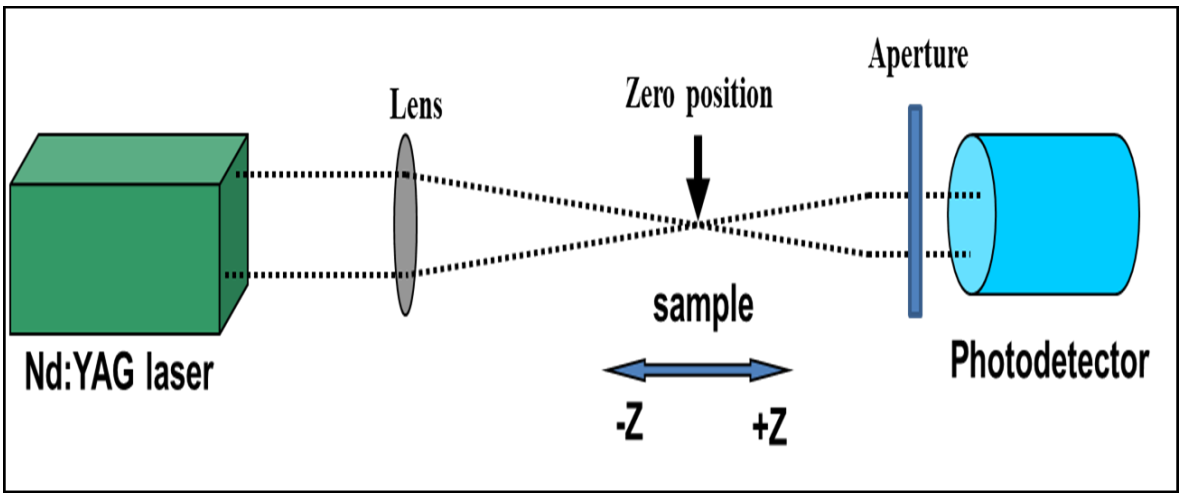

Figure 1.11: Z-scan measurement set up.

Information about the light-matter interaction can be extracted by measuring the transmittance through the sample as a function of Z-position of the sample. The two nonlinear interactions that can be determined in this fashion are the sample's nonlinear index of retraction and nonlinear absorption coefficient [29, 82,84]. Determination of nonlinear absorption coefficient measurements is done by the removal of the aperture thus making the scan insensitive to nonlinear refraction. Nonlinear index of refraction is measured by placing the aperture in front of the detector measuring the transmitted light. This makes the measurements sensitive to beam spreading or focusing and relates to a transformation of phase distortion into amplitude distortion. Sample displaying nonlinear refraction will act as a lens of variable focal length as it is moved along the z-axis [81, 84].

1.8.1 Theory behind Z-scan measurements

Second order NLO parameter (β) was determined experimentally by measuring the normalised transmittance from an open aperture Z-scan experiment. The normalised transmittance is given by **Equation 1** [85, 86]:

$$T_n(z_s) = \frac{1}{Aq_0(Z_s)} \int_{-\infty}^{+\infty} \ln[1 + q_0(z_s) f(\tau)] d\tau \quad (1)$$

where $f(\tau)$ is a function of time describing the temporal profile of the pulse for Gaussian pulses and has the form $f(\tau) = e^{(-\tau^2)}$. A is a normalization constant equal to $\int_{-\infty}^{+\infty} f(\tau) d\tau$ and $q_0(z_s)$ is a parameter characterizing the strength of the nonlinearity. When using circular Gaussian beam q_0 is represented by **Equation 2** [87, 88]:

$$q_0(z_s) = \frac{2\beta P_0 L_{eff}}{\pi w^2(z_s)} \quad (2)$$

where β is the nonlinear absorption coefficient of the material, P_0 is the peak power of the pulses and the L_{eff} is the effective propagation length in the material, given by the relation

$$L_{eff} = \frac{1-e^{-(\alpha L)}}{\alpha} \quad (3)$$

where L is the sample length (or the thickness of the sample respectively) and α is the linear absorption coefficient. α can be determined using **Equation 4:**

$$\alpha = \frac{hv}{N}\beta \quad (4)$$

where N corresponds the number of active species per unit volume, h is Planck's constant and v is the frequency of a laser excitation. The parameter $w(z_s)$ (in **Equation 2**) is the beam width at the sample plane defined as the distance from the beam centre to the point where the intensity reduces to $1/e^2$of its axis value. $w(z_s)$ is defined by **Equation 5** [85]:

$$w(z_s) = w_0\sqrt{1 + \left(\frac{z_s - z_0}{z_R}\right)^2} \quad (5)$$

where w_0 is the beam width at the focus and $z_0$is the location of the beam focus. The parameter z_R is the Rayleigh length, defined by **Equation 6**:

$$z_R = \frac{\pi w_0^2}{\lambda} \quad (6)$$

where λ is the bean wavelength. **Equations (1)-(6)** are used to determine the nonlinear absorption coefficient (β) from experimentally measured transmittance. Tsigaridas et al. [85] have produced an analytical formula given by **Equation 7:**

$$q_0(z_s) = \begin{cases} a_0 + a_1 T_n(z_s) + a_2 T_n^2(z_s) + a_3 T_n^3(z_s) \ \ for \ \ T_n(z_s) \leq 0.75 \\ \\ c_0 + c_1 [T_n(z_s)]^{c_2} \ for \ T_n(z_s) \geq 0.75 \end{cases} \quad (7)$$

where, the coefficients $a_0, a_1, a_2, a_3, c_0, c_1, c_2$ for Gaussian pulses are given as 15.66, -37.45, 30.76, -8.97, -2.301, 2.156, -1.563 respectively [85]. **Equation7** provides values of $q_0(z_s)$ directly from the normalized transmittance $T_n(z_s)$. Tsigaridas again demonstrated that the technique allows straight forward determination of β and is very robust to noise [85]. Absorption coefficient (β), as well as the beam parameters z_0 and Z_R can be determined from $q_0(z_s)$ values obtained from **Equation (7)**. Substituting **Equation 5** into **Equation 2** $q_0\,(z_s)$ is then defined by **Equation 8**:

$$q_0(z_s) = \frac{Q_0}{1+(z_s - z_0)^2 / z_R^2} \quad (8)$$

Where

$$Q_0 = \frac{2\beta P_0 L_{eff}}{\pi w_0^2} = \frac{2\beta P_0 L_{eff}}{\lambda z_R} \quad (9)$$

Equation 7 gives a Gaussian plot with Q_0 as the maximum value at the beam waist ($z_s = z_0$). The full width at half maximum (FWHM) of the $q_0(z_s)$ is equal to $2z_R$. The peak value and the FWHM of the plot gives values of Q_0 andz_R. **Equation 10** is then used to calculate the nonlinear absorption coefficient (β).

$$\beta = \frac{\lambda z_R Q_0}{2 P_0 L_{eff}} \quad (10)$$

1.9 Density Functional Theory

Density functional theory (DFT) is a modelling tool used in computational physics, computational chemistry and materials sciences. This computational method is used to obtain general properties of the compound due to the presence of the electron density within the molecule. DFT theory puts more emphasis on one electron density function than the wave function. DFT could be used to investigate the electronic molecular structure of atoms and molecules [89]. In the recent past, understanding of chemical structure and the natural of the chemical reaction of different molecules based on the calculations of the electronic structure has gained a lot of interest by different researchers. The interest arose as a result of the fact that, DFT calculations can be done correctly while maintaining the time of calculating.

1.9.1 DFT calculations for NLO properties.

DFT calculation of hyper-Rayleigh Scattering (HRS) response coefficient (β_{HRS}) is done in order to calculate the first static hyperpolarizability [20, 90,91 92]. As mentioned earlier, HRS β values when compared with Z-scan β values show consistence results (same trend). Therefore, theoretical HRS β values from DFT calculations are compared with experimentally determined β values from Z-scan measurements. The advantage of DFT calculation method is that octupolar and dipolar second order NLO contributions are theoretically separated compared to other methods [93]. The values of both dipolar ($\beta_{J=1}$) and octupolar ($\beta_{J=3}$) are known to be significantly influenced by the number of electrons in the system [20]. Due to symmetry constraints there is no permanent dipole moment for octupolar molecules [91], hence octupolar molecules present an isotropic β tensor.

It is to be noted that the equations presented below are only valid in the off-resonance region [94].The following equations were used to calculate the β_{HRS} response. In **Equation 11**, $\langle\beta_{ZZZ}^2\rangle$ and $\langle\beta_{ZXX}^2\rangle$ are the orientation average of the molecular β tensor components.

$$\beta_{HRS}(-2\omega;\omega,\omega) = (\langle\beta_{ZZZ}^2\rangle + (\langle\beta_{ZXX}^2\rangle)^{1/2} \quad \textbf{(}11\textbf{)}$$

The molecular β tensor was calculated using **Equations 12** and **13** [95]:

$$\langle\beta_{ZZZ}^2\rangle = \frac{1}{7}\sum_{\zeta}^{x,y,z}\beta_{\zeta\zeta\zeta}^2 + \frac{6}{35}\sum_{\zeta\neq\eta}^{x,y,z}\beta_{\zeta\zeta\zeta}\,\beta_{\zeta\eta\eta} + \frac{9}{35}\sum_{\zeta\neq\eta}^{x,y,z}\beta_{\eta\zeta\zeta}^2 + \frac{3}{35}\sum_{\zeta\neq\eta\neq\xi}^{x,y,z}\beta_{\eta\zeta\zeta}\,\beta_{\eta\xi\xi} + \frac{2}{3}\sum_{\zeta\neq\eta\neq\xi}^{x,y,z}\beta_{\zeta\eta\xi}^2 \quad (12)$$

$$\langle\beta_{ZXX}^2\rangle = \frac{1}{35}\sum_{\zeta}^{x,y,z}\beta_{\zeta\zeta\zeta}^2 - \frac{2}{105}\sum_{\zeta\neq\eta}^{x,y,z}\beta_{\zeta\zeta\zeta}\,\beta_{\zeta\eta\eta} + \frac{11}{105}\sum_{\zeta\neq\eta}^{x,y,z}\beta_{\eta\zeta\zeta}^2 - \frac{1}{105}\sum_{\zeta\neq\eta\neq\xi}^{x,y,z}\beta_{\eta\zeta\zeta}\,\beta_{\eta\xi\xi} + \frac{4}{105}\sum_{\zeta\neq\eta\neq\xi}^{x,y,z}\beta_{\zeta\eta\xi}^2 \quad (\textbf{13})$$

In addition, the molecular geometric information is given by the depolarization ratio (DR), which is expressed by $DR = \langle\beta_{ZZZ}^2\rangle/\langle\beta_{ZXX}^2\rangle$. The nature of the symmetric Rank-3 β tensor is further clarified by decomposing $\langle\beta_{HRS}^2\rangle$ as the sum of the dipolar ($\beta_{J=1}$) and octupolar ($\beta_{J=3}$) tensorial components [91], which are expressed as **Equation 14 to 16**:

$$\beta_{HRS} = \sqrt{(\beta_{HRS}^2)} = \sqrt{\frac{10}{45}\left|\beta_{J=1}\right|^2 + \frac{10}{105}\left|\beta_{J=3}\right|^2} \quad \textbf{(14)}$$

$$\left|\beta_{J=1}\right|^2 = \frac{3}{5}\sum_{\zeta}^{x,y,z}\beta_{\zeta\zeta\zeta}^2 + \frac{6}{5}\sum_{\zeta\neq\eta}^{x,y,z}\beta_{\zeta\zeta\zeta}\,\beta_{\zeta\eta\eta} + \frac{3}{5}\sum_{\zeta\neq\eta}^{x,y,z}\beta_{\eta\zeta\zeta}^2 + \frac{3}{5}\sum_{\zeta\neq\eta\neq\xi}^{x,y,z}\beta_{\eta\zeta\zeta}\,\beta_{\eta\xi\xi} \quad \textbf{(15)}$$

$$\left|\beta_{J=3}\right|^2 = \frac{2}{5}\sum_{\zeta}^{x,y,z}\beta_{\zeta\zeta\zeta}^2 - \frac{6}{5}\sum_{\zeta\neq\eta}^{x,y,z}\beta_{\zeta\zeta\zeta}\,\beta_{\zeta\eta\eta} + \frac{12}{5}\sum_{\zeta\neq\eta}^{x,y,z}\beta_{\eta\zeta\zeta}^2 - \frac{3}{5}\sum_{\zeta\neq\eta\neq\xi}^{x,y,z}\beta_{\eta\zeta\zeta}\,\beta_{\eta\xi\xi} \quad \textbf{(16)}$$

$$+ \sum_{\zeta\neq\eta\neq\xi}^{x,y,z}\beta_{\zeta\eta\xi}^2$$

The ratio of octupolar $\left[\Phi_{J=3} = \rho/(1+\rho)\right]$ and dipolar $\left[\Phi_{J=1} = 1/(1+\rho)\right]$ contribution to the hyperpolarizability tensor is determined by substituting the nonlinear anisotropy parameter $\rho = \left|\beta_{J=3}\right|/\left|\beta_{J=1}\right|$ [91]. The nonlinear anisotropy parameter values run from 0 (pure dipole) to ∞ (pure octupole).

The theoretical normalized HRS intensity ($I_{\Psi V}^{2\omega}$) is determined by using Bersohn's expression [91], **Equation 17**, which assumes a general elliptically polarised incident light propagating along the X direction, see **Figure1.12** as an example, reported in literature [64].

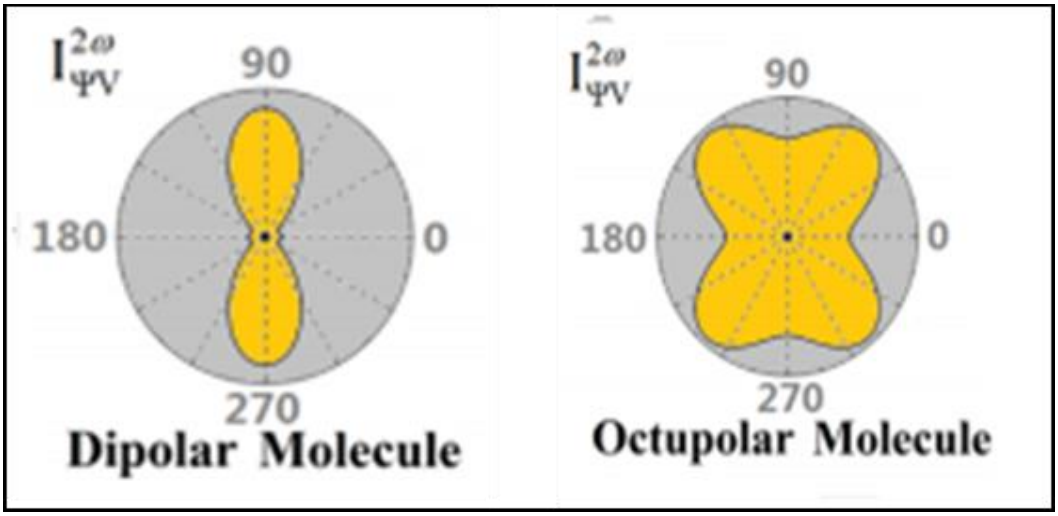

Figure 1.12: Dipolar and Octupolar plots [64]

Equation 17 further assumes that the intensity of the harmonic light is scattered at 90° along the Y direction and the vertically (V) polarised light along the Z axis [91].

$$I_{\Psi V}^{2\omega} \propto \langle \beta_{ZXX}^2 \rangle cos^4\Psi + \langle \beta_{ZZZ}^2 \rangle sin^4\Psi + sin^2\Psi cos^2\Psi \times \langle (\beta_{ZXZ} + \beta_{ZZX})^2 - 2\beta_{ZZZ}\beta_{ZXX} \rangle \qquad \textbf{(17)}$$

The orientational averages $\langle (\beta_{ZXZ} + \beta_{ZZX})^2 - 2\beta_{ZZZ}\beta_{ZXX} \rangle$ in **Equation 17** is expressed as **Equation 18**:

$$\langle (\beta_{ZXZ} + \beta_{ZZX})^2 - 2\beta_{ZZZ}\beta_{ZXX} \rangle = 7\langle \beta_{ZXX}^2 \rangle - \langle \beta_{ZZZ}^2 \rangle$$

$$= \frac{2}{35}\sum_{\zeta}^{x,y,z} \beta_{\zeta\zeta\zeta}^2 - \frac{32}{105}\sum_{\zeta\neq\eta}^{x,y,z} \beta_{\zeta\zeta\zeta}\,\beta_{\zeta\eta\eta} + \frac{10}{21}\sum_{\zeta\neq\eta}^{x,y,z} \beta_{\eta\zeta\zeta}^2 \qquad \textbf{(18)}$$

$$-\frac{16}{105}\sum_{\zeta\neq\eta\neq\xi}^{x,y,z} \beta_{\eta\zeta\zeta}\,\beta_{\eta\xi\xi} + \frac{22}{105}\sum_{\zeta\neq\eta\neq\xi}^{x,y,z} \beta_{\zeta\eta\xi}^2$$

1.10 Summary of thesis Aims

The aims of this thesis are:

(1) To synthesise metal-free and nickel monomeric 4-(4-*t*ert-butyphenoxy) phthalocyanines, biphenyl bridged binuclear 4-tert-butyphenoxy phthalocyanines and naphthalene bridged binuclear 4-tert-butyphenoxy phthalocyanines, **Figure 1.12 (19-21)**. These complex molecules will be characterised by mass spectroscopy (MS), UV-Vis spectroscopy, Infrared (IR) spectroscopy and Magnetic circular dichroism (MDC) spectroscopy.

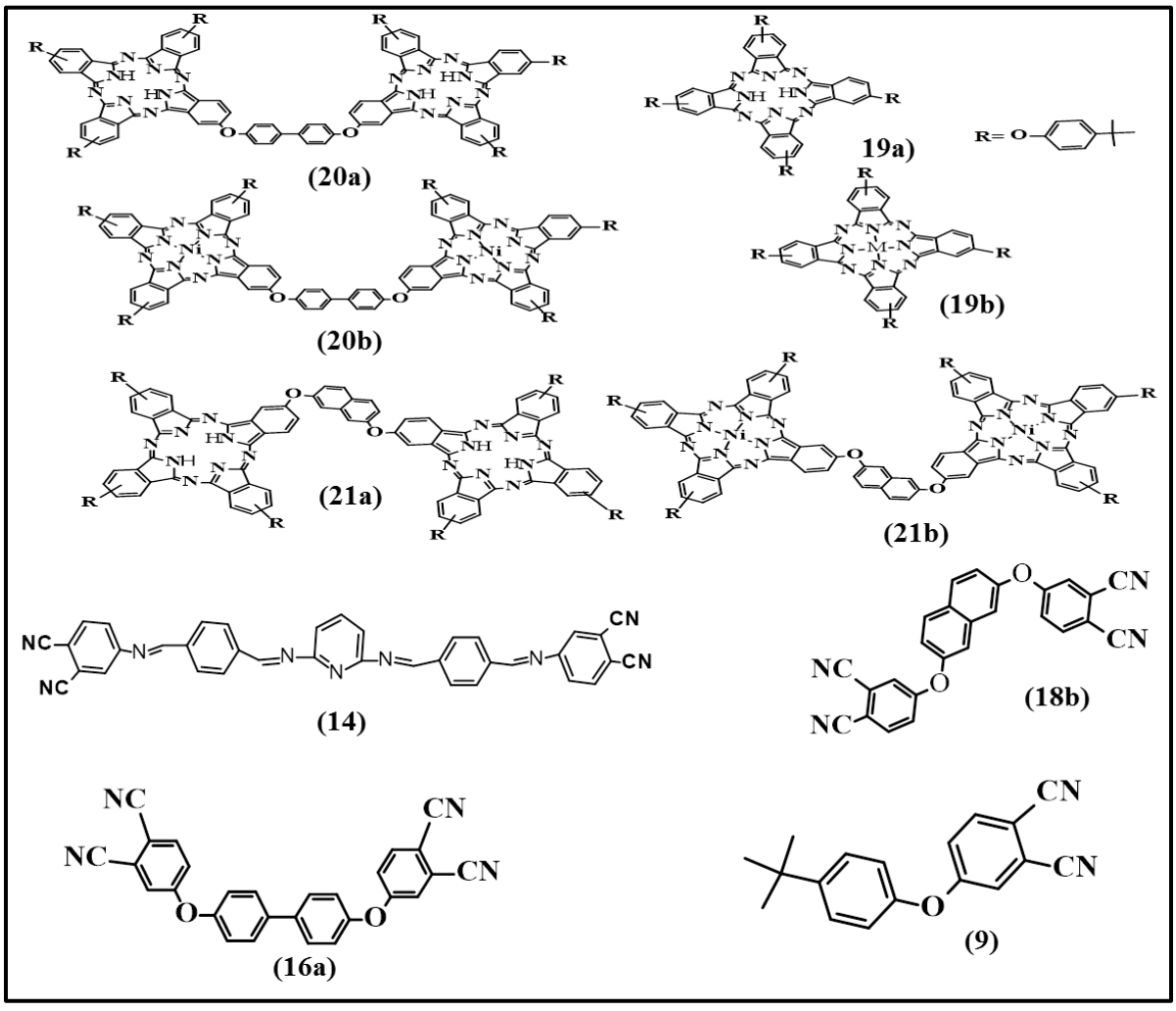

Figure 1.13: Synthesised molecules studied in this thesis

(2) To investigate fluorescence lifetimes and rotational correlation time of these metal-free complexes using time correlated single photon counting (TCSPC).

(3) Nature of second- order nonlinear optical activity of biphenyl bridged binuclear phthalocyanines and naphthalene bridged phthalocyanines in comparison with monomeric phthalocyanines will be investigated.

(4) Octupolar/Dipolar contributions to the second-order nonlinear optical response of all the synthesised complexes using density functional theory will be studied

CHAPTER TWO: EXPERIMENTAL

2 Experimental

2.1 Materials

4-Nitrophthalonitrile, 4, 4-dihydroxybiphenyl, and 4-tertbutylphenol were purchased from Sigma-Aldrich and were used without further purification. The solvents dimethylsulfoxide (DMSO), dichloromethane (DCM), 1-octanol, dimethylformamide (DMF) and tetrahydrofuran (THF) were purchased from Merk and were used as received, whereas, dichlorobenzene and hexane were purchased from Sigma-Aldrich. Other solid materials that were purchased from the sigma-Aldrich include; potassium carbonate, aluminium oxide and Silica gel. Bio-beads were purchased from the Bio-Rad laboratories.

2.2 Equipment

Ground state electronic absorption spectra were performed on Shimadzu UV-2550 spectrophotometer in THF. Magnetic Circular Dichroism (MCD) spectra were run on Chirascan plus spectrometer as solution in THF. IR spectra were recorded with the Perkin Elmer spectrum 2000 FT-IR spectrometer. Elemental analyses were performed on an Elementar vario micro cube (**CHNS** analysis). Mass spectra data were collected on a Bruker AutoFLEX III smart-beam MALDI-TOF mass spectrometer using alpha cyano as the matrix in the positive mode. Column chromatography was carried out on silica gel, aluminium oxide and on Bio-beads^{TM} S-x1 support. ^{1}H- NMR and ^{13}C- NMR were recorded on Bruker AM-300 equipment.

Fluorescence lifetimes were measured with a FluoTime 300 EasyTau spectrometer (PicoQuant GmbH) using a time correlated single photon counting (TCSPC) technique. The samples were excited at 670 nm with a diode laser (LDH-P-670, 20 MHz repetition rate, 44 ps pulse width,

PicoQuant GmbH).The detector employed was a Peltier cooled photomultiplier (PMA-C 192-M, PicoQuant GmbH).

All Z-scan experiments described in this study were performed using a frequency-doubled Nd: YAG laser (Quanta-Ray, 1.5 J/10 ns fwhm pulse duration) as the excitation source. The laser was operated in a near Gaussian transverse mode at 532 nm (second harmonic), with a pulse repetition rate of 10 Hz and an energy range of 0.1 μJ - 0.1 mJ, which was monitored with an energy detector (Coherent J5-09). The low repetition rate of the laser prevents cumulative thermal nonlinearities. The beam was spatially filtered to remove the higher order modes and tightly focused with a 15 cm focal length lens. No damage was detected between runs when the sample was moved or replaced.

The Gaussian 03 software package [96] running on an Intel/Linux cluster was used to perform all DFT calculations. The calculations were done at the B3LYP geometry optimizations with 6-31G (d) and SDD basis sets. Gaussview 4.1 was used for all visualizations of molecular orbitals (MOs) and properties. The B3LYP exchange-correlation density functional employs Becke's method for using Lee-Yang Parr's gradient-correction, which includes a hybrid of semi-empirical Hatree-Fock and DFT exchange.

2.3 Synthesis of peripheral substituted phthalonitriles

2.3.1 Synthesis of 4β- (4-tert-butylphenoxy) phthalonitrile (9)

1.04g, (6.00 mmol), of 4-nitrophthalonitrile (**1)** and 0.90g, (5.98 mmol) of 4-tert-butyphenol **(2**) were dissolved in 10 ml dry DMF under nitrogen gas at room temperature. Anhydrous K_2CO_3 (2.50g, 18 mmol) was crushed and added portion-wise every 15 minutes. The reaction was allowed for 24 hrs. After 24 hrs of total reaction, 1.00 M HCl (50 ml) was added to the reaction mixture to allow formation of precipitates. The reaction was then filtered, and recrystallized in methanol and small amount of water to yield a pale yellow product. Yield: 72%, Elemental: expected values (%): (C=75.7), (H=2.9), (N=13.6), results (%): (C=74.5), (H=3.04), (N=13.7) IR [(KBr) vmax, cm^{-1})]: (C≡N = 2228.01), (C-H = 2964).

2.4 Syntheses of Bisphthalonitriles (linkers)

2.4.1 Synthesis of conjugated bisphthalonitrile (14)

Telethaldehyde (0.20 g, 0.15 mmol) and 4-aminophthalonitrile (0.21 g, 0.15 mmol) in the ratio 1:1 were refluxed in toluene overnight at 110°C. After the reaction time, the product was filtered and recrystallizes in acetonitrile to obtain a yellow compound referred to as compound **12**. The yellow product was then dried in oven overnight at 50°C. Compound **12** (0.30 g, 0.12 mmol) and 2, 6-diaminopyridine (0.06 g, 0.06 mmol) in the ratio 2:1 were refluxed in methanol at 65°C overnight. After the total reaction time, the product was filtered and recrystallizes in acetonitrile to obtain a pure brown compound referred to as compound **14**. The pure compound **14** was then dried in oven at 60°C overnight. Yield: 64%. Elemental: Expected results (%) (C=75.11),

(H=3.5), (N=21.31), Results (%) (C=74.78), (H=4.46) (N=20.76). IR [(KBr) vmax, cm^{-1})]: (C≡N = 2219.67), (=C-H =3100)

2.4.2 Synthesis of 4, 4- Diphthalonitrileoxybiphenyl (16a)

Dihydroxybiphenyl (**15**) (0.10 g; 0.54 mmol) and 4-nitrophthalonitrile (**1**) (0.19 g; 1.1 mmol) were dissolved in 2.00 ml of DMSO, stirred at 70 °C for 30 hrs. After 6 hrs of the reaction, K_2CO_3 (0.50g, 3.60 mmol) was added at once and the reaction continued for 24 hrs. After the total reaction time (30 hrs), 1.00 M HCl (13.00 ml) was added to the reaction mixture to precipitate out the desired product. The product was filtered and recrystallizes in methanol to obtain a yellow compound. The yellow product was purified using flash chromatography on silica gel and eluting with chloroform to afford 4, 4-diphthalonitrileoxybiphenyl as a white solid. Yield: 69%, and the melting point of the compound was found to be between 154-156°C. Elemental: expected values (%) (C=76.7), (H=3.2), (N=12.8), results (%): (C=75.56), (H=3.25), (N=12.44). IR [(KBr) vmax, cm^{-1})]: (C≡N = 2219.67), (=C-H =3100). $^{1}H^{1}$NMR: δH (300 MHz; CDCl3) 7.19 (4H, d, J = 8.6 Hz, ArH), 7.31-7.35 (4H, m, overlapping signals, ArH), 7.68 (4H, d, J = 8.6 Hz, ArH) and 7.76 (2H, d, J = 8.4 Hz, ArH). $^{13}C^{1}$NMR: δC (150 MHz; $CDCl_3$) 109.2 (Ar-C), 114.9 and 115.3 (CN), 117.8, 121.1, 121.6, 121.7, 129.3, 135.5 and 138.1 (Ar-C), 153.4 and 161.6 (ArC-O).

2.4.3 Synthesis of 2, 7-Diphthalonitrileoxynaphthalene (18b)

2, 7-dihydroxynaphthalene (**17**) (0.08 g, 0.50 mmol) and 4-nitrophthalonitrile (0.17 g, 1.00 mmol) were dissolved in 2.5 mL of DMSO, stirred at 70 °C for 30 hrs. After 6 hrs of the reaction, K_2CO_3 (0.50 g, 3.60 mmol) was added at once and the reaction continued for 24 h.

After the total reaction time (30 hrs), 1M HCl (10 mL) was added to the reaction mixture to precipitate out the desired product. The product was filtered and recrystallizes in methanol to obtain a yellow compound. The yellow product was purified using flash chromatography on silica gel and eluting with chloroform to afford a white solid. Yield: 60%. Elemental: expected values (%) (C=78.2), (H=5.8), (N=10.1), results (%): (C=77.5), (H=5.43), (N=10.8). IR [(KBr) vmax, cm^{-1})]: (C≡N = 2219.67), (=C-H = 3100). ^{1}H NMR: δ_H (300 MHz; DMSO) 7.40(2H, dd, *J* = 8.8 and 2.2 Hz, ArH), 7.51 (2H, dd, *J* = 8.8 and 2.5 Hz, ArH), 7.68 (2H, d, *J* = 2.2 Hz, ArH), 7.91 (2H, d, *J* = 2.5 Hz, ArH) and 8.14 (4H, d, *J* = 8.8 Hz, ArH); ^{13}C NMR: δ_C (75 MHz; DMSO) 108.7 (Ar-C), 115.5 and 116.0 (CN), 116.3, 116.9, 119.8, 122.8, 123.3, 128.7, 131.0, 135.1 and 136.5 (Ar-C), 152.7 and 160.8 (ArC-O).

2.5 Synthesis of monomeric and binuclear phthalocyanines.

2.5.1 Synthesis of metal-free 4β-(4-tert-butylphenoxy) phthalocyanine (19a) and biphenyl-bridged binuclear 4β-(4-tert-butylphenoxy) phthalocyanine (20a)

A ratio of (1:20) compound **16a** (0.01 g, 0.03 mmol) and compound **9** (0.16 g; 0.59 mmol), were dissolved in the mixture of o-dichlorobenzene and 1-octanol in the presence of lithium (as a catalyst). The mixture was stirred and refluxed at 120 $^{\circ}C$ for 6 hrs and left to cool to room temperature. Acetic acid was then added to the mixture (to remove lithium metal), and stirred for 30 minutes. Methanol was then added to precipitate the product out. The mixture was then filtered and the solid green product dried. The product was purified on column chromatography using silica gel. The mixture of DCM and methanol (10:1) was used to elute the first fraction (green in colour), which consisted of a monomeric phthalocyanine. THF was then used as the

second eluent in order to elute out the second fraction which was blue in colour. The second fraction was further purified on Bio-beads using THF to obtain a pure metal-free monomeric Pc (**19a**) and metal-free binuclear Pc (**20a**). Compound **20a** came out first in the column because of its lager molar mass and the compound **19a** came out last.

Compound (**19a**): Yield: 35%, IR [(KBr) vmax, cm^{-1})]: (N-H=3700), (C-H=2964.99).UV/Vis (THF): λmax nm (log ε): 700 (6.00), 665 (5.96), 637 (5.54), 605 (5.35), 338 (5.75).MS (MALDI-TOF) m/z: Calculated 1107.34; Found 1109.88 [M + H^+].

Compound (**20a**): Yield: 15%, IR [(KBr) vmax, cm^{-1})]: (N-H=3700), (C-H=2964.99).UV/Vis (THF): λmax nm (log ε): 698(6.09), 663(6.14), 629 (6.02), 603 (5.99), 325 (6.23). MS (MALDI-TOF) m/z: Calculated 2100.5; Found 2101.39 [M + H^+].

2.5.2 Synthesis of metal-free naphthalene-bridged binuclear 4β-(4-tert-butylphenoxy) phthalocyanine (21a)

Naphthalene binuclear metal-free 4β-(4-tert-butylphenoxy) phthalocyanine (**21a**) was synthesised as described above for compounds (**20a**), the difference being that, compound **18a** (0.02 g, 0.05 mmol) and **9** (0.27 g, 0.98 mmol) were used.

Compound (21a): Yield: 13%, IR [(KBr) vmax, cm^{-1})]: (N-H=3700), (C-H=2964.99).UV/Vis (THF): λmax nm (log ε): 699 (6.42), 664 (6.48), 631 (6.42), 610 (6.39), 331 (6.57). MS (MALDI-TOF) m/z: Calculated 2074.4; Found 2080.8 [M + H^+].

2.5.3 Synthesis of nickel 4β-(4-tert-butylphenoxy) phthalocyanine (19b) and biphenyl-bridged binuclear nickel 4β-(4-tert-butylphenoxy) phthalocyanine (20b)

Compound **16a** (0.01 g; 0.03 mmol) and compound **9** (0.15 g; 0.55 mmol), in the ratio 1:20, were dissolved in the mixture of o-dichlorobenzene, 1-octanol and Nickel (II) acetate in the presence of three drops DBU as a catalyst. A similar reaction and purification procedure was followed as above **(2.51**). The difference being that nickel acetate was used instead of lithium metal and hence no need for the acetic acid

Compound (**19b**) Yield: 37% IR [(KBr) vmax, cm^{-1})]: (C-O-C=1246), (C-H=2964.99).UV/Vis (THF): λmax nm (log ε): 668 (5.86), 601 (5.16), 375 (5.13), 323 (5.92). MS (MALDI-TOF) m/z: Calculated 1164.00; Found 1166.19 [M + H^+].

Compound (**20b**): Yield: 17%, IR [(KBr) vmax, cm^{-1})]: (C-O-C=1246), (C-H=2964.99).UV/Vis (THF): λmax nm (log ε): 664 (6.07), 608 (6.29), 327 (6.29). MS (MALDI-TOF) m/z: Calculated 2113.8; Found 2215.07 [M + H^+].

2.5.4 Synthesis of Naphthalene-bridged binuclear nickel 4β-(4-tert-butylphenoxy) phthalocyanine (21b)

Naphthalene binuclear nickel 4β-(4-tert-butylphenoxy) phthalocyanine (**21b**) was synthesised using (0.01 g, 0,02 mmol) of compound **18b** and (0.16g, 0,58 mmol) of compound **9**. Similar method and purification procedure was followed as above for compound **20b**.

Compound (21b) Yield: 15% IR [(KBr) vmax, cm^{-1})]: (C-O-C=1246), (C-H=2964.99). UV/Vis (THF): λmax nm (log ε) 661(6.12), 610(6.30), 319(6.39). MS (MALDI-TOF) m/z: Calculated 2187.8; Found 2193.86 [M + H^+].

CHAPTER THREE: SYNTHESIS AND CHARACTERISATION

3 Synthesis and Characterisation

3.1 Synthesis of Phthalonitriles

In order to prepare binuclear phthalocyanines, two different types of phthalonitriles have been synthesised. The two types of phthalonitriles are; substituted phthalonitrile, which was synthesised from 4-nitro phthalonitrile and the linking (bridging) phthalonitrile referred to as bisphthalonitrile, which is used to join two monomeric Pcs together .Three different linking phthalonitriles have been synthesised. One of the linkers synthesised is conjugated in order to make conjugated Bi-Pcs. This conjugated phthalonitrile was synthesised from 4-aminophthalonitrile.The two other bridging phthalonitriles are not conjugated but covalently bonded so as to make covalent bonded Bi-Pcs. These two bridging phthalonitriles have been synthesised from 4-nitrophthalonitrile.

3.1.1 Synthesis of 4-(4-tert-butylphenoxy) phthalonitrile (9)

The substituted phthalonitrile needed for this work was derived from 4-nitrophthalonitrile, following synthetic method [97].The synthesis of 4-nitro phthalonitrile is routine or sometimes can be bought from Sigma-Aldrich, hence not repeated here. The synthesised 4-nitrophthalonitrile **(1**) was reacted with 4-*tert*-butulphenol (**8**) in dry DMF in the presence of Potassium carbonate (K_2CO_3) as a catalyst at RT for 24 hours to form 4-(4-*tert*-butylphenoxy) phthalonitrile, yield 72%, **Scheme 3.1.**

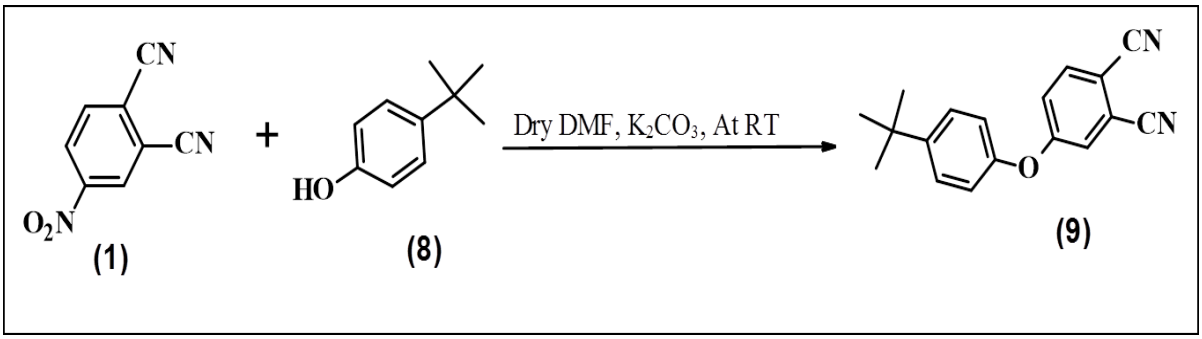

Scheme 3.1: Synthesis of 4-(4-*tert*-butylphenoxy) phthalonitrile (**9**)

The IR spectra of compound **9** showed a strong C≡N stretch band at 2228.01 cm^{-1}. Strong C-O-C bond stretch was found between 1220 -1350 cm^{-1} ranges. Expected C-H stretching band at 2964.99 cm^{-1} was observed. Elemental results for compound **9** correlated very well with calculated values.

3.1.2 Synthesis of bridging conjugated phthalonitrile (14)

Scheme 3.2 shows a synthetic route for compound **14.** Telethaldehyde **(10)** and 4-aminophthalonitrile **(11)** in the ratio 1:1 were refluxed together in toluene overnight at 110 °C to form compound **12**. Compound **12** together with 2, 6-diaminopyridine **(13)** in the ratio 2: 1 were refluxed in methanol at 65°C overnight to obtain a yellow product**.** The product was then recrystallised in hot acetonitrile to yield 64 % of pure compound **14.**

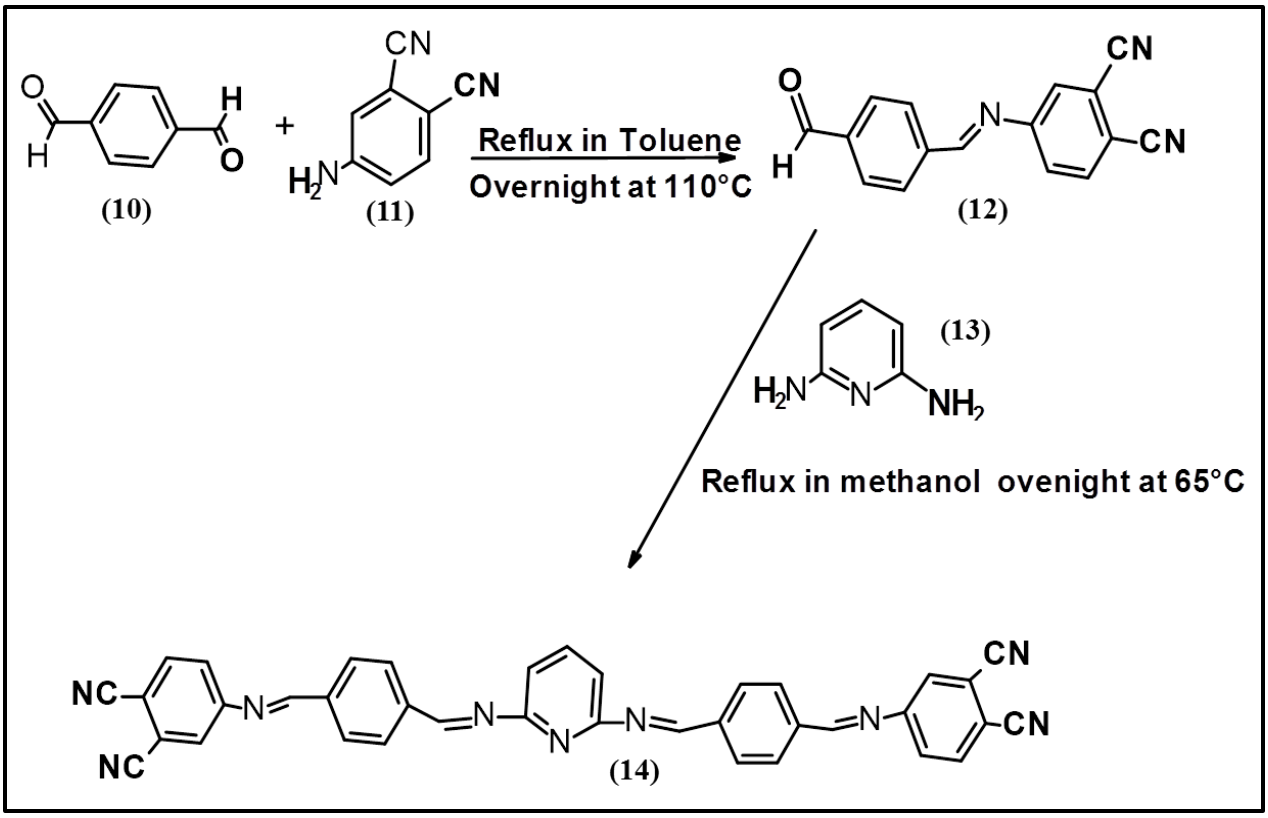

Scheme 3.2: Synthesis of bridging conjugated phthalonitrile (compound 14)

IR Spectrum of compound 14 showed a C≡N stretch band at 2235 cm^{-1}, C-N band at 1215 cm^{-1} and small C=N peak was observed at 1626, **Figure 3.1.** Elemental results for compound **14** agreed very well with calculated values.

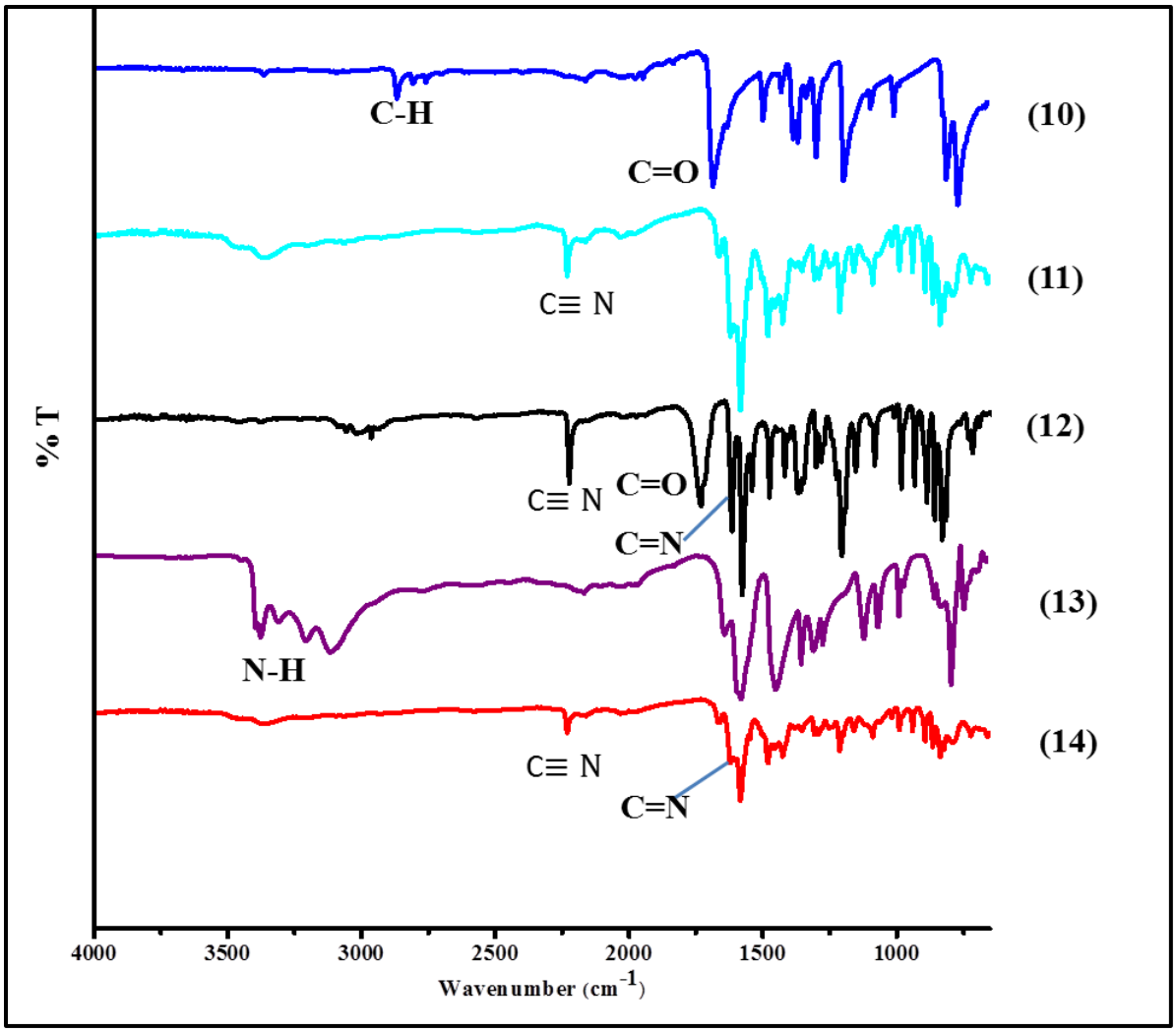

Figure 3.1: IR Spectra for compounds **10**, **11**, **12**, **13** and **14**

3.1.2 Synthesis of 4, 4-diphthalonitrileoxybiphenyl and 2,7-diphthalonitrileoxynaphthalene phthalonitrile

Dihydroxybiphenyl **(15)** and 2, 7-diphthalonitrileoxynaphthalene **(17)** were used to synthesise 4, 4-Diphthalonitrileoxybiphenyl phthalonitriles **(16a)** and 2, 7 diphthalonitrileoxynaphthalene phthalonitriles (**18b**). The synthesis was carried by reacting compound **1** with compounds **15** and **17** respectively, in dry DMSO in the presence of K_2CO_3 at room temperature for 30 hours. The resulting products where further purified by column chromatography using chloroform and methanol (10:1) to afford 69 % and 60 % yields of compounds **16a** and **18b** respectively, **Scheme 3.2.**

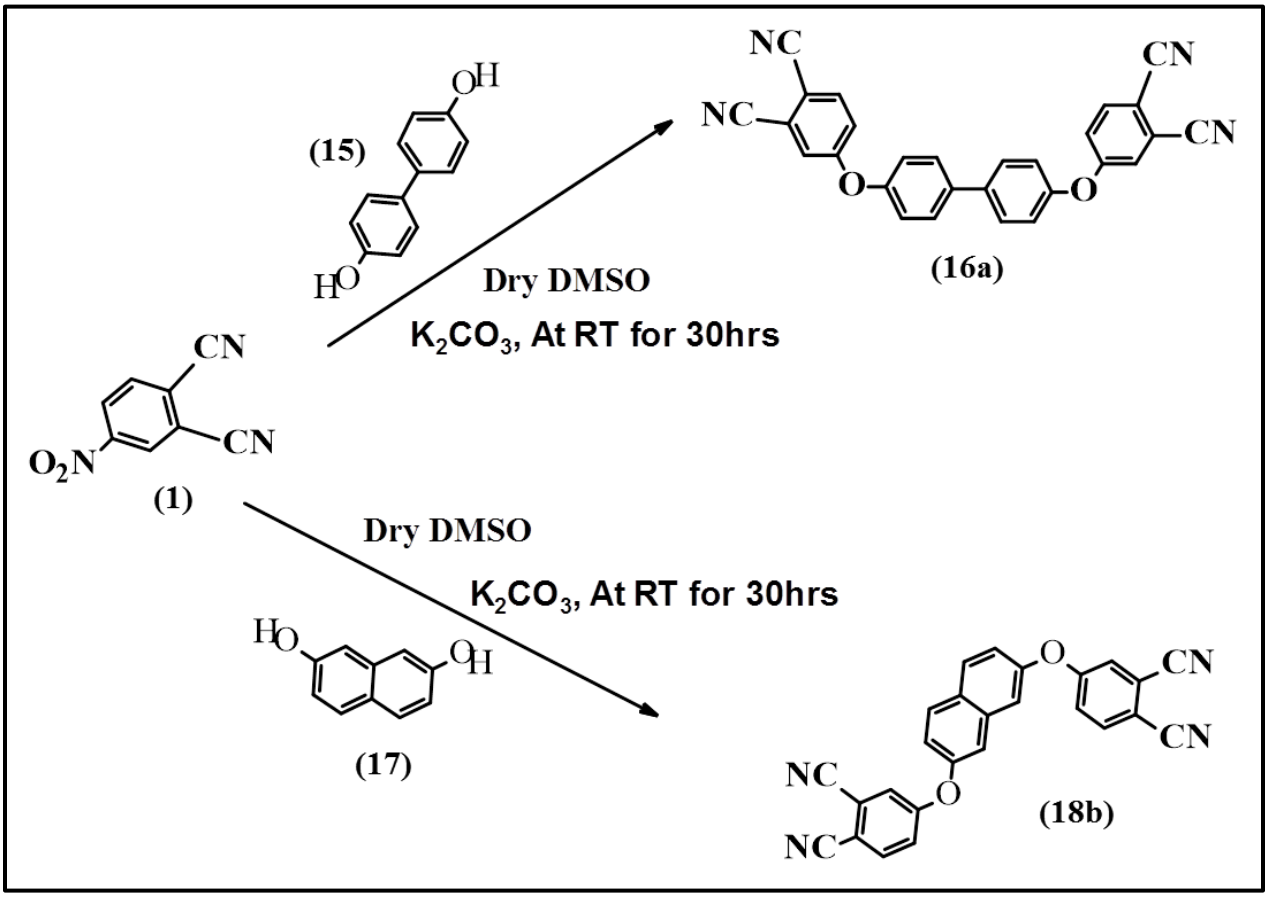

Scheme 3.3: Synthesis of bisphthalonitriles (compounds **16a** and **18b)**

IR spectra of compounds **16a** and **18b** showed a C≡N stretch band at 2228cm^{-1} and the C-H stretching band at 2964 cm^{-1}, **Figure 3.2**. Elemental results for compounds, **16a** and **18b** correlated very well with the measured values. The ^{1}H NMR and ^{13}C NMR data obtained were in agreement with the structures of compound **16a** and **18b.** The ^{1}H NMR aromatic region of compound **16** exhibited peaks at 7.19 ppm, 7.31-7.35ppm, 7.68ppm and 7,76ppm. These were assigned to the protons on the phthalonitrile and benzene rings. The ^{13}C NMR data showed aromatic carbon (Ar-C) signal at 109.2, 117.8, 121.1,121.6, 121.7, 129.3,135.5 and 138.1 ppm,

CN signal at 114.9 and 115.3 ppm and ArC-O at 153.4 and 161,6 ppm. The melting point of compound **16a** was found to be between 154-156 ˚C.

For compound **18b,** the ^{1}HNMR exhibited aromatic protons peaks at 7.41.7.53, 7.67. 7.91 and 8.16 ppm. The ^{13}C NMR data also showed aromatic carbon (Ar-C) signals at 108.9, 116.5, 117.1, 120.0, 123.1, 123.6, 128.9, 131.3, 135.4 and 136.7 ppm. CN signal at 115.8 and 116.2 and Ar-O at 152.8 and 160.9 ppm.

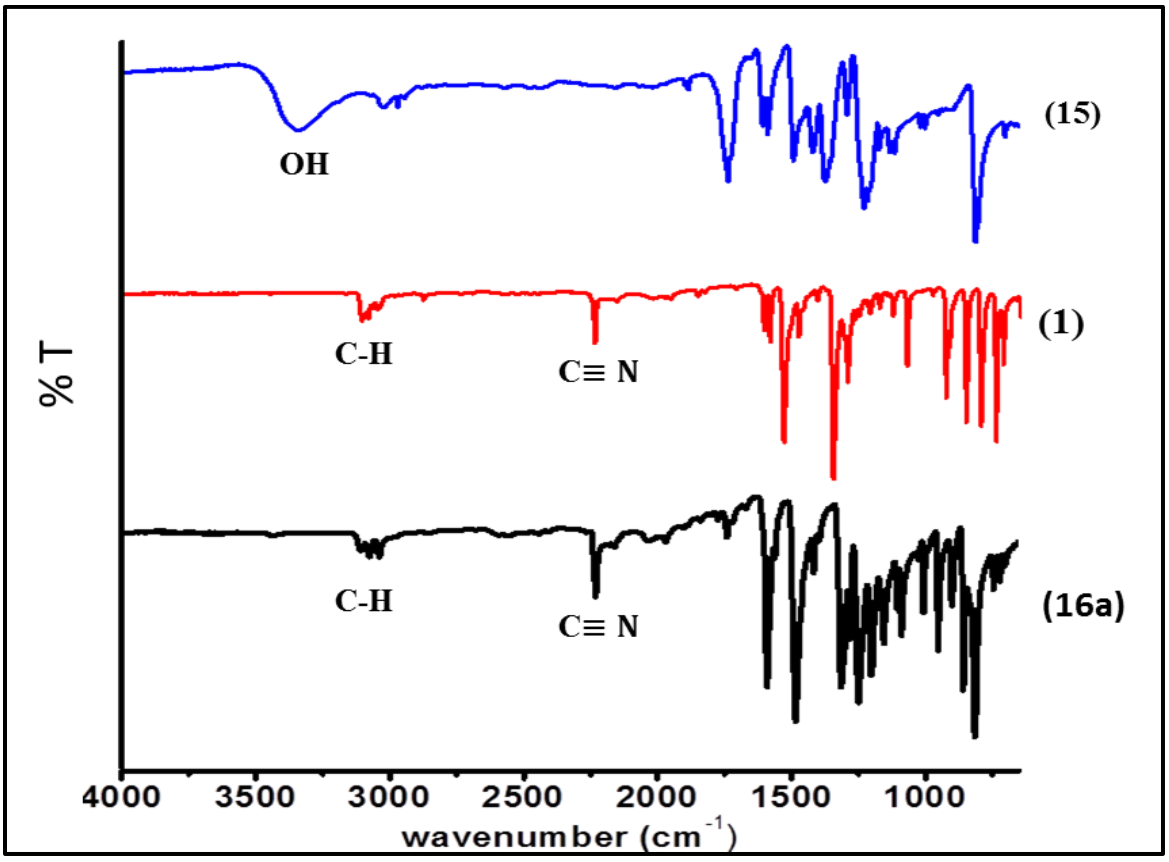

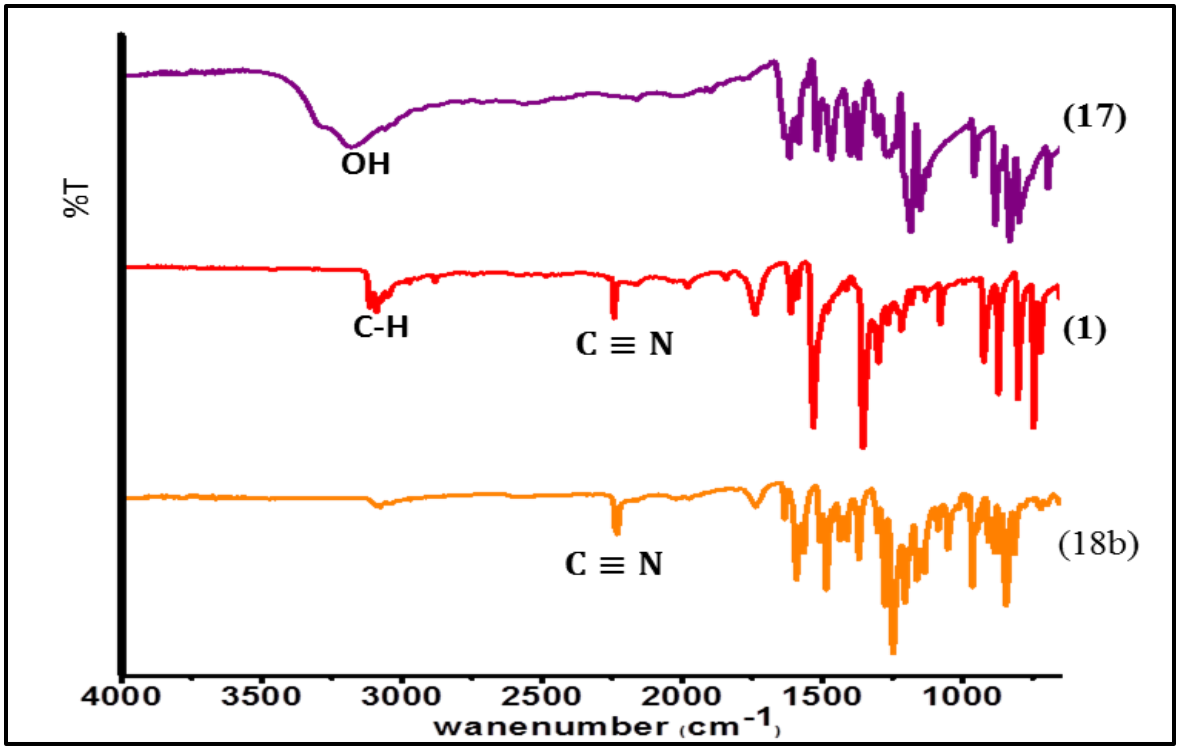

Figure 3.2: IR spectra compounds **15**, **1** and **16a** (top) and compound **17**, **1** and **18b** (bottom)

3.2 Synthesis of binuclear Phthalocyanines

Binuclear phthalocyanines are formed as the result of mixed condensation of bisphthalonitriles and substituted phthalonitriles. Substituted phthalonitrile used should be in large excess to prevent self-condensation of the bisphthalonitriles. An attempt was made to try and make conjugated Bi-Pcs using substituted phthalonitrile **9** and conjugated bisphthalonitrile **14.** Unfortunately**,** the Bi-Pc was not formed only the monomeric Pc instead was formed. It was suspected that the bisphthalonitrile was not active enough to cyclise. Therefore, bisphthalonitrile was converted to bisisoindoline as reported in literature [56, 98, 99], to improve reactivity. However, Bi-Pc did not form despite the activation. Covalently bonded Bi-Pcs formed by using

the other two covalently bonded bisphthalonitriles **(16a** and **18b**) as wanted. However, the Bi-pcs were obtained in low yields.

3.2.1 Synthesis of metal-free 4β-(4-*tert*-butylphenoxy) phthalocyanine (19a), biphenyl bridged binuclear 4-*tert*-butylphenoxy phthalocyanine (20a) and naphthalene bridged binuclear 4-*tert*-butylphenoxy phthalocyanine (21a).

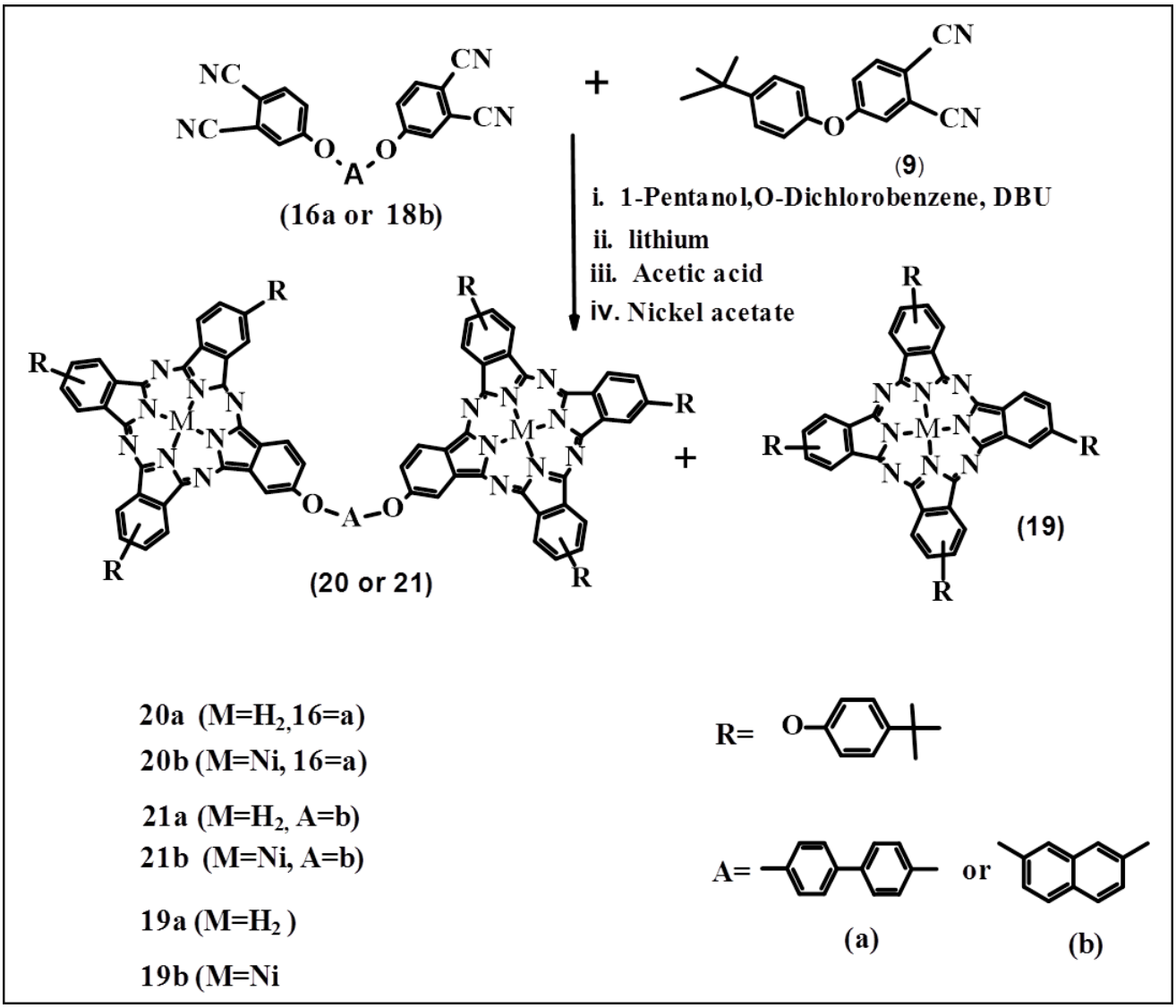

Scheme 3.4: Synthesis of metal-free and nickel compounds **19a, 19b**, **20a**, **20b**, **21a** and **21b**

The synthesis of metal-free and nickel 4β-(4-*tert*-butylphenoxy) phthalocyanine (**19a** and **19b**),) and biphenyl bridged binuclear 4-*tert*-butylphenoxy phthalocyanine **(20a** and **20b)** and synthesis of metal-free naphthalene bridged binuclear 4-*tert*-butylphenoxy phthalocyanine (**21a** and **21b**) is depicted in **Scheme 3.4.**

Using statistical condensation method, substituted phthalonitriles (9) was reacted with bisphthalonitrile (**16a**) and (**18b**) in the presence I-octanol, o-dichlorobenzene and lithium metal or nickel acetate to afford Bi-Pcs **(20a, 20b, 21a and 21b**)**.** Compound **19a** and **19b** were obtained as by-products of the reaction. The Bi-Pcs (**20a, 20b, 21a** and **21b)** were purified by size exclusion method using bio-bead column, eluting with THF.

MS-MALDI-TOF data were in agreement with the structure of complexes **19a, 19b, 20a, 20b, 21a** and **21b**, **Figure 3.3.** MS-MALDI-TOF was used to analyse these large complexes because it is very fast, easy to use, very sensitive, tolerant to buffer and does not fragment large molecules into smaller charged particles, rather it turns the large molecules being ionised into small droplets. These droplets can then be further desolvated into even smaller droplets, which creates molecules with attached protons [100, 101]. Due to aggregation and paramagnetic nickel metal centre, poor H^1NMR signals were observed for these complexes.

IR spectra of complexes **19a, 19b**,**20a**,**20b**, **21a** and **21b,** clearly showed the absence of C≡N stretching band at 2228 cm^{-1}, the presence of =C-H band at 2928 cm^{-1} , C-O-C vibrational at 1260 $cm^{-1}$and N-H stretching band at 3700 cm^{-1} for metal-free complexes. For nickel complexes, N-H stretch was not observed due to metalation.

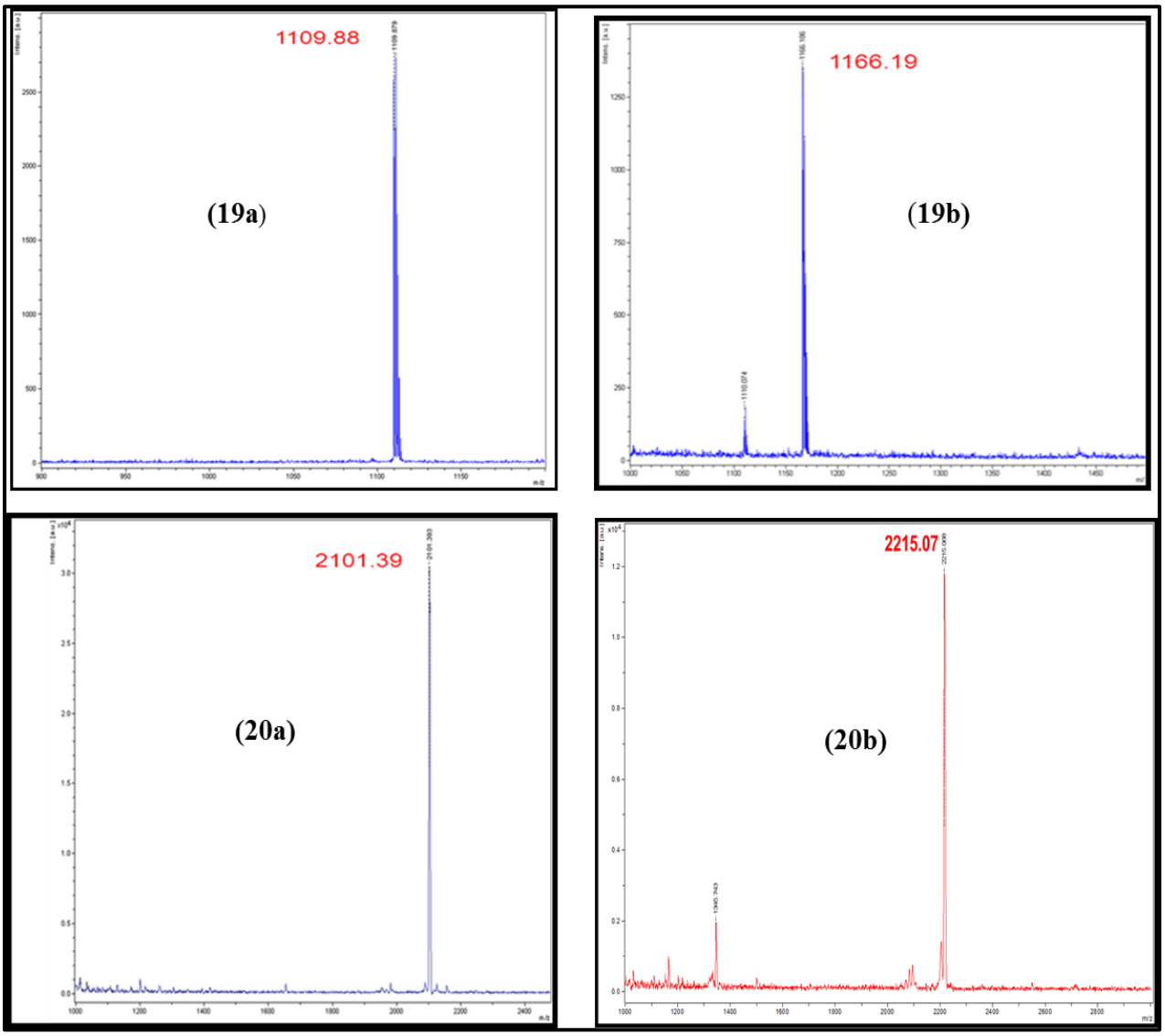
1109.88
(19a)
1166.19
(19b)
2101.39
(20a)
2215.07
(20b)

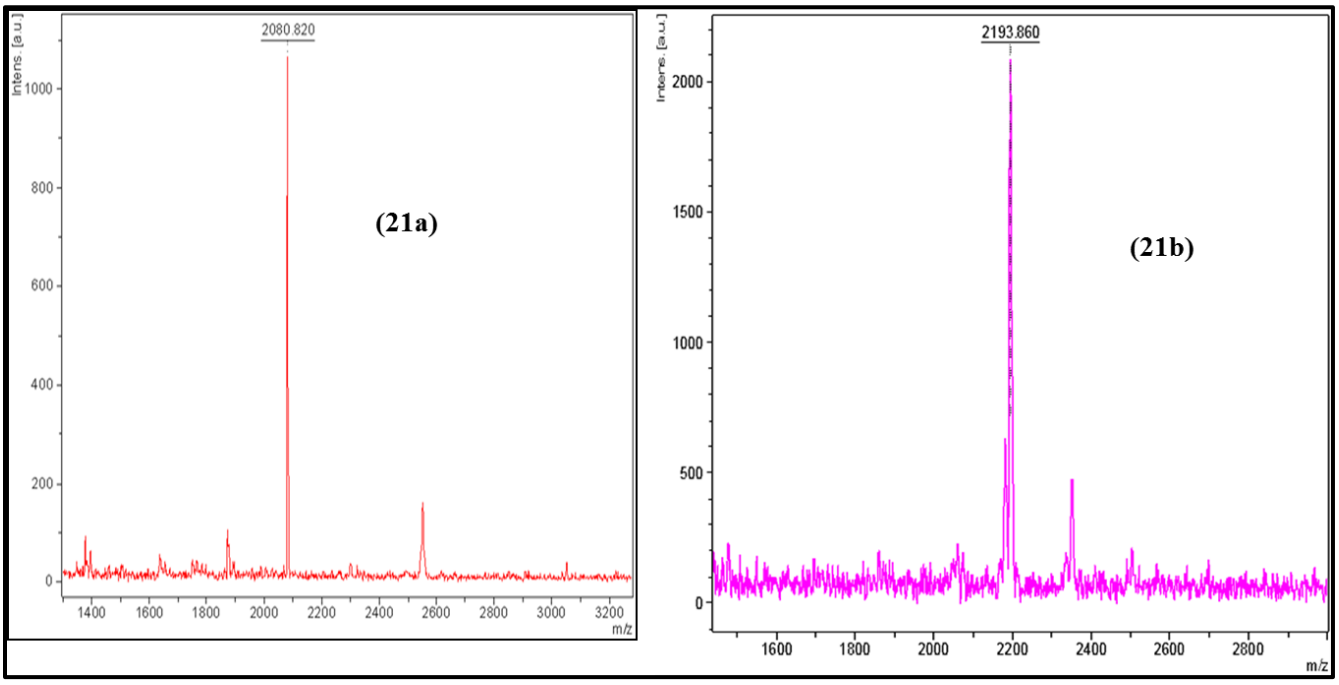

Figure 3.3: Mass spectra (MALDI- TOF) for complexes **19a**, **19b**, **20a**, **20b**, **21a** and **21b**

3.3 Electronic absorption and MCD spectroscopy

MCD spectroscopy can be used to identify the main electronic Q (0, 0) and B (0, 0) bands, due to the presence of intense Faraday $\boldsymbol{A_1}$ terms or coupled pairs of oppositely-signed Faraday $\boldsymbol{B_0}$ terms [102].The band assignment was modified by the Stillman group [103-107] on this basis to, in ascending energy, determine the Q (ca. 670 nm), B1 (ca. 370 nm), B2 (ca. 330 nm), N (ca. 275 nm), L (ca. 245 nm) and C (ca. 210 nm) bands. **Figure 3.4** contains the absorption and MCD spectrum of compounds **19a, 19b, 20a, 20b, 21a** and **21b**. The presence of intense Faraday $\boldsymbol{B_0}$ term intensity for all the complexes demonstrates that the B_1 and B_2 bands lie in the **300-400** nm region.

The UV-visible absorption and MCD spectra (in **Figure 3.4**) of metal-free binuclear **(20a** and **21a)** and mononuclear 4β-(4-*tert*-butyphenoxy) phthalocyanines **(19a)** are consistent with those reported previously for D_{2h} symmetry [**108, 109**]. Similarly for nickel complexes **19b, 20b** and **21b** are consistent with those reported for D_{4h} symmetry [108]. MCD and UV/vis spectra of compounds **20a, 20b, 21a,** and **21b** (in **Figure 3.4 B, C, E and F)** shows an intense blue shifted band between **600-350** nm, which is associated with H-aggregation through the exciton coupling of the Pc units [110]. The intensity of the peak and wavelength indicates a strong intramolecular coupling and thus reflects a co-facial arrangement of the binuclear phthalocyanines aggregates [**110**].

Pcs with D_{2h} symmetry are known to produce negative MCD troughs associated with the Q band absorption peak in the longest wavelength [78]. The metal-free Pc (**19a**) has D_{2h} symmetry and each unit of the metal-free Bi-Pcs (**20a** and **21a**) also approximate D_{2h} symmetry. Therefore the π system of compounds **20a** and **21a** is predicted to contain four lowest unoccupied molecular orbitals (LUMOs) of b_{3g}, b_{2g}, b_{1u} and a_u symmetry and two highest occupied molecular orbitals (HOMOs) each from the $1a_{1u}$ and $1a_{2u}$ molecular orbitals (MOs). These MOs are associated with Counterman's 4-orbital model [111], with b_{3g} and a_u, and b_{2g} and b_{1u} symmetry, respectively. The MCD spectra of **20a** and **21a** (**Figure 3.4** (**B**) and (**C**) respectively) show negative MCD troughs associated with Faraday $\boldsymbol{B_0}$ term for the Q band (**630-700** nm) in the longest wavelength. The presence of Faraday $\boldsymbol{B_0}$ terms indicate that no degeneracy exists in either the ground or the excited states [78].

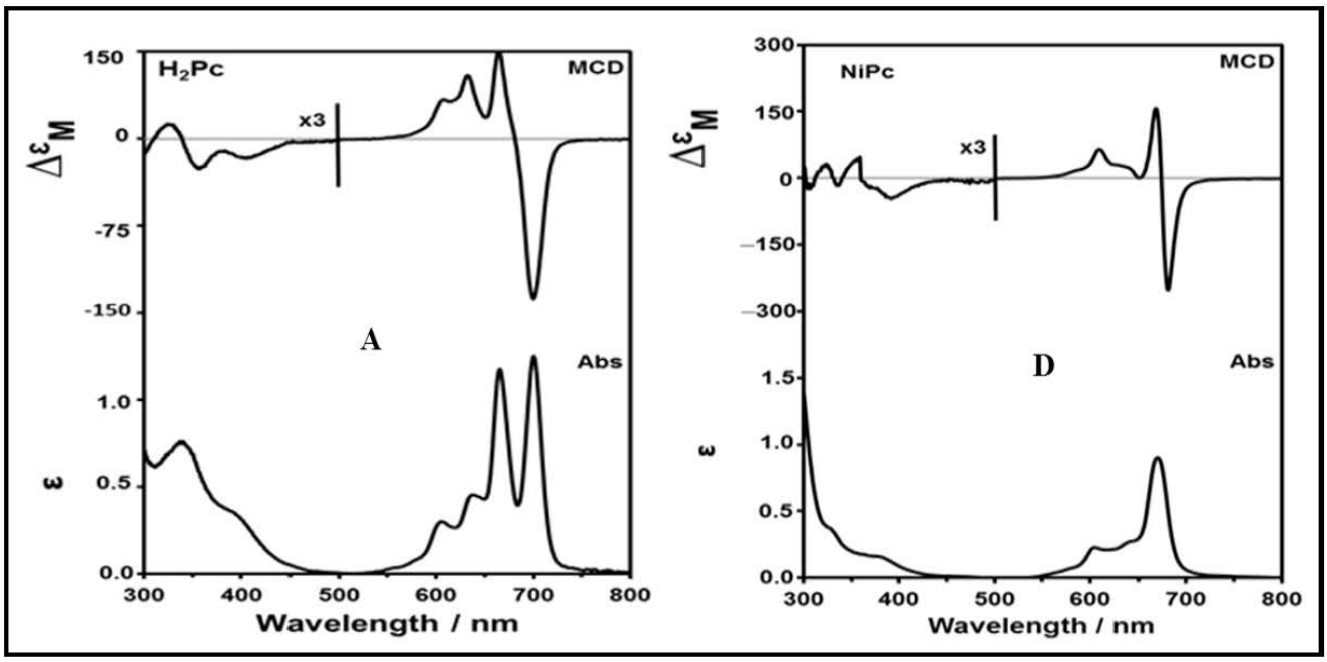
H2Pc
MCD
x3
A
Abs
Wavelength / nm
NiPc
MCD
x3
D
Abs
Wavelength / nm

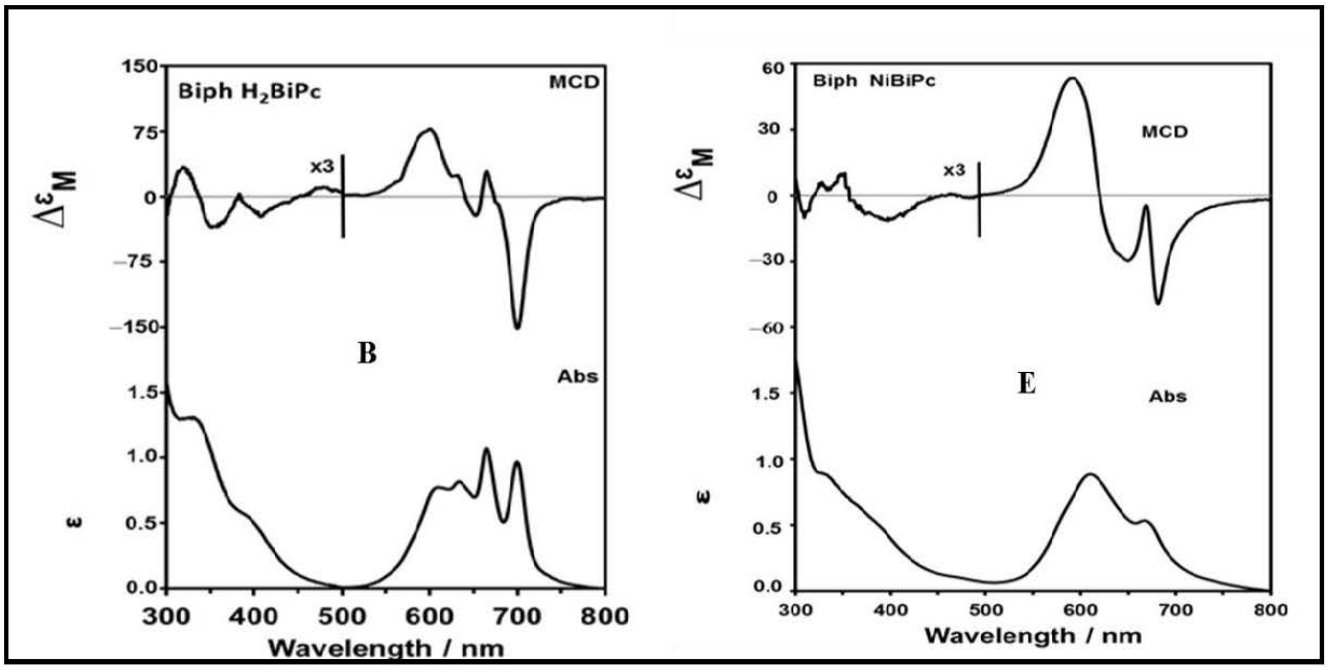
Biph H2BiPc
MCD
x3
B
Abs
Wavelength / nm
Biph NiBiPc
MCD
x3
E
Abs
Wavelength / nm

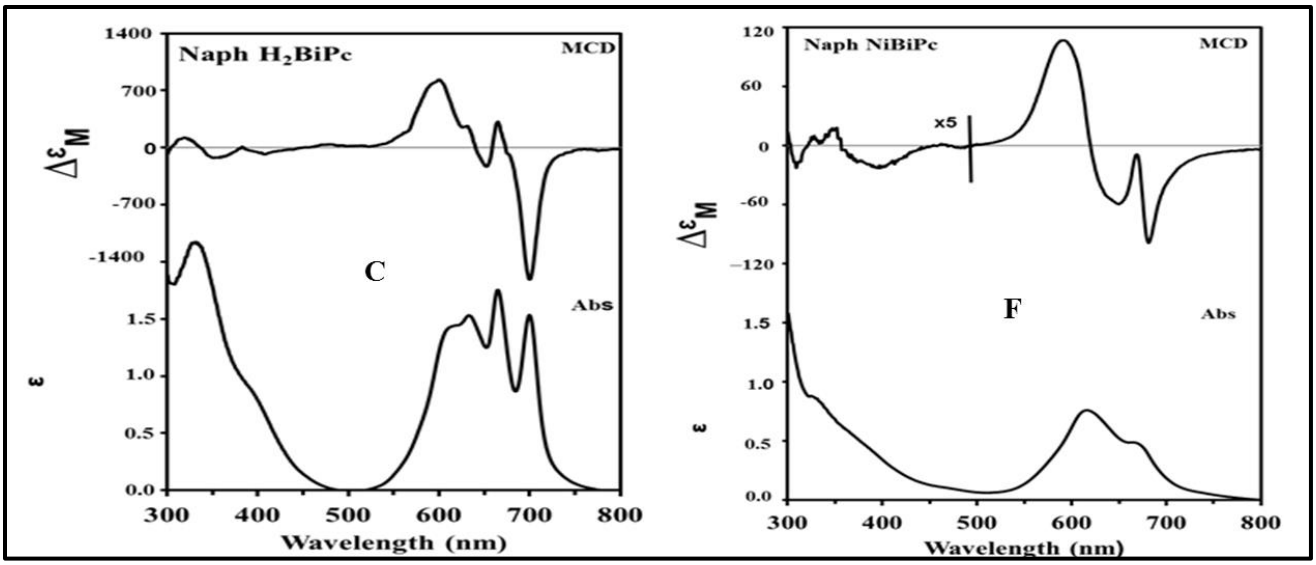

Figure 3.4 UV-VIS (bottom) and MCD (top) spectra for: Left hand side (LHS) A (**19a**), B (**20a**), C (**21a**). Right hand side (RHS) D (**19b**), E (**20a**) and F (**21b**) in THF.

The split Q-band for compound **19a** (**Figure 3.4 A**) attributed to the π - π* transition is assigned as the Q_{x00} and Q_{y00} of the Pc^{2-} ring [112]. The split Q-band is due to the presence of low symmetry (D_{2h}) which lifts the degeneracy of the two LUMO levels. The B band in the UV region arises from the deeper π level - LUMO transition.

Similarly a split Q-band is observed for compounds **20a** and **21a** and its assigned transitions follow a similar assignment as compound **19a**, see **Figure 3.4**, the difference being in the number of MOs as discussed above. However, the Q-bands observed for **20a** and **21a** in the longer wavelength consist of superposition of Faraday $\boldsymbol{B_0}$ terms from individual phthalocyanine units.

The envelope of absorption intensity in the **400-470** nm region has been assigned previously to n → π* transitions associated with the lone pairs on the peripheral oxygen atoms [113], or to the destabilizing effect of the electron donating effect of the sp^3

hybridized oxygen atoms on the π-MOs that are associated primarily with the fused-ring-expansion of the ligand with benzo rings [114].

The MCD Q-band of nickel phthalocyanine (**19b**) and binuclear phthalocyanine (**20b and 21b**), **Figure 3.4 (D), (E)** and **(F)** respectively, shows a single Q-band (700 nm) with a Faraday $\boldsymbol{A_1}$ term which is consistent with phthalocyanine possessing a D_{4h} symmetry [78]. The observed Q-band Faraday $\boldsymbol{A_1}$ terms for both complexes suggest that the LUMOs energy levels in both complexes are degenerate. However, the nickel binuclear phthalocyanines (**19b** and **21b**) MCD Q band consists of superimposition of two Faraday $\boldsymbol{A_1}$ terms, since each phthalocyanine unit has an approximate D_{4h} symmetry. The prominence of the blue shifted aggregation bands observed in **Figure 3.4 (E)** and **(F)** again is an indication of strong intramolecular coupling and thus reflecting a co-facial arrangement of the nickel binuclear phthalocyanines. A monomer-like species is expected in the Q band region if the solution contains a monomer-like species with an intense and negative MCD absorption peak around **700-710** nm [115], which is the case for compounds **19a, 20b, 21a** and **21b**. The intensity of the aggregated peak for **20b** and **21b** is higher with respect to that of **20a** and **21a**, suggesting that **20b and 21b** are more prone to aggregation. The insertion of nickel atom in the central cavity may promote aggregation, because the binuclear Pc units will assume a flatter geometry compared to its metal-free counterpart.

3.4 Fluorescence lifetimes and rotational correlation lifetimes.

Figure 3.5 A, B and **C** shows the normalised absorption, excitation and emission spectra of metal free **19a**, **20a** and **21a**. The excitation spectrum of **19a** is identical to its ground state absorption spectrum, whereas **20a** and **21a** differ in the intensity of the aggregation band. The excitation spectra of **20a** and **21a** confirm that the bands between **600-650** nm

correspond to aggregation, since aggregated species do not fluoresce. As expected no emission or excitation spectra was obtained for nickel complexes. This is because nickel atom is known to quench the excited state, due to the unpaired electron in the d orbial

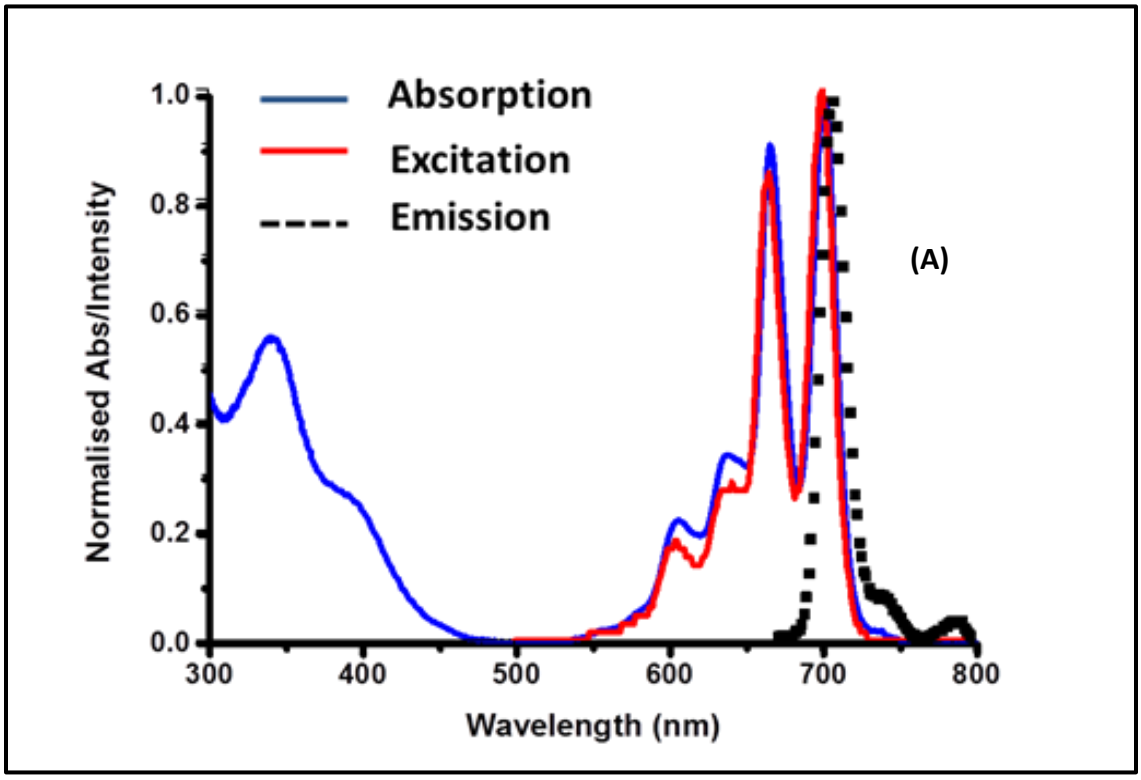

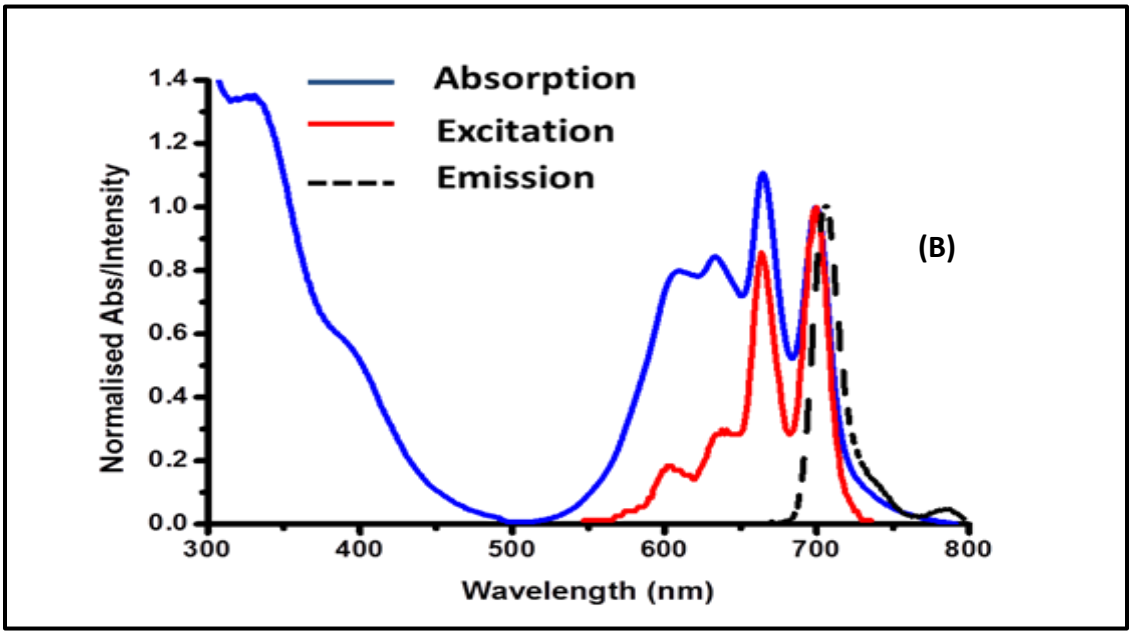

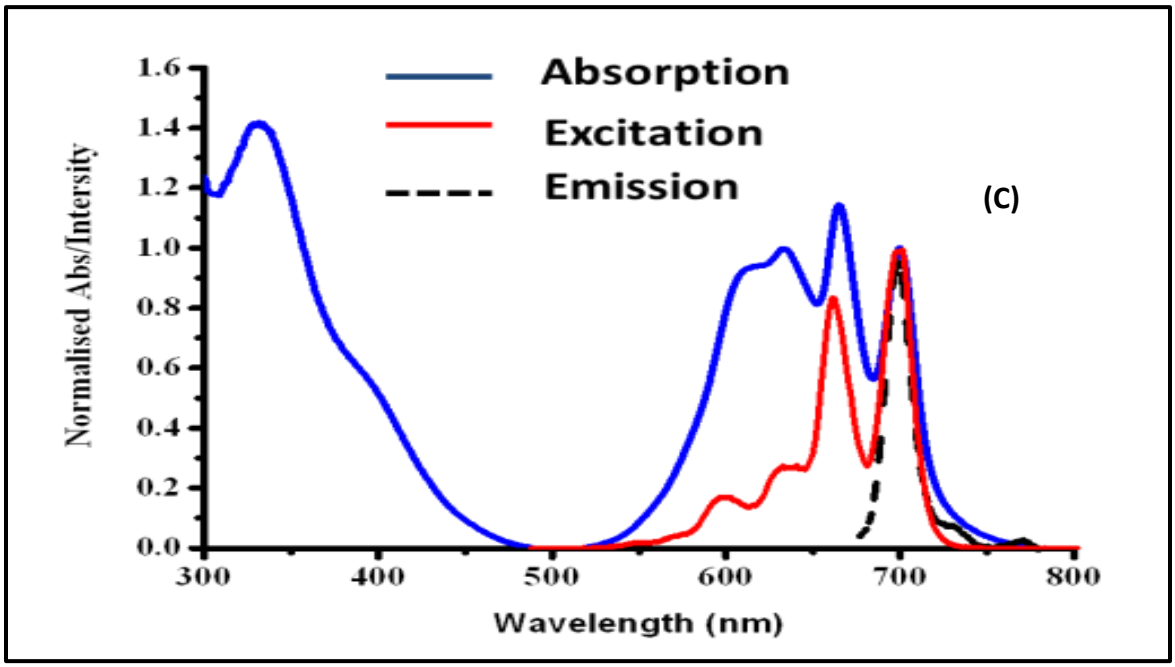

Figure 3.5: Absorption, excitation and emission of A(**19a**), B(**20a**) and C(**21a**) in THF.

Typical time resolved mono-exponential fluorescence decay curves (obtained from TCSPC) for complexes **19a**, **20a** and **21a** in THF are shown in **Figure 3.6**. One fluorescence life time (τ) for **19a, 20a and 21a** were obtained (in THF and DCM) and were found to be between 5.0-5.8 ns range, see **Table 3.1**, which falls within the typical range for monomeric phthalocyanine compounds [115]. A single fluorescence lifetime also suggests that the compounds are relatively pure

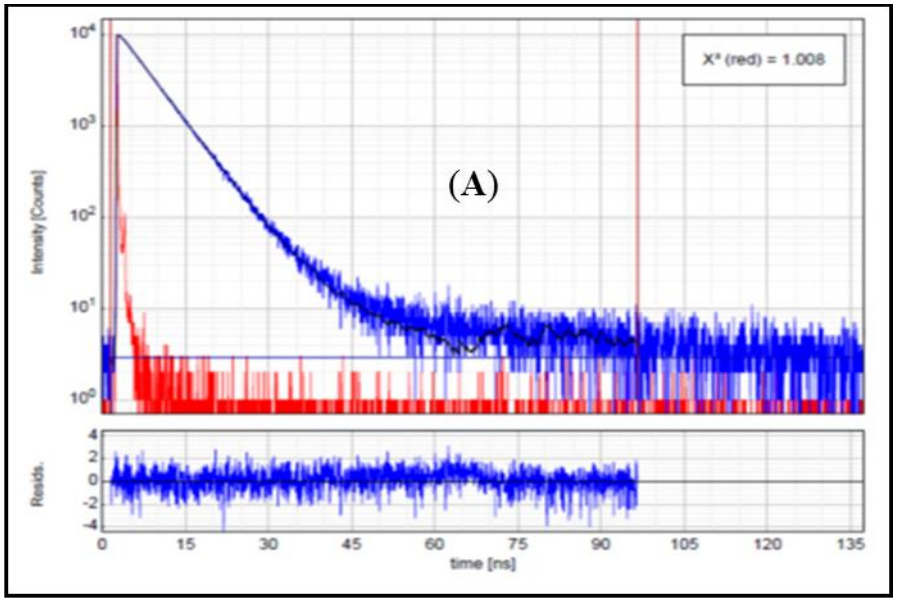
X² (red) = 1.008
(A)
Intensity [Counts]
Resids.
time [ns]

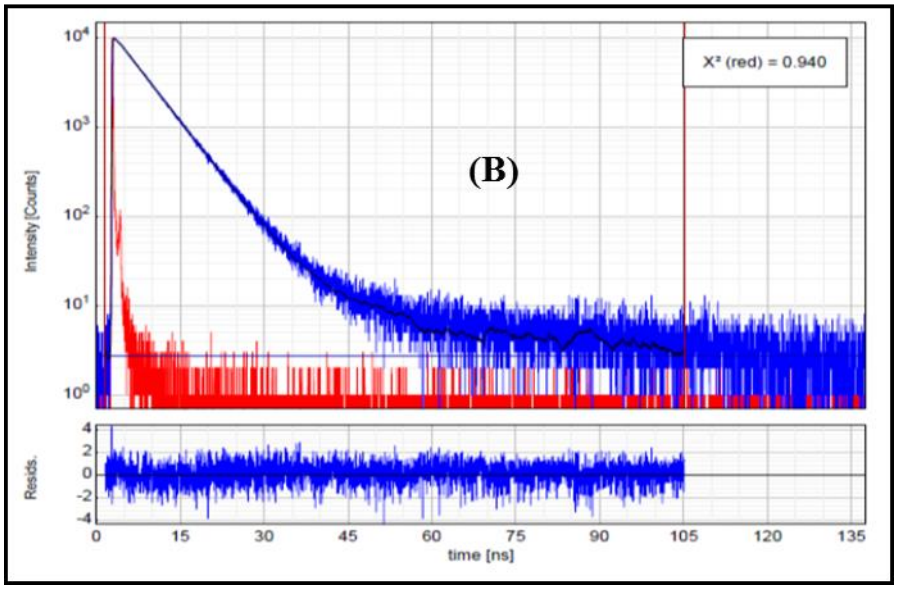
X² (red) = 0.940
(B)
Intensity [Counts]
Resids.
time [ns]

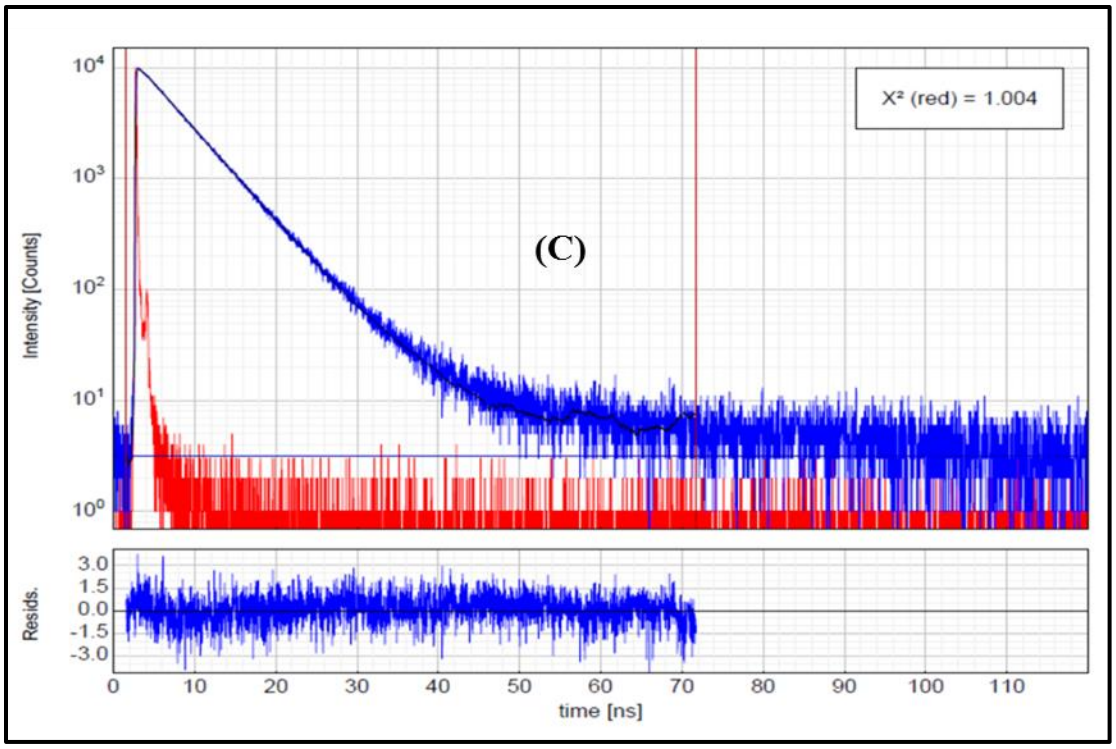

Figure 3.6: Fluoresces decay curves for compounds **19a** (A), **20a** (B) and **21a** (C) in THF. Excitation wavelength of 638 nm.

The rotational correlation times (Φ) in THF and DCM (in brackets) for **19a**, **20a** and **21a** were found to be 0.52 (0.49), 0.73 (0.58) and 0.57(0.43) ns respectively. Compound **21a** has a significantly greater correlation time in both solvents. Φ is usually controlled by solvent viscosity, size and shape of the molecule. The difference in (Φ) can be attributed to the differences in the molecular structures. The correlation times suggest that compound **21a** has a greater interaction with the solvent molecules.

Table 3.1: Q band maxima in the absorption (Abs), fluorescence excitation (Exc), emission (Em) spectra, fluorescence lifetime (τ), anisotropy rotational correlation time (Φ) values and molecular volumes (V_m) in THF and DCM.

	λ_{max} (nm)			τ (ns)	Φ (ns)	V_m	Solvent
	Abs	Exc	Em			($10^{-27}m^3$)	
19a	664:699	639	649	5.3±0.024	0.57±0.19	4.88	THF
	665:700	635	645	5.7±0.084	0.43±0.13	4.32	DCM
20a	663:698	634	644	5.2±0.019	0.52±0.31	4.46	THF
	660:694	634	644	5.4±0.031	0.49±0.15	4.91	DCM
21a	663:698	638	648	5.2±0.021	0.73±0.02	6.25	THF
	660:698	640	650	5.6±0.020	0.58±0.19	5.82	DCM

The rotational correlation times (Φ) were further used to calculate the molecular volume occupied by each compound using **Equation 19** [116]

$$\phi = \frac{\eta V}{kT} \qquad (\mathbf{19})$$

Where k is the Boltzman constant, η the viscosity, V the molecular volume and T the absolute temperature. The results of molecular volume using the above equation are summarised in **Table 3.1**. The molecular volumes from **Equation 19** are within range of theoretically calculated molecular volume of $1.29 \times 10^{-27} m^3$ for an unsubstituted phthalocyanine compound.

The unsubstituted phthalocyanine diameter was estimated to be 13.5 Å. The theoretical value was calculated from DFT optimised structures at the B3LYP/6-31G (d) level of theory.

Compounds **19a, 20a** and **21a** molecular volumes are experimentally determined in THF and DCM (in brackets) to be 4.46 x 10^{-27} (4.91 x 10^{-27}), 6.25 x 10^{-27} (5.82 x 10^{-27}) and 4.88 x 10^{-27} (4.32 x 10^{-27}) m^3 respectively (see **Table 3.1**). THF has higher viscosity compared to DCM (0.46 and 0.41 mPa.s respectively). The experimentally determined molecular volume is expected to be more accurate in more viscous solvents. This is because viscous solvents tend to slow down the rotation of the molecules in solution, hence the determined rotational lifetimes become more reliable.

3.4 Nonlinear optical (NLO) parameters

Figure 3.7 A, **B**, **C D**, **E** and **F** shows the open aperture Z-scan curves obtained for compounds **19a, 19b, 20a, 20b, 21a** and **21b** respectively in THF. All the compounds showed a strong nonlinear absorption behavior with reverse saturable absorption (RSA) profile. The experimental and theoretical nonlinear absorption coefficient (β) values for all the six complexes were obtained and are tabulated in **Table 3.2**. The experimental β values were obtained by a nonlinear fit q_o (z_s), a parameter that characterises the strength of the nonlinearity, in the curve depicted in **Figure 3.7 (A')**, (**B'**), (**C'**) (**D'**), (**E'**) and (**F'**), using **Equations 7** and **10**. The highest measured β value of 5.36 X 10^{-10} m/W was obtained for the metal-free compounds (**19a**) and the lowest β value of 1.78X10^{-10} m/W was obtained for nickel complex (**19b**). The measured β values lie within the range of those reported previously for phthalocyanine complexes [117]. The reduction in the β value upon metalation of compound (**19a**) is expected since metalation leads to a more centrosymmetric compound (**19b**). Low β values are expected for centrosymmetric compounds [118]. Therefore upon metalation all complexes showed lower β values as expected with respect to their metal-free counterpart. Aggregation in monomeric Pc is also known to leads to the reduction of β values [12, 39, 40, 119]. However despite severe aggregation, Bi-Pcs (**20a, 20b,**

21a and **21b**) measured β values were found to be in range of monomeric Pc β values, see **Table 3.2**. Metal-free Bi-Pcs (**20a** and **21a**) showed higher β values of 4.10 X 10^{-10} m/W and 3.37 X 10^{-10} m/W respectively, compared to that of nickel Bi-Pcs (**20b** and **21b**) with β values of 3.33 X 10^{-10} m/W and 2.25 X 10^{-10} m/W respectively. The differences in β values between nickel Bi-Pcs (**20b**) and (**21b**) is attributed to the differences in the bridge compound. Restricted rotation could cause compounds (**21a** and **21b**) to be more prone to aggregation compared to Bi-Pcs (**20a** and **20b**). Hence higher β values are observed for Bi-Pcs **20a** and **20b**.

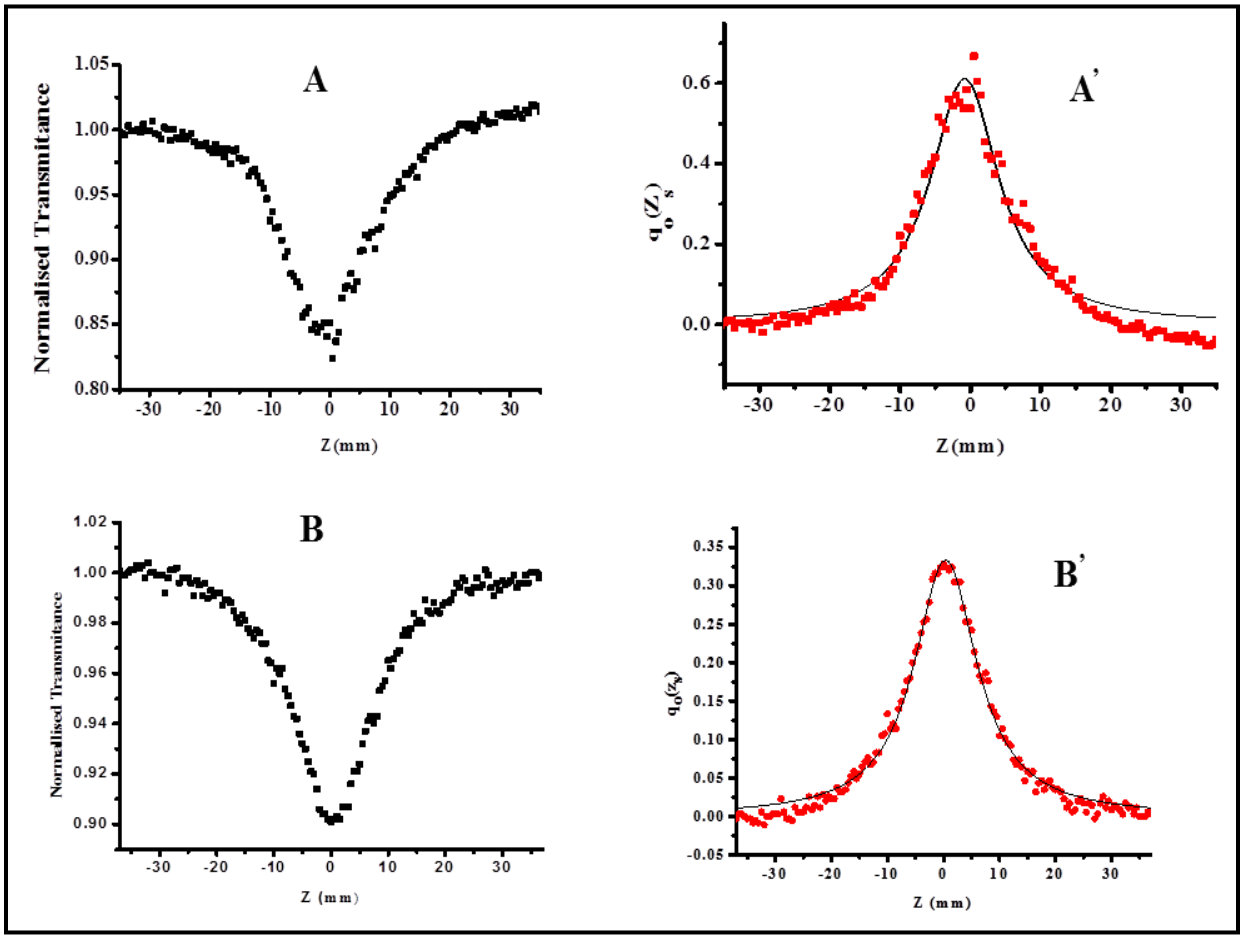

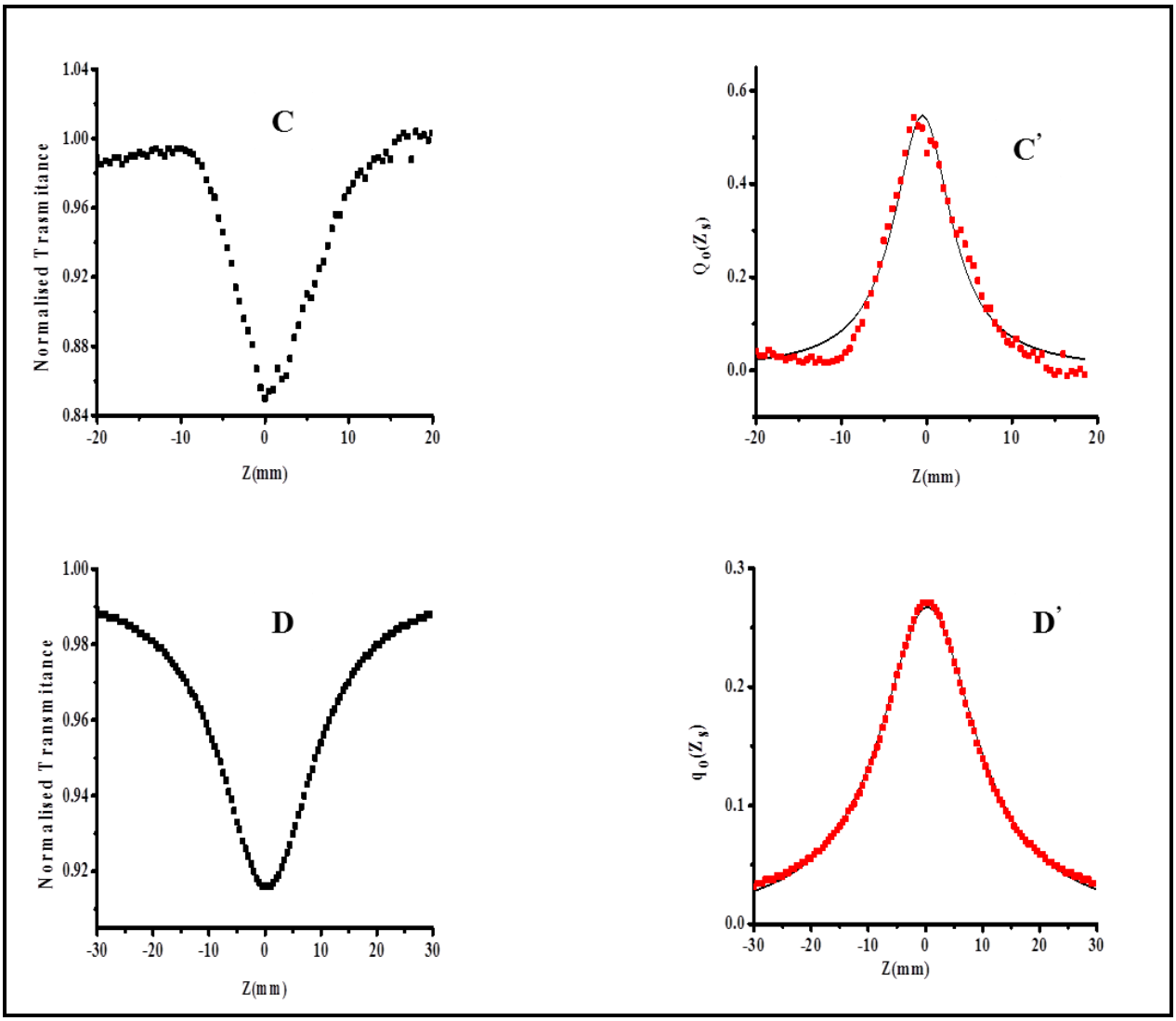
C
Normalised Trasmitance
Z(mm)
C'
$Q_0(Z_g)$
Z(mm)
D
Normalised Transmitance
Z(mm)
D'
$q_0(Z_g)$
Z(mm)

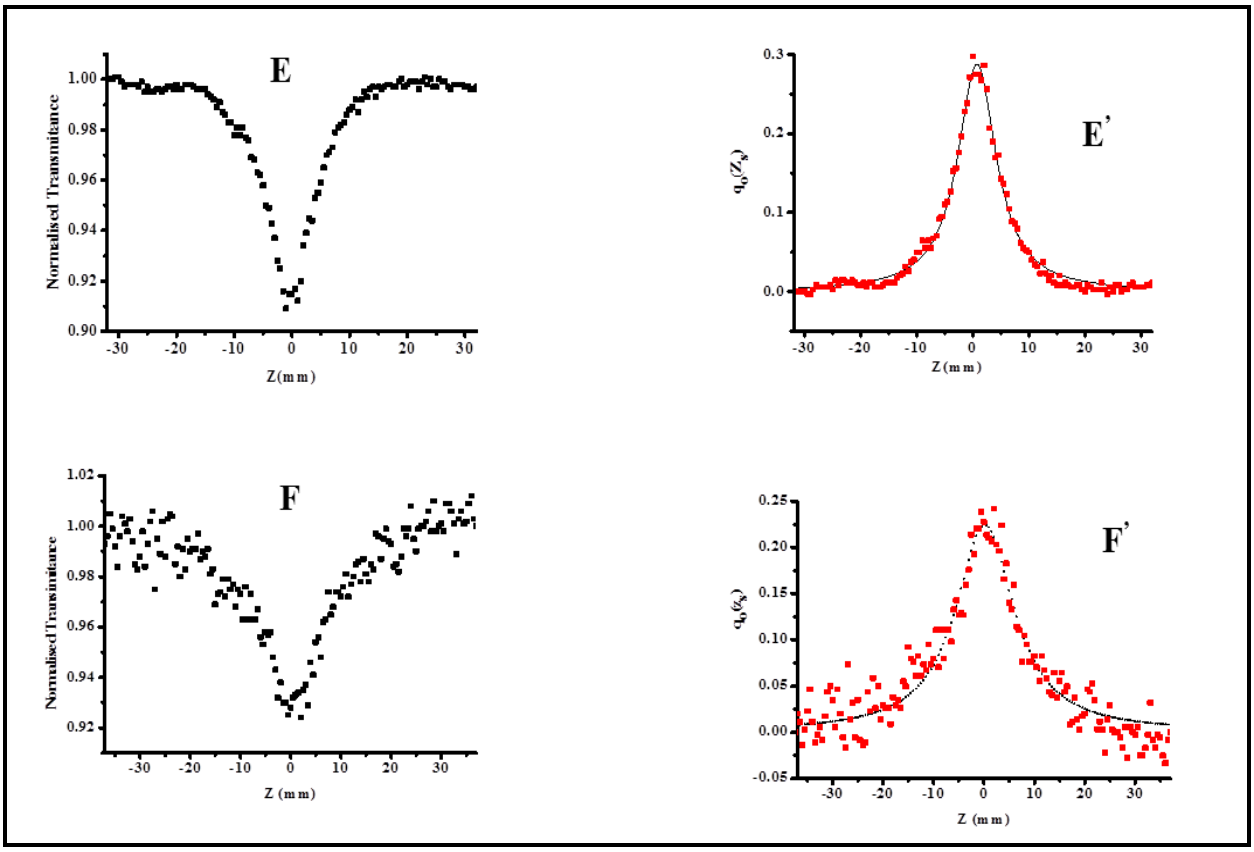

Figure 3.7: Z-Scan (left) and nonlinear fit curves (right) for compounds: A (**19a**), B **(19b**), C (**20a**), D **(20b**), E (**21a)** and F (**21b**) in THF**.**

The observed differences in β values between Bi-Pc **20b** and Bi-Pc **21b** are explained by the same reasoning as above**.** Insertion of nickel atom also makes the Bi-Pc units to be more planar, thus increasing aggregation tendency between the Pc units. This could also contribute to the observed differences in β values between metalated and metal-free Bi-Pcs.

Table 3.2: Experimental and theoretical Z-scan results for second order nonlinear polarizability, β, in THF. DFT calculated with the B3LYP functional and SDD basis sets.

	Q_0	z_R(mm)	$\beta\left(\frac{m}{W}\right) \times 10^{-10}$(Exp.)	β_{HRS}(esu) $\times 10^{-28}$(Theor)	$\Phi_{J=1}$	$\Phi_{J=3}$	ρ	DR
19a	0.612	5.93	5.36	0.65	0.78	0.28	0.36	6.34
20a	0.544	4.14	4.10	7.12	0.50	0.49	0.98	4.27
21a	0.33	6.85	3.37	7.38	0.39	0.61	1.54	3.56
19b	0.288	4.20	1.78	0.46	0.75	0.26	0.35	6.35
20b	0.267	10.38	3.33	6.02	0.57	0.43	0.77	4.74
21b	0.23	7.06	2.35	6.07	0.43	0.57	1.34	3.77

3.5 DFT calculations

DFT calculations were done in order to calculate the theoretical β values and to theoretically determine dipolar and octupolar ($\Phi_{J=1}$ and $\Phi_{J=3}$) contribution to the NLO response. **Equations 11** to **18** were used to theoretically calculate β, $\Phi_{J=1}$ and $\Phi_{J=3}$ values of compounds **19a, 19b, 20a, 20b, 21a** and **21b**, see **Table 3.2**. All DFT calculations were carried out using SDD basis set at B3LYP level of theory. Theoretically determined β values for compounds **19a, 19b, 20a, 20b, 21a** and **21b** showed a similar trend to experimentally determined values in terms of lowering of β values upon metalation. A trend peculiarity occurred for the β value for **19a**, which shows the largest experimentally determined β value compared to **20a** and **21a**, but a much smaller theoretical β value compared to **20a** and **21a**. The large β value for compound **19a** is explained by the fact that compound **19a** is monomeric in solution, whilst Bi-Pcs compounds **20a** and **21a**

are considerably aggregated. The theoretically determined β values suggest that without aggregation compounds **20a, 20b, 21a** and **21b** should show much higher β values compared to compounds **19a**. This trend peculiarity was not observed for the metalated Pc and Bi-Pcs. The experimental results correlates well with theoretical prediction and Bi-Pcs β values are still within range of β values determined for monomeric Pcs despite considerable aggregation. Aggregation is known to significantly reduce β values for monomeric Pcs **[**65]. This fact suggests that higher β values are expected for disaggregated Bi-Pcs. However compounds **20a**, **20b**, **21a** and **21b** could not be disaggregated.

The theoretically determined β values were further separated into dipolar and octupolar contribution using **Equation 11** to **18**. **Table 3.2** and **Figure 3.8** summarize the theoretical results. **Figure 3.8** plots the Harmonic light intensity as a function of the polarization angle by polar representation for compounds **19a, 19b, 20a, 20b, 21a** and **21b** with increasing octupolar contribution and their corresponding DR values. The nonlinear anisotropy parameter (ρ), in **Table 3.2**, was used to calculate the the ratio of dipolar/octupolar contribution. Anisotropy parameter of a value less than one suggest a more pronounced dipolar character and greater than one a more pronounced octupolar character [63]. The theoretical results suggest that Bi-Pcs **20a**, **20b**, **21a** and **21b** β values have greater octupolar contributions compared to monomeric Pcs (**19a** and **19b)**. Octupolar contribution presents an isotropic β tensor (hence free from symmetry restriction) and a complex charge distribution within the compound. The large octupolar contribution and two dimensional nature of Bi-Pcs suggest that the large β value is due to an increase in π- orbital energy [120]. DFT results suggest that in general the presence of the central metal does not significantly affect the ratio of dipolar/octupolar contribution. Hence the experimentally observed higher β values for Bi-Pcs could be attributed to the increased octupolar

nature. The molecular geometric information is given by the depolarization ratio (DR) [63]. Upon metalation there is a decrease in DR values for compounds **19a and 19b** and an increase in DR values for compounds **20a, 20b, 21a** and **21b** (see **Table 3.2**). An increase in DR values suggests lowering of symmetry [63]. An increase in DR values of Bi-Pcs (**20a,** and **21a**) upon metalation suggests that the nickel Bi-Pcs (**20b** and **21b**) have slightly lower symmetry compared to their metal-free counterpart. These results together with the shape of the polar plots in **Figure 3.8**, suggest a preservation of a dipole nature of the molecule after metalation.

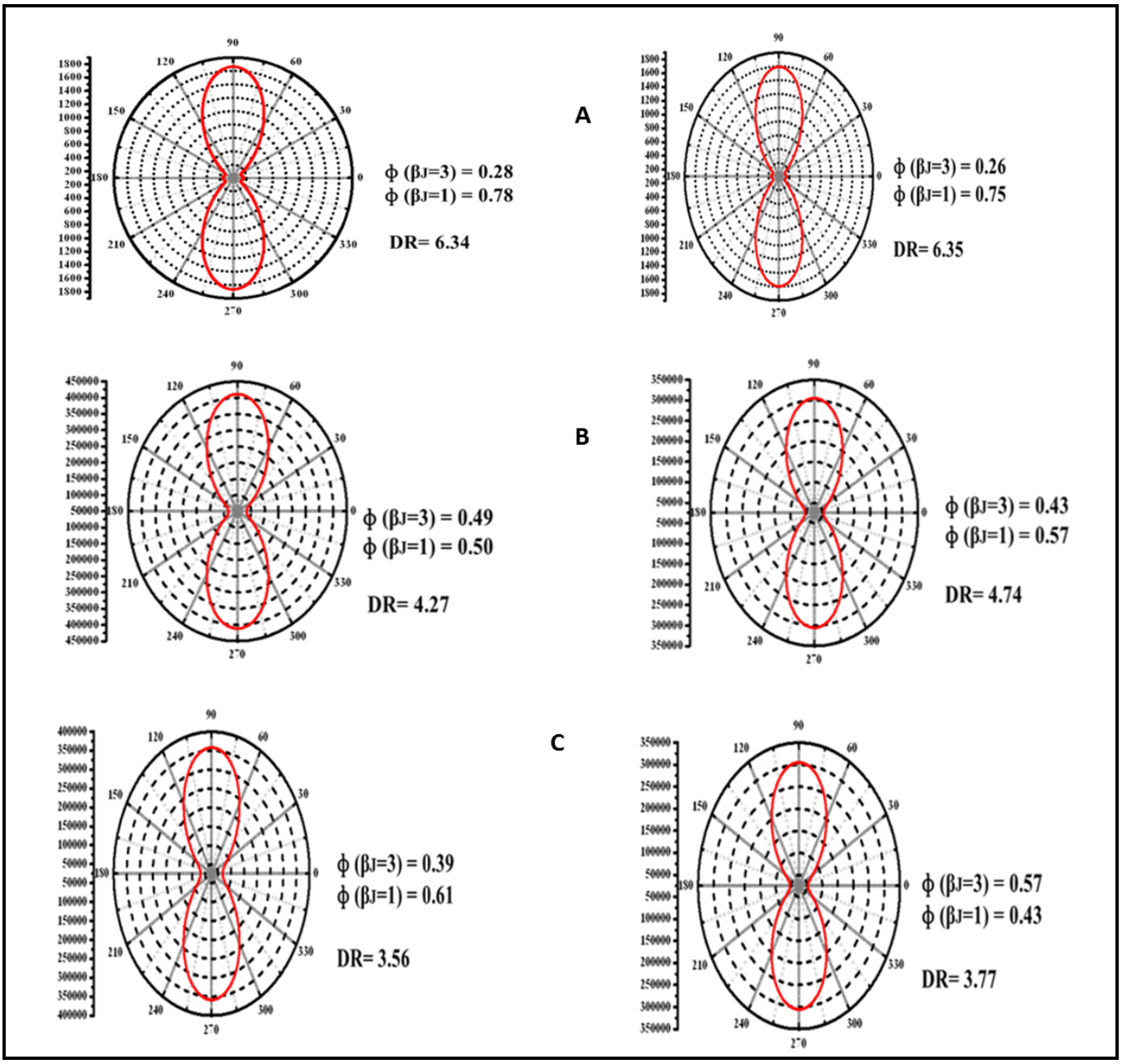

Figure 3.8: Polar plots for compounds (Left): A (**19a**), B (**20a**), C (**21a**). (Right): A(**19b**), B (**20b**) and C (**21b**).

Bi-Pcs have the potential to transform their approximated D_{2h} symmetry to a D_2 or D_{2d} symmetry, by changing the angles (θ and ϕ) corresponding to the torsional relationship between their Pc units and the bridge least square plane [44]. Torsional angle of $\theta = -\phi < 45^{\circ}$ correspond to D_2 symmetry, $\theta = -\phi = 45^{\circ}$ correspond to D_{2d} symmetry and $\theta = -\phi = 0^{\circ}$ correspond to D_{2h} symmetry [56]. As an example **Figure 3.9** shows the DFT optimize compounds **21b** and **20b**

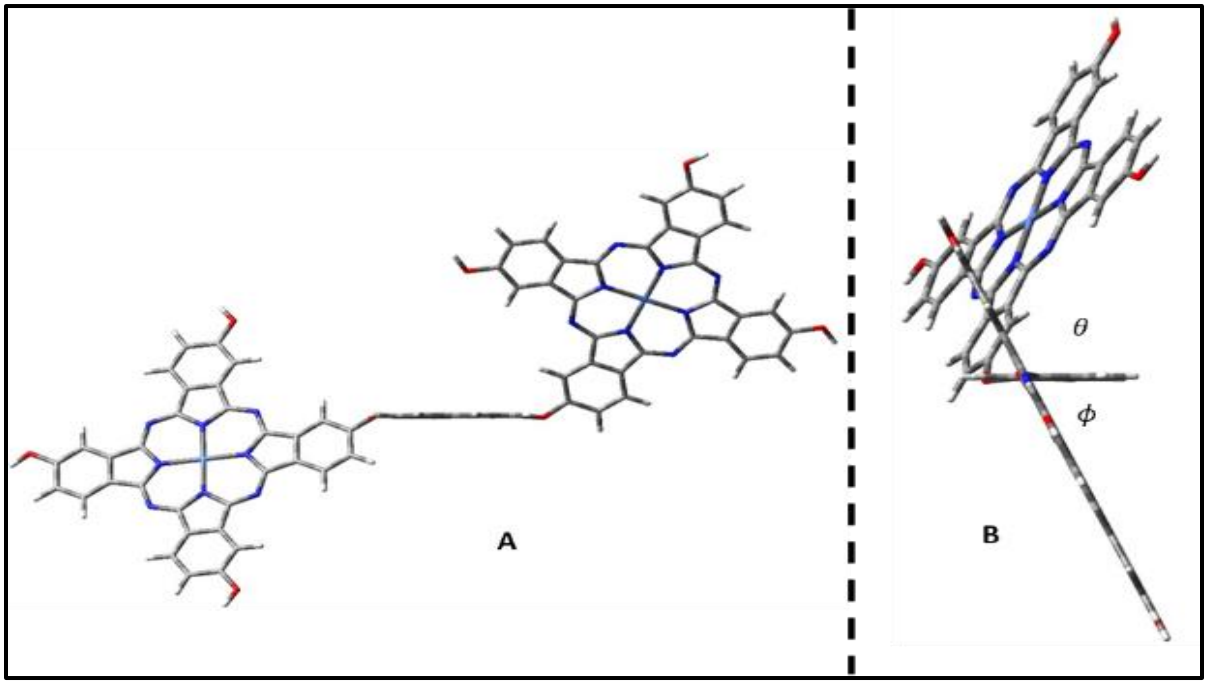

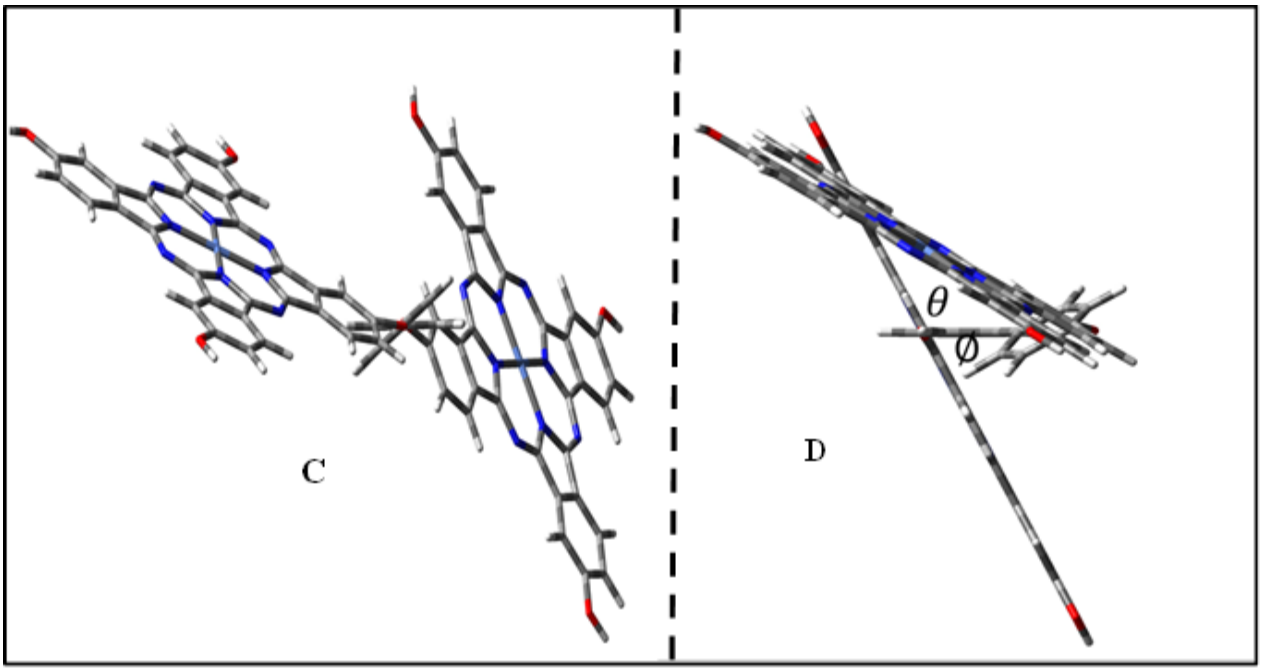

Figure 3.9: Front (**A and C**) and side (**B and D**) view of compounds **21b (**top**) 20b (**bottom**)**

The angles θ and ϕ corresponding to the torsional relationship between the Pc units and the naphthalene bridged least square plane are measured to be $\theta = -\phi \approx 64^{\circ}$, which approximate a D_{2d} symmetry [56]. The Pc units with biphenyl bridged least square plane are measured to be $\theta = -\phi \approx 61.5^{\circ}$, approximating a D_{2d} symmetry. The above results suggest that the enhanced β value for both **20b** and **21b** is also due to the approximation of the D_{2d} symmetry. Similar improvements in β value due to D_{2d} symmetry have been observed in literature [56]. The D_{2d} symmetry, similar to D_{3h} or T_d symmetry, is responsible for the increase in octupolar contribution. The highly aggregated Bi-Pc complexes (**20a**, **20b**, **21a**, and **21b**) suggest that the measured β value is mainly due to the octupolar contribution. The calculated $\boldsymbol{\rho}$ and **DR** values also supports the above interpretation.

CHAPTER FOUR: CONCLUSIONS

4. General Conclusion

Metal-free and nickel 4β-(4-tert-butylphenoxy) phthalocyanines (**19a, 19b),** biphenyl bridged binuclear 4-tert-butylphenoxy phthalocyanines (**20a, 20b**) and naphthalene bridged binuclear 4-tert-butylphenoxy phthalocyanines (**21a**, **21b**) were successfully synthesised and characterised. UV-vis absorption, MCD and fluorescence spectroscopy of these compounds have been studied. The Fluorescence life time where determined to be in range of literature values for Pcs ~5 ns and anisotropy rotational correlation time was found to be between 0.45 and 0.75 ns. The mass spectrometry results showed the m/z of 1109.88,1166.6, 2101.39, 2215.07, 2080.8, and 2193.86, which are close to the calculated m/z peak of 1107.34,1164.00,2100.5,2213.8,2074.4 and 2187.8 for the compounds **19a**,**19b**, **20a**, **20b**, **21a** and **21b** respectively.

Nonlinear optical activities of the compounds **19a, 19b, 20a, 20b, 21a** and **21b** were investigated. The profiles of the open aperture for the compounds revealed reverse saturable excited state absorption in THF solution. The highest and lowest β value of 5.36 X 10^{-10} m/W and 1.78X10^{-10} m/W were measured for compound **19a** and **19b** respectively. Metal-free Bi-Pcs (**20a** and **21a**) showed higher β values of 4.10 X 10^{-10} m/W and 3.37 X 10^{-10} m/W respectively, compared to that of nickel bi-Pcs (**20b** and **21b**) with β values of 3.33 X 10^{-10} m/W and 2.25 X 10^{-10} m/W respectively. These results suggest that these compounds **20a**, **20b, 21a**, and **21b** can find potential applications in nonlinear optics, similar to compounds **19a** and **19b.**

The DFT determined β values suggested that without aggregation compounds **20a** and **21a** should show much higher β values compared to compound **19a.** The theoretically determined β values were further separated into dipolar and octupolar contributions. The

depolarization ratio (DR) and nonlinear anisotropy parameter (ρ) of these synthesized compounds were determined. The theoretical results suggest that Bi-Pcs (**20a, 20b, 21a** and **21b)** have more octupolar contributions compared to monomeric Pcs (**19a** and **19b)**. This has been observed due to the decrease of DR values of Bi-Pcs and increase of ρ values of monomeric Pcs. The presence of the central metal does not significantly affect the ratio of dipolar/octupolar contribution. Hence the experimentally observed higher β values for Bi-Pcs could be attributed to the increased octupolar nature. The improvement in Bi-Pcs β values is also attributed to D_{2d} symmetry approximation.

REFERENCES

[1] C. G . Claessens , T. Torres, Chem. Eur . J, 2000, 6, 2168.

[2] P. Gregory, J. Porphyrins Phthalocyanine, 2000, 4, 432.

[3] N. B. McKeown, Chem. Ind, 1999, 11, 67.

[4] A.P. Castano, T. N. Demidova, M. R. Hamblin, Photodiagnosis and photodynamic therapy, 2004, 1, 279.

[5] S.Vilakazi, T.Nyokong, Polyhedron, 2000, 19, 229.

[6] K.T. Ranjit, I.Willner, J. phys.chem,B, 1998, 02, 9397.

[7] D.Worhle, D. Meissener, Adv mater, 1991, 3,129.

[8] C.C Leznff, A.B.P Lever (eds) phthgalocyanines:properties and applications,VCH, publishers,NewYork, 1989, 1, 245.

[9] C. J. Walsh, B.K.Mandal, J.mater, 2000, 12, 287.

[10] M. J. Stillman, T. Nyokong , C. C. Leznff , A. B. P. Lever, Phthalocyanines: Properties and applications, 1989, 1, 133.

[11] S. Khene, Synthesis photophysics and electrochemical study on tin macrocycles, Rhodes University, MSc thesis, 2008, pp 5 and 11.

[12] X. F Zhang, H. J Xu, J. Chem. Soc. Faraday Trans, 1993, 89, 347.

[13] W. A. Nevin, M. R. Hempstead, W. Liu, C. C. Leznoff, A. B. P. Lever, Inorg. Chem, 1987, 26, 540.

[14] N.Kobayashi, H. Ogata, N. Nonaka, E A. Lukyanets, Chemistry, Eur.J, 2003, 9, 5123

[15] M. Hanack, H. Heckmann, R. Polley, in Methoden der Organischen Chemie (Houben–Weyl), Thieme Verlag: Stuttgart, 1997, 170, 244.

[16] K.D.Modibane, Synthesis and photo physical properties of lead phthalocyanines, Rhodes University, MSc thesis, 2009, pp 18.

[17] M. Hanack, M. Lang, Adv. Mater, 1994, 6, 819.

[18] A. W. Snow, J. R. Griffith, N. P. Marullo, Macromol, 1984, 17, 1614.

[19] D. A. Davies, C. Schnik, J. Silver, J. L. Sosa-Sanchez, J. Porphyrins and Phthalocyanines, 2001, 5, 376.

[20] P.C. Ray, Chem. Rev. 2010, 110, 5332.

[21] S. Haqu, J. Nelson, Science, 2010, 327, 1466.

[22] G. Lim, J. Chen, J. Clark, S.G.R. Goh, H.W. Ng, W.H. Tan, H.R. Friend, K.P.Ho, K.L.Chua, Nature Photonics, 2011, 5, 554.

[23] J.M. Hales, J. Matichak, S. Barlow, S. Ohira, K. Yesudas, L J. Bredas, W. J Perry, R.S. Marder, Science, 2010, 327, 1485.

[24] P. N. Williams, J. Introduction to Nonlinear Optical Effects in Molecules and Polymers; John Wiley: NewYork, NY, USA, 1991, 17, 969.

[25] N. Nikogosyan, Nonlinear Optical Crystals: A Complete Survey. Springer Science and Business Media, Inc.: NewYork, NY, USA, 2005, 20, 1656.

[26] L.De Boni, E. Piovesan, L.Gaffo, C.R.Mendanca, J.phys.Chem.A, 2008, 112, 6803.

[27] T. Pritchett, Sensors and electron devices directorate, ARL, Adelphi, MD, 2002, 39, 20783.

[28] B. Sheehy, L.F. Di Mauro, Ann. Rev. Phys. Chem, 1996, 47, 463

[29] H. S. Nalwa, J. S. Shirk, in Phthalocyanines, Properties and Applications Eds: (C. C. Leznoff, A. B. P. Lever), VCH, New York, 1996, 4, 79.

[30] M. B. Askari, P. Jalilpour, F. Ahmadi. Optical Nonlinear Absorption Coefficient of PbS Nano Particles Studied by the Z-Scan Technique. American Journal of Nanoscience and Nanotechnology, 2014, 2, 28.

[31] P.Kaatz, D. P. Shelton, J. Chem. Phys, 1996,105, 3918.

[32] O. B. Bankole, T. Nyokong, J. Molecular structure, 2015, 1089, 107.

[33] O.B. Bankole, J. Britton, T. Nyokong, Polyhedron, 2015, 88, 73.

[34] S. O. Sanusi, E. Antunes, T. Nyokong, J. Porphyrins and Phthalocyanines, 2013, 17, 920.

[35] S. J. Mathews, S. C. Kumar, L. Giribabu, S.V. Rao, Materials letters, 2007, 6, 4426.

[36] S.V. Rao, P.T. Anusha, T. S. Prashant, D. Swain, S.P Tewari, Material sciences and applications, 2011, 2, 299.

[37] K.Sanusi, T. Nyokong, J.coordination chemistry, 2014, 67, 2911.

[38] K. Sanusi, S. Khene, T. Nyokong, Optical materials, 2014, 37, 572.

[39] A. Tuhla, H. Manaa, S. Makhseeda, N. Al-Awadi, J. Mathew, H. M. Ibrahim, T. Nyokong, H. Behbehan, Optical materials, 2012, 34,1869.

[40] S. Tekin, H. G. Yaglioglu, A. Elmali, U. Kürüm, H. Yanık, D. A. Tekdas, M. Durmus, V. Ahsen, Material chemistry and physics, 2013, 138, 270.

[41] E. M. García-Frutos , S. M. O'Flaherty , E. M. Maya , G. de la Torre , W. Blau , P. Vázquez T. Torres, J. mater. Chem, 2003, 13, 749.

[42] M. Yuksek, A. Elmali, M. Durmus, H. G. Yaglioglu, H. Unver, T. Nyokong, J. Opt, 2012, 12, 015208.

[43] E.T. Saka, C. Gol, M. Durmus, H. Kantekin, Z. Biyikhoglu, J. Photochemistry and photobiology .A, 2012, 241, 67.

[44] G.de la Torre, P.Vazquez, F. Agullo-Lopez, T. Torres, Chem.Rev, 2004, 104, 3723.

[45] H. S. Nalwa, S. Miyata, Nonlinear optics of Organic molecules and polymers, CRC Press, New York, USA, 1997,33, 261.

[46] M. M Ayhan, A. Singh, C. Hirel, A.G. Gürek, V. Ahsen, E. Jeanneau, I. Ledoux-Rak, J. Zyss, C. Andraud, Y. Bretonniè re, J. Am. Chem. Soc, 2012, 134, 3655.

[47] D. Dini, M. J. F. Calvete, M. Hanack, M. Meneghetti, J.Phys.Chem.A, 2008, 112, 8515.

[48] J. S. Shirk, R.G. S. Pong, S. R. Flom, H. Heckman, M. Hanack. J. Phys. Chem. A, 2000, 104,1438.

[49] J. L. Bredas, C. Adant, P. Tackx, A. Persoons, B. M. Pierce. Chem. Rev, 1994, 243, 94.

[50] V. Chauke, M. Durmus, T.Nyonkong, J. Photochem. Photobial, A, 2007, 179, 192.

[51] M. Calvete, M. Hanack, Eur. J. Org. Chem, 2003, 11, 2080.

[52] G.de la Torre, G. Bottari, M. Sekita, A. Hausmann, D. M. Guidi, T. Torres, Chem. Soc, 2013, 42, 8049.

[53] N. Kobayashi, T. Fukuda, D. Lelieve, Inorg. Chem, 2000, 39, 3632.

[54] A.Y. Tolbin, V.E. Pushkarev, L.G. Tomilova, N.S.Zefirov, Macroheterocycles, 2010, 3, 30.

[55] A.Y. Tolbin, A.V. Avanon, L. G. Tamilova, N. S. Zefirov, J. Porphyrin and phthalocyanines, 2003, 7, 162.

[56] K. M. Kadish, K. M. Smith, R. Guilard, (Eds), The Porphyrin Handbook, Academic press, New York, 2003, 7, 187.

[57] T.V.Duncan, K. Song, S. T. Hung, I. Miloradovic, A. Nayak, A. Persoons, T. Verbiest, M. J. Therien, K. Clays, Augew. Chem. Int. Ed, 2008, 47, 2978

[58] J. L. Bredas, C. Adant, P. Tackx, A. Persoons, B. M. Pierce, A. Chem. Rev, 1994, 94, 243.

[59] M. J. F. Calvete, D. Dini, M. Hanack, J. C. S. Garcıa, W. Chen, W. Ji, J. Mol Model, 2006, 15, 543.

[60] K. E. Sekhosana, E. Amuhaya, T. Nyokong, Polyhedron, 2015, 85, 347.

[61] M. Quintiliani, J. P. Moreno, I. Asselberghs, P. Vázquez, K. Clays, T. Torres, J. Phys. Chem. B, 2010, 114, 6309.

[62] L. Xu, E. Wang, Z. Li, D. G. Kurth, X. Du, H. Zhang, C. Qin, New J. Chem, 2002, 26, 782.

[63] G. Lu, J. Li , S. Yan , C. H , M. Shi , W. Zhu ,Z. Ou, K. M. Kadish, Dyes and Pigments, 2015,121, 38.

[64] L. Zhang, D. Qi, L. Zhao, C. Chen, Y. Bian, W. Li, J. Phys. Chem. A, 2012, 116, 10249.

[65] D. Qi, Y. Zhang, L. Zhang, J. Jiang, J. Phys. Chem A, 2010, 114, 1931.

[66] N. Kobayashi, Y. Yanagisawa, C. C. Leznoff, Analytical Sciences, 1990, 6, 813.

[67] E. M. Maya, P. Vazquez, T. Torres, Chem. Commun, 1997,43, 1175.

[68] M. J. F. Calvete, D. Dini, S. R Flom, M. Hanacks, R. G. S. Pong, J.S. Shirk, Eur. J. org. chem, 2005, 23, 3499.

[69] T.V. Dubinina, N.E Borisova, M.V. Sedova, L.G. Tamilova, T.Furuyama, N. Kobayashi, Dyes and pigments, 2015, 117, 1.

[70] G. Bottari, T. Torres, chem. commun, 2004, 10, 216.

[71] H.Yoshiyama, N.shibata, T. Sato, S.Nakumuru, T. Toru, Org.Biomol, chem, 2008, 6, 4498.

[72] S. O. Malley, B. Schazmann, D. Diamond, K. Nolan, Tetrahedron letters, 2007, 48, 9003.

[73] T. Ceyhan, A. Altindal, M. K. Erbil, O. Bekarodu, Polyhedron, 2006, 25, 737.

[74] [66] Z. Li, F. Gao, Z. Xiao, G. Ao, X. Wu, Y. Fana, Z. Nie, T. H. Wei, J. yana, Y. Wang, X. Zhang, J. Zuo, Y. Song, Dyes and pigments, 2015, 119, 70.

[75] Y. Cimen, E. Ermis, F. Dumludag, A.R. Ozkaya, B. Salih, O. Bekaroglu, Sensors and Actuators B, 2014,202, 1137.

[76] R. Jung, K. H. Schweikart, M. Hanack, Synthetic metals, 2000, 453, 112.

[77] F. Paulat, N. Lehnert, Inorg. Chem, 2008, 47, 4963.

[78] J. Mack, X .Liang, T. V. Dubinina, L.G.Tomilova, T. Nyokong, N. Kobayashi, J. Porphyrins and phthalocyanine, 2013, 17, 489.

[79] J. Mack, M. J. Stillman, N. Kobayashi, Coordination chemistry reviews, 2007,251, 429.

[80] N. Kobayashi, Y. Yanagisawa, T. Osa, H. Lam, C. C. Leznoff, Analytical sciences, 1990, 6, 1907.

[81] H. Isago, Optical spectra of phthalocyanines and other related compounds, National Institute of Material Sciences, Japan, published by Springer, Japan, 2015.

[82] D.V. O'Connor and D. Phillips, Time Correlated Single Photon Counting, Academic Press, London, 1984.

[83] S. C. Frances photophysics evaluation of substituted Zinc phthalocyanines as sensitisers for photodynamic therapy, Durham University, 1997, pp 45.

[84] G. Tsigaridas, I. Polyzos, P. Persephonis, V. Giannetas, Opt. Commun., 2006, 266, 284.

[85] E. W. V. Stryland, M. Shaik-Bahae; Characterization technique and tabulations for organic nonlinear material, Marcel Dekker Inc, 1998, 1, 655.

[86] P. Neethling Determining nonlinear optical properties using z-scan technique, University of Stellenbosch, 2005,1, 12.

[87] M. Sheik-Bahae, A. A. Said, T. H. Wei, D, J. Hagan, E. W. Van Stryland, IEEE J. Quantum Elect., 1990, 26, 760.

[88] M. Kandaz, A. R. Özkaya, Özer Bekaroğlu, Monatsh. Chem, 2001, 132, 1013.

[89] M. J. MacLachlan, In Frontiers in Transition Metal-Containing Polymers, ed. A. S. Abd -El-Aziz and I. Manners (Eds.) Wiley & Sons: New York, 2007, 12, 208

[90] P. Hohenberg, W. Kohn, physical review, 1964, 136, 864.

[91] A. Plaquet, M.Guillaume, B. Champagne, F. Castet, L. Ducasse, L. Pozzo, V. Rodriguez, Phys. Chem. Chem. Phys, 2008,10, 6223.

[92] F. Castet, E. Bogdan, A. Plaquet, L. Ducasse, B. Champagne, V. Rodriguez, J. Chem. Phys, 2012,136, 024506.

[93] P.S. Liyanage, R.M. de Silva, K.M.N. de Silva, J. Mol. Struct., Theochem, 2003, 639, 195.

[94] C. Wang, C. Chen, Q. Zhang, D. Qi, J. Jiang, Turk J Chem, 2014, 38, 1046.

[95] P. C. Ray, Chem Rev, 2010,110, 5332.

[96] M.J. Frisch, G.W. Trucks, H.B. Schlegel, G.E. Scuseria, M.A. Robb, J.R. Cheeseman, J.A. Montgomery Jr., T. Vreven, K.N. Kudin, J.C. Burant, J.M. Millam, S.S. Iyengar, J. Tomasi, V. Barone, B. Mennucci, M. Cossi, G. Scalmani, N. Rega, G.A. Peters son, H. Nakatsuji, M. Hada, M. Ehara, K. Toyota, R. Fukuda, J. Hasegawa, M. Ishida, T. Nakajima, Y. Honda, O. Kitao, H. Nakai, M. Klene, X. Li, J.E. Knox, H.P. Hratchian, J.B. Cross, V. Bakken, C. Adamo, J.

Jaramillo, R. Gomperts, R.E. Stratmann, O. Yazyev, A.J. Austin, R. Cammi, C. Pomelli, J.W. Ochterski, P.Y. Ayala, K. Morokuma, G.A. Voth, P. Salvador, J.J. Dannenberg, V.G. Zakrzewski, S. Dapprich, A.D. Daniels, M.C. Strain, O. Farkas, D.K. Malick, A.D. Rabuck, K. Raghavachari, J.B. Foresman, J.V.D.J. Fox, T. Keith, M.A. Al-Laham, C.Y. Peng, A. Nanayakkara, M. Challacombe, P.M.W. Gill, B. Johnson, W. Chen, M.W. Wong, C. Gonzalez, J.A. Pople, Gaussian 03, Revision E.01, Gaussian Inc., Wallingford, CT, 2004.

[97] W. Worhle, M. Eskes, K. Shigehara, A. Yamada, Synthesis, 1993, 5, 194.

[98] J. A. Elvidge, R. P Linstead, J. Chem. SOC, 1952, 10, 5000.

[99] K.Venkataraman, chemistry of synthetic dyes, Academic press, New York and London, 1972, 6, 1.

[100] O.Vorm, P. Roepstroff, M. Mann, Improved resolution and very high sensitivity in MALDI-TOF of matrix surfaces made by fast evaporation, Anal Chem, 1994, 66, 3281.

[101] D. C. Reiber, T.A. Grower, Identifying proteins and matrix-assisted laser desorption/ionization in source fragmentation data combined with data base researching. Anal Chem, 1998, 70, 673.

[102] J. Mack, N. Kobayashi, *Chem. Rev*, 2011, 111, 281.

[103] T. Nyokong, Z. Gasyna, M. J. Stillman, Inorg. Chem, 1987, 26, 548.

[104] T. Nyokong, Z. Gasyna, M. J. Stillman. Inorg. Chem, 1987, 26, 1087.

[105] E. A. Ough, T. Nyokong, K. A. M. Creber, M. J. Stillman, Inorg. Chem, 1988, 27: 2724.

[106] J. Mack, M. J. Stillman, J. Phys. Chem, 1995, 95, 7935.

[107] J. Mack, M. J. Stillman, Inorg. Chem, 1997, 36, 413.

[108] N. Kobayahsi, K. Nakai, Chem. Commun, 2007, 64, 4077.

[109] G. N. Ngubeni, J. Britton, J. Mack, E. New, I. Hancox, M.Walker, T. Nyokong, T. S. Jones, S. Khene, J. Mater. Chem. C, 2015, 3, 10705.

[110] N. Kobayashi, Y. Yanagisawa, C. C. Leznoff, Analytical Sciences, 1990, 6, 813.

[111] M. Gouterman, In the Porphyrins, D. Dolphin (Ed.) Academic Press: New York, 1978, 3, 1.

[112] Z. Gasyna, N. Kobayashi, M. J. Stillman, J. Chem. Soc. Dalton Trans, 1989, 2397.

[113] J. Mack, N. Kobayashi, M. J. Stillman, J. Inorg. Biochem, 2010, 102, 472.

[114] N. Nombona, W. Chidawanyika, T. Nyokong, J. Mol. Struct, 2012, 1012, 31.

[115] J. W. Borst, M. A. Hink, A. van Hoek, A. J. W. G. Visser, J. Fluoresc, 2005, 15, 153.

[116] D. Dini and M. Hanack. In the Porphyrin Handbook: Physical Properties of Phthalocyane-based Materials, Vol K. M. Kadish, K. M. Smith and R. Guilard (Eds.) Academic Press: USA, 2003, 17, 22.

[117] T. Verbiest, S. V. Elshocht, A. Persoons, C. Nuckolls, K. E. Phillips, T. J. Katz, Langmuir, 2001, 17, 4685.

[118] H. M. Kim, B. R. Cho, J. Mater.Chem, 2009, 19, 7402.

[119] P. Tau, T. Nyokong, Electrochim. Acta, 2007, 52, 3641.

[120] M. Cho, S.-Y. An, H. Lee, I. Ledoux, J. Zyss, J. Chem. Phys, 2002, 116, 9165.